NASA Technical Memorandum 80203

Aeroacoustic Wind-Tunnel Tests of a Light Twin-Boom General-Aviation Airplane With Free- or Shrouded-Pusher Propellers

H. Clyde McLemore and Robert J. Pegg

NASA

NASA Technical Memorandum 80203

Aeroacoustic Wind-Tunnel Tests of a Light Twin-Boom General-Aviation Airplane With Free- or Shrouded-Pusher Propellers

H. Clyde McLemore and Robert J. Pegg
Langley Research Center
Hampton, Virginia

SUMMARY

Tests have been conducted in the Langley Full-Scale Tunnel to determine the aerodynamic and acoustic characteristics of four different pusher-propeller arrangements on a twin-boom, general-aviation airplane. The propellers included a 2-blade free propeller, two 3-blade shrouded propellers, and a 5-blade shrouded propeller.

The tests were conducted for a range of airplane angles of attack from 0° to about 16° for test speeds from 0 to about 36 m/sec (118 ft/sec) and for a range of propeller-blade angles and rotation speeds.

The free propeller provided the best overall aerodynamic propulsive performance. For forward-flight conditions, the free-propeller noise levels were lower than those of the shrouded propellers, and in the static conditions, the free-propeller noise levels were as low as those for the shrouded propellers, except for the propeller in-plane noise where the shrouded-propeller noise levels were lower.

INTRODUCTION

In recent years, increased emphasis has been placed on the development of propulsion systems which reduce the noise and engine-emissions pollution of civil airplanes without overly penalizing aerodynamic performance. One proposed method of accomplishing this objective for light, propeller-driven, general-aviation airplanes is the use of a small-diameter shrouded propeller with a direct-drive rotary engine. Such a propulsive system is expected to offer several advantages over the free-propeller system, including: (1) a more compact propulsion package, (2) acoustic shielding, (3) minimization of pollutants, and (4) less weight.

The present investigation was conducted to determine the aeroacoustic characteristics of a preliminary design of a proposed shrouded-propeller configuration which would be used in such a propulsion system. The tests were conducted in the Langley Full-Scale Tunnel with a twin-boom, general-aviation airplane powered by three different shrouded-pusher-propeller configurations and a free-pusher-propeller configuration. Aeroacoustic data were obtained for airspeeds ranging from 0 to 36 m/sec (118 ft/sec) for a range of propeller-blade angles and advance ratios.

SYMBOLS AND ABBREVIATIONS

Aerodynamic data presented herein are referred to the stability system of axes shown in figure 1. The moment reference center was located horizontally at 37.5 percent of the mean aerodynamic chord and vertically at water line 1.399 m (4.59 ft). Dimensional quantities are given in the International

System of Units (SI), with U.S. Customary Units given in parentheses. Definitions and conversion factors between the systems are presented in reference 1.

B number of propeller blades

BW bandwidth

C_D drag coefficient, Drag/qS

C_L lift coefficient, Lift/qS

C_m pitching-moment coefficient, $\dfrac{\text{Pitching moment}}{qS\bar{c}}$

C_p propeller power coefficient, $\dfrac{2\pi Q}{\rho n^2 D^5}$

C_T propeller thrust coefficient, $\dfrac{T}{\rho n^2 D^4}$

$C_T{}'$ airplane thrust coefficient, $\dfrac{T}{qS}$

$\bar{c}$ mean aerodynamic chord, 1.490 m (4.89 ft)

$\bar{c}_t$ mean aerodynamic chord of horizontal tail, 1.018 m (3.34 ft)

D propeller diameter, m (ft)

d local propeller chord, m (ft)

d_e propeller equivalent chord, $\dfrac{3}{R^3}\displaystyle\int_0^R dr^2\,dr$

FM propeller figure of merit; ratio of power required by an actuator disk producing same thrust to power required by propeller: $\dfrac{0.798 C_T^{3/2}}{C_p}$ for free propeller; $\dfrac{0.564 C_T^{3/2}}{C_p}$ for shrouded propeller

J propeller advance ratio, $\dfrac{V}{nD}$

M_t propeller tip Mach number

N_{Re} Reynolds number

2

n	propeller revolutions per second
P_b	brake power, watts (ft-lb/sec)
P_s	shaft power, watts (ft-lb/sec)
p	acoustic pressure, N/m^2 (lb/ft^2)
P_o	reference acoustic pressure, 0.2 μN/m^2 (4.19 $\times$ 10^{-7} lb/ft^2)
Q	propeller torque, N-m (lb-ft)
q	tunnel dynamic pressure, N/m^2 (lb/ft^2)
R	propeller radius, m (ft)
r	radius station of propeller, m (ft)
S	wing area, 16 258 m^2 (175.00 ft^2)
SPL	sound pressure level, $20 \log \dfrac{p}{p_o}$, dB
T	effective propeller thrust, Drag$_{\text{prop off}}$ - Drag$_{\text{prop operating}}$
t	propeller-blade thickness, cm (in.)
V	velocity, m/sec (ft/sec)
W	airplane weight, kg
WL	water line
wnmlg	windmilling
X,Y,Z	stability system of axes
α	angle of attack, deg (propeller shaft axis is used as zero reference)
β	propeller-blade angle at any radius station, deg
β_o	propeller-blade reference angle at 0.768R (free propeller) and 0.803R (shrouded propeller), deg
δ_f	flap-deflection angle, deg
η	propeller propulsive efficiency, $\left(\dfrac{C_T}{C_P}\right)\left(\dfrac{V}{nD}\right)$
θ	microphone acoustic angle, deg

3

ρ mass density of air, kg/m^3 (slugs/ft^3)

ϕ microphone azimuth angle, deg

2B   2-blade free propeller

3B   3-blade shrouded propeller, normal tip

3BT   3-blade shrouded propeller, unloaded tip

5BT   5-blade shrouded propeller, unloaded tip

AIRPLANE AND TEST SETUP

The airplane used in the tests was a modified version of a twin-engine, twin-boom, general-aviation airplane. A three-view sketch of the airplane is shown in figure 2; geometric characteristics of the free and shrouded propellers are shown in figure 3; and photographs of the airplane mounted for tests in Langley Full-Scale Tunnel are presented in figure 4.

The forward propeller and engine of the airplane were removed and the aft fuselage contours were modified so as to be compatible with a rotary combustion engine and a shrouded propeller. A direct-drive electric motor was used for the present tests to minimize engine noise and thereby permit measurements of the noise produced by the propulsor unit. The airplane was designed to accept either a free-propeller or a shrouded-propeller arrangement as shown in figure 3. In addition to a conventional 2-blade free propeller, the tests included two 3-blade shrouded propellers and a 5-blade shrouded propeller. Some of the important geometric characteristics of the propellers were:

Propeller	Diameter, m (ft)	Equivalent chord, m (ft)	Solidity
2-blade free	1.981 (6.50)	0.150 (0.50)	0.098
3-blade shrouded, normal tip	1.006 (3.30)	0.140 (0.46)	0.266
3-blade shrouded, unloaded tip	1.006 (3.30)	0.140 (0.46)	0.266
5-blade shrouded, unloaded tip	1.006 (3.30)	0.091 (0.30)	0.289

One of the 3-blade propellers and the 5-blade propeller were twisted abruptly near the tip (unloaded), whereas the other 3-blade propeller had a

4

more conventional (normal) twist distribution from root to tip. The reduced tip loading was designed by the manufacturer to alleviate acoustical problems without unduly affecting the aerodynamic performance. Blade-form curves for the test propellers are presented in figure 5. The shrouded propellers had NACA 16-series airfoil sections, and the free propeller had Clark Y sections. The direction of propeller rotation was clockwise when viewed from the rear for all of the test propellers.

The shrouded propellers originally had a diameter of 1.015 m (3.33 ft); however, during initial static tests, the propeller tips scraped the inner shroud surface as a result of flexibility in the shroud and shroud support systems. The diameter of the shrouded propellers was therefore decreased by 0.953 cm (0.375 in.) to insure adequate tip clearance for the remaining tests. Based upon data presented in reference 2, the tip clearance would be expected to reduce propulsive thrust by about 1.5 percent.

Pressure-type microphones with nose cones were used in the acoustic portion of the investigation. As shown in figure 4, 11 microphones were used, and the microphones were mounted on 1.52-m (4.99 ft) stands placed in a semicircular array around the right side of the airplane at a radius about the propeller axis of 5.791 m (19.00 ft), as depicted in figure 6. The propeller axis was about 3.322 m (10.90 ft) above the microphone array when the airplane was at $\alpha = 0°$. As shown in figure 6, the acoustic angle θ (the angle between the hub-microphone line and the propeller axis) and the azimuth angle ϕ were generally different for each microphone position. For the present tests, the airplane support struts were wrapped with 1.27-cm- (0.5 in.) thick wool-pile matting (fig. 4), and a special sound-absorbing ground board was used which consisted of a 10.16-cm- (4 in.) thick layer of fiberglass covered with 40-percent porosity, 0.158-cm- (0.0625 in.) thick perforated plate with 0.3175-cm- (0.125 in.) diameter holes (fig. 7).

CORRECTIONS

The aerodynamic data have been corrected for support strut tares, buoyancy, and airflow angularity. Wall corrections have been applied somewhat arbitrarily because of the unique installation of the airplane in the wind tunnel. Normally, tests similar to the present one are conducted with a nonporous ground board installed in the tunnel beneath the model and with wall corrections applied to the data as obtained by the theory of reference 3. Since the present tests were concerned with acoustic as well as aerodynamic performance, the ground board was covered with acoustic devices as explained in the previous section. Since this acoustic material did not provide a finite, hard boundary (such as the original ground board) nor was the tunnel jet completely open (all four walls unrestrained by solid boundaries), the approach to applying meaningful wall corrections to the subject data was subject to considerable question. There was no convenient way to determine the wall corrections experimentally, so calculations were made to estimate the lift characteristics of the basic unpowered airplane, and these calculated results were then compared with uncorrected wind-tunnel test data and flight test data for an original Cessna 327 airplane. The wind-tunnel test data were then corrected by methods of reference 3, using both the open-test-section approach and the approach with one

solid boundary. The wall correction method that resulted in the best correlation of wind-tunnel and flight data and of calculations was that for an open-test-section tunnel, so the wall corrections of the subject report were applied as determined for the open test section without a ground board.

TESTS AND METHODS

Aerodynamic Tests

The aerodynamic tests were conducted for a speed range from 0 to about 36 m/sec (118 ft/sec), with most of the tests conducted at about 29 m/sec (95 ft/sec). High tunnel speeds were found to be unnecessary from a Reynolds number standpoint, and structural loading of the airframe was minimized by the relatively low speed tests. The lower speed was also better for the acoustic measurements since the tunnel ambient noise level was considerably lower for the reduced speed.

In order to conduct the zero-speed tests (static tests), a cloth curtain was drawn across the wind-tunnel test-section entrance throat to prevent the propeller slipstream from circulating through the tunnel passages and thus back to the test propeller. The static tests were conducted for a range of propeller-blade angles and revolution speeds. The static-test variables for the various propeller arrangements investigated are given in table I.

With the wind tunnel operating, tests were conducted for a range of angles of attack from 0° to 16°. Propeller-blade angle and revolution speed were varied from a windmilling condition to the revolution speed for maximum allowable motor current, but not exceeding 2700 rpm for the free propeller and 5000 rpm for the ducted propellers. In general, maximum motor current resulted in a value of power very near the design value required for the actual airplane (i.e., 134 kW (180 hp) at 2700 rpm for the free propeller or 138 kW (185 hp) at 5000 rpm for the ducted propeller). Propeller drive power for the subject tests was determined by recording the minimum current required for drive motor operation and determining the torque used from a motor calibration curve of minimum current versus torque. Propeller thrust for the tests was determined by subtracting the drag measurement obtained while the propeller was operating from the drag of the configuration with the propeller and propeller shroud removed. The tunnel-operating propeller test conditions are listed in table II.

Acoustic Tests

Measurement system.- Figure 8 shows a system block diagram for a typical microphone channel. The principal system components were a pressure microphone with accessory nose cone, preamplifier, power supply, variable-gain amplifier, and FM tape recorder (operated at 76.2 cm/sec (30.00 in./sec)).

Prior to the wind-tunnel test, the systems were assembled and the critical parameters of frequency response, distortion, linearity, and electronic noise floors were documented. These procedures and test results are summarized in

6

table III. A typical system frequency-response curve, obtained by voltage insertion into the preamplifier, is shown in figure 9. The roll-off beginning at about 12 kHz is caused by the low-pass filter in the tape-recorder reproduce electronics. Daily piston-phone level calibrations were also made on site at a level of 124-dB SPL at 250 Hz.

Because the analyses in this report were based mainly on A-weighted sound pressure levels, no system corrections have been included. The microphone response was obtained from electrostatic laboratory calibrations, and the signal conditioning response was obtained from the voltage insertion sweeps discussed previously. The nose-cone response came from manufacturer's data. The effect of the wind tunnel on the recorded noise data was obtained from data in reference 4.

Eleven microphone systems were used in this test. The microphones were mounted about the vertical projection of the propeller hub on the tunnel acoustic ground board. The microphones were oriented so that the nose cone was parallel to the free stream. A plan view of the airplane and microphone array is shown in figure 6.

From the photographs of the test configuration presented in figure 4, it can be noted that the airplane propeller axis was above the microphone array plane for $\alpha = 0°$. Thus, the acoustic angle (the angle between the hub-microphone line and the propeller axis) of each microphone was not the same as the angular location of the microphone with respect to the hub projection on the microphone array plane. Included in figure 6 are both the array plan-view angle and the acoustic angle for each microphone position with the airplane at $\alpha = 0°$.

Data description.- The data points listed in table IV were chosen for acoustic analysis. These data were chosen to provide the widest possible variation of power, thrust, blade angle, and noise at $\alpha = 0°$ and zero sideslip. Seventy seconds of acoustic data were recorded for most of these data points. The tunnel-operating ambient noise levels were determined at test speeds of about 25 m/sec (82 ft/sec) and about 29 m/sec (95 ft/sec) with the airplane propeller removed.

Data acquired for the conditions listed in table IV were analyzed to provide A-weighted sound pressure levels and narrow-band spectra (BW = 50 Hz). The A-weighted sound pressure levels were used to provide noise directivity patterns and trend plots for each propeller configuration, whereas the narrow-band spectra were used to show the detailed acoustic differences between propellers and between static and tunnel-operating conditions.

RESULTS AND DISCUSSION

Aerodynamic Characteristics

Effect of Reynolds number.- The results of the Reynolds number tests with propellers removed for a flap deflection of 0° are shown in figure 10. There is a fairly large effect of Reynolds number on the maximum lift and associated

drag characteristics at test Reynolds numbers of 1.0×10^6 and 2.1×10^6, but for Reynolds numbers at and above 2.8×10^6, there is little effect of Reynolds number. Most of the tests were therefore conducted for a Reynolds number of 2.8×10^6.

Effect of free propeller.- The effects of the 2-blade free propeller on the aerodynamic characteristics of the airplane are shown in figure 11. Increasing propeller thrust is seen to provide a small increase in lift-curve slope; for tests in which maximum lift was achieved, the maximum lift was increased with increasing thrust as expected. In general, increasing thrust resulted in a small increment of diving moment and resulted in slightly increased longitudinal stability.

Effect of shrouded propellers.- The effects of shrouded propellers on airplane aerodynamic characteristics are given in figures 12 to 14. These data show the effects of thrust and blade angle for three different propellers. The data presented in figure 12 are for a 3-blade propeller with highly twisted (unloaded) tips. Figure 13 shows data for the same 3-blade arrangement but with a normal tip-twist distribution, and figure 14 presents data for the unloaded-tip, 5-blade propeller arrangement. In each case, propeller thrust and blade angle are seen to have very little effect on the longitudinal stability characteristics of the airplane.

Propeller Characteristics

The aerodynamic characteristics of the test propellers in forward flight are presented in figures 15 to 18, and the static-thrust characteristics of the four test configurations are shown in figures 19 to 22. All the propeller data are seen to vary fairly uniformly with increasing blade angle, revolution speed and velocity (V/nD), and angle of attack. It should be noted that the efficiency data presented represent propulsive efficiencies (differences in airplane drag with propellers removed or operating) rather than propeller efficiencies (shaft thrust). This actual shaft thrust may be masked somewhat if the basic drag characteristics change with propeller operation since thrust herein is defined as drag measured on the scale system with propellers off minus drag measured with propellers operating.

Propeller Performance

Since one of the main purposes of the subject investigation was to determine the relative merits of four different propulsive configurations, the thrust required was calculated for the airplane and plotted (along with the available thrust) as a function of flight speed in figure 23. The calculations were made for full- and partial-power conditions for each of the four test configurations. The thrust-required calculations were for a wing loading W/S of 957.6 N/m^2 (20 ft-lb) for standard sea-level conditions. The operating conditions assumed for the calculations were as follows:

8

<u>Maximum speed for free propeller</u> -

100-percent power = 134 kW (180 hp) at 2700 rpm, variable β

<u>Maximum speed for shrouded propeller</u> -

100-percent power = 138 kW (185 hp) at 5000 rpm, variable β

<u>Cruise speed for free and shrouded propeller</u> -

P_b = 75 percent of full power and 80 percent of full revolution speed, variable β

The results of the calculations, along with maximum static-thrust values for the four test propeller configurations, are shown in figure 23. It should be noted here that all of the propeller configurations have the same basic airframe and, therefore, the same "propulsive system off" drag. The shroud and propeller of the shrouded arrangement are considered to be the propulsive device that produces the net thrust for the propeller thrust coefficient.

It is readily apparent in figure 23 that the free propeller provides much more available thrust in flight than the other propulsors and that the 5-blade, shrouded-propeller arrangement was the poorest. Maximum speeds of the free propeller, 3-blade, normal-tip, 3-blade, unloaded-tip; and 5-blade, unloaded-tip, shrouded propellers were, respectively, 130 knots, 121 knots, 118 knots, and 109 knots. It is also seen that unloading the shrouded-propeller tip was detrimental to the thrust.

The airplane cruise performance varies in almost the same manner as maximum speed conditions vary with maximum cruise speeds for the free propeller, the 3-blade, normal-tip, the 3-blade, unloaded-tip, and the 5-blade, unloaded-tip, shrouded propellers of 115 knots, 101 knots, 98 knots, and 94 knots, respectively. Again, the free propeller was the best of the four arrangements tested. The data also indicate large penalties in rate of climb for the shrouded propellers.

An interesting point can be noted for the static-thrust points shown in figure 23(a). The free propeller provided 3527 N (793 lb) of thrust, whereas the 3-blade, normal-tip, shrouded propeller provided 3438 N (773 lb) of thrust. In other words, the smaller, 3-blade, normal-tip, shrouded propeller did produce values of static thrust about equal to those of the free propeller, but at forward-flight conditions, the drag of the shroud arrangement severely degraded performance. It should be noted that the propeller-blade angles investigated for the 3-blade, normal-tip, shrouded propeller were not large enough to absorb the available horsepower, so in order to obtain data comparable to the other configurations (i.e., full rpm and P_s), the data were extrapolated to larger values of β. The extrapolation showed that a blade angle of about 21° would be required, with a resulting FM of about 0.74. Another point is that unloading the propeller tip reduced the static thrust.

9

Of particular interest is the fact that the 5-blade configuration was very poor in both the static and flight regimes. The 5-blade chord is somewhat shorter than the 3-blade arrangement, but the total solidity was somewhat higher, which would be expected to produce similar results. Under static-test conditions, the electric-motor drive which powered the propeller used excessively high values of electrical power and the tests were terminated before the design rpm was reached. Because of this excess power usage, only two blade angles (12° and 16°) were investigated for the 5-blade shrouded propeller at static thrust. In order to obtain the static-thrust characteristics for comparison with the other configurations, the data were extrapolated to a comparable tip Mach number (0.771) and power coefficient ($C_p = 0.181$). For this condition, the blade angle was estimated to be 16°, with a figure of merit of only about 0.48. Thrust was calculated by the use of FM and C_p.

Of the four propeller configurations investigated, the free propeller provided the best propulsive characteristics, followed by the 3-blade, normal-tip, shrouded propeller, the 3-blade, unloaded-tip, shrouded propeller, and the 5-blade, unloaded-tip, shrouded propeller.

Acoustic Characteristics

The acoustic objectives of the subject tests were to measure the noise levels generated by the free- and shrouded-propeller configurations under simulated static and forward-flight conditions and to identify any systematic differences between the propeller configurations at the static and forward-speed conditions. The results pertaining to these objectives will be discussed herein.

Data are presented which show typical A-weighted SPL directivity patterns for two typical propeller configurations, a trend chart of A-weighted SPL versus power, and typical narrow-band acoustic spectra for the free and shrouded propellers. The data are presented for both static and forward-speed conditions.

A-weighted SPL directivity patterns.- The values of A-weighted SPL obtained at microphone positions 1 to 11 were plotted against acoustic incidence angle for all four propeller configurations at the maximum obtainable (although not necessarily equal) continuous power for each. Typical results for the free and shrouded propellers are plotted in figures 24 and 25, respectively. Figures 24(a) and 24(b) show directivity patterns for the free propeller under static and tunnel-operating conditions. It can also be seen that the levels for the tunnel-operating condition are about 5 dB lower than for the static condition. This characteristic will be discussed in further detail in the section entitled "Narrow-Band Acoustic Data."

Figures 25(a) and 25(b) show representative directivity patterns for a 5-blade, shrouded-propeller configuration. The other shrouded configurations are similar. Comparison of the two acoustic patterns of figure 25 shows no noise reduction going from static to tunnel-operating conditions. Comparison of the free- and shrouded-propeller static-noise levels (figs. 24(a) and 25(a)) indicates that the value of SPL between $\theta = 48^\circ$ and $\theta = 132^\circ$ are generally

10

lower, by as much as 10 dB, for the shrouded configuration. This result may be caused by shroud shielding. Comparison of figures 24(b) and 25(b) show that there is no difference in the in-plane noise under tunnel-operating conditions.

A-weighted SPL variation with power.- A comparison of the A-weighted sound pressure levels for various propeller configurations plotted against power for microphone position 2 is shown in figure 26. Data for both static and tunnel-operating conditions are shown. The free-propeller noise levels are generally lower than other configurations regardless of power or flight condition. This conclusion is typical of the results from the other microphone locations.

Narrow-band acoustic spectra.- Narrow-band spectra for microphone position 2 are plotted in figures 27 and 28 for several propeller configurations. Based on the experimental and theoretical results published in references 5 and 6, increased noise from shrouded propellers occurring at high tunnel speeds may be caused by inflow turbulence. Reference 5 indicates that a multiplicity of harmonically related tones is generated when a rotor encounters inflow turbulence. These tones, combined with traditional rotational noise harmonics, result in a discrete acoustic spectrum at higher sound pressure levels and at higher frequencies than for nonturbulent inflow. In reference 6, data are presented which indicate that propeller noise may be expected to decrease when going from static run-up to forward flight. The reason given for this effect is that, for a static run-up, atmospheric turbulent eddies are stretched by the contracting flow into the propeller disk. This causes a long-period turbulence disturbance and many acoustic blade-passage harmonics to be generated. In forward flight, these same eddies are not stretched to nearly the same extent as for static run-up; thus, the period of turbulence ingestion reduced, and lower noise levels are obtained. Unpublished turbulence data from the Langley Full-Scale Tunnel indicate that turbulence levels increase with tunnel velocity and approach 10 percent. Tunnel turbulence characteristics are not representative of those occurring in free air. The spectra for the free and shrouded propellers are compared directly for static and tunnel-operating conditions in figures 27 and 28, respectively. As shown in the tables on each figure, the spectra were obtained at maximum and as nearly equal power settings as possible. For every comparison, the free-propeller noise levels were generally as low as, or lower than, those for the shrouded propeller for most of the power and thrust range investigated.

CONCLUDING REMARKS

Aerodynamic and acoustic tests of four different pusher-propeller configurations on a twin-boom, general-aviation airplane configuration in the Langley Full-Scale Tunnel show the following results:

1. The free propeller had the best propulsive characteristics in both static and forward-flight conditions, followed next by the 3-blade, normal-tip, shrouded propeller, the 3-blade, unloaded-tip propeller, and finally the 5-blade, unloaded-tip propeller.

2. The free-propeller noise levels were generally as low as, or lower than, those for the shrouded propellers under tunnel flow conditions for most of the power and thrust range investigated.

3. Statically, the propeller in-plane noise levels of the shrouded propellers at high power conditions were less than for the free propeller. At other than the in-plane positions, the free- and shrouded-propeller noise levels were about equal.

Langley Research Center
National Aeronautics and Space Administration
Hampton, VA 23665
January 30, 1980

REFERENCES

1. Mechtly, E. A.: The International System of Units - Physical Constants and Conversion Factors (Second Revision). NASA SP-7012, 1973.

2. Black, Donald M.; Wainauski, Harry S.; Rohrbach, Carl: Shrouded Propellers - A Comprehensive Study. AIAA Paper No. 68-994, Oct. 1968.

3. Heyson, Harry H.: Use of Superposition in Digital Computers To Obtain Wind-Tunnel Interference Factors for Arbitrary Configurations, With Particular Reference to V/STOL Models. NASA TR R-302, 1969.

4. Abrahamson, A. L.; Kasper, P. K.; and Pappa, R. S.: Acoustical Characteristics of the NASA-Langley Full-Scale Wind Tunnel Test Section. NASA CR-132604, 1975.

5. Hanson, Donald B.: Study of Noise Sources in a Subsonic Fan Using Measured Blade Pressures and Acoustic Theory. NASA CR-2574, 1975.

6. Metzger, Frederick B.; and Magliozzi, Bernard: New Directions in Aircraft Propulsor Noise Research. [Preprint] 750515, Soc. Automot. Eng., Apr. 1975.

TABLE 1.- STATIC-TEST PARAMETERS

Propeller	Blade angle, deg	rpm range
2B, 1.981-m (6.50 ft) diameter	10, 12	500 to 2700
	14	500 to 2500
	16	500 to 2250
	18	500 to 2000
	20	500 to 1750
	22	500 to 1740
	24	500 to 1600
3BT, 1.006-m (3.30 ft) diameter	12, 16, 20	500 to 500
	24	500 to 4500
3B, 1.006-m (3.30 ft) diameter	12, 16, 20	1000 to 5000
5BT, 1.006-m (3.30 ft) diameter	12, 16	500 to 5000

TABLE II.- TUNNEL-OPERATING PARAMETERS

[Angle-of-attack range, 0° to 16°; flap deflections of 0°, 20°, 30°]

Propeller	Blade angle, deg	rpm range	Speed range, m/sec (ft/sec)
Removed	---	-------------	15 (49) to 36 (118)
2B, 1.981-m (6.50 ft) diameter	12	1000 to 2700	29 (95)
	16	800 to 2250	
	20	700 to 2000	
	24	500 to 1800	
	28	500 to 1500	
3BT, 1.006-m (3.30 ft) diameter	12	1400 to 5000	29 (95)
	16	1300 to 5000	
	20	1100 to 5000	
	24	1000 to 4500	
	28	900 to 3500	
	32	800 to 3500	
3B, 1.006-m (3.30 ft) diameter	12	1500 to 5000	29 (95)
	16	1300 to 5000	
	20	1100 to 5000	
	24	1000 to 4500	
	28	900 to 3500	
	32	800 to 3500	
	36	700 to 3000	
5BT, 1.006-m (3.30 ft) diameter	12	1400 to 5000	29 (95)
	16	1300 to 5000	
	24	1100 to 4000	
	32	800 to 3500	
	36	700 to 3000	

TABLE III.- SUMMARY OF SYSTEM LEVEL TESTS

Test	Procedure	Test results
Frequency response	Apply oscillator signal at preamplifier input. Record system frequency response through tape-recorder output.	+2 dB⎱ Through −1 dB⎰ 10 Hz
Distortion	Apply signal at microphone using acoustic calibrator. Check system distortion through tape-recorder output.	<2 percent
Linearity	Apply oscillator signal at preamplifier input. Check system linearity at tape-recorder output over expected range settings of variable-gain amplifier.	±1.0 percent of full-scale tape-recorder deviation
Noise floor (ref. 0.2 $\mu N/m^2$)	Short circuit preamplifier input and monitor system noise level at tape-recorder output.	40 to 61 dB

15

TABLE IV.- DATA POINTS CHOSEN FOR ACOUSTIC ANALYSIS

(a) Static conditions

Tunnel condition	Runs	Propeller	Velocity, m/sec	α, deg	β, deg	δ_f, deg	rpm	Sideslip, deg	Power, kW	Thrust, N
Static	20(05)	2B	0	0	10	0	1500	0	13	979
Static	20(07)	2B	0	0	10	0	2000	0	34	1802
Static	20(08)	2B	0	0	10	0	2250	0	51	2335
Static	20(09)	2B	0	0	10	0	2500	0	75	2985
Static	20(10)	2B	0	0	10	0	2700	0	98	3403
Static	21(02)	2B	0	0	12	0	1500	0	17	1085
Static	21(03)	2B	0	0	12	0	2000	0	43	2033
Static	21(04)	2B	0	0	12	0	2250	0	65	2656
Static	21(05)	2B	0	0	12	0	2500	0	96	3360
Static	21(06)	2B	0	0	12	0	2700	0	128	4014
Static	22(02)	2B	0	0	14	0	1500	0	21	1263
Static	22(03)	2B	0	0	14	0	2000	0	57	2349
Static	22(04)	2B	0	0	14	0	2250	0	83	2949
Static	22(05)	2B	0	0	14	0	2500	0	127	3839
Static	23(02)	2B	0	0	16	0	1500	0	28	1379
Static	23(03)	2B	0	0	16	0	2000	0	75	415
Static	23(04)	2B	0	0	16	0	2250	0	110	3132
Static	24(02)	2B	0	0	18	0	1500	0	37	1450
Static	24(03)	2B	0	0	18	0	2000	0	98	2624
Static	25(03)	2B	0	0	20	0	1750	0	78	2055
Static	26(04)	2B	0	0	22	0	1740	0	96	2082
Static	116(02)	3B	0	0	12	0	3000	0	10	609
Static	116(03)	3B	0	0	12	0	4000	0	26	1099
Static	116(04)	3B	0	0	12	0	4500	0	37	1392
Static	116(05)	3B	0	0	12	0	5000	0	53	1717
Static	125(03)	3B	0	0	16	0	3000	0	16	845
Static	125(05)	3B	0	0	16	0	4000	0	40	1535
Static	125(06)	3B	0	0	16	0	4500	0	57	1944
Static	125(07)	3B	0	0	16	0	5000	0	79	2438

16

TABLE IV.- Continued

(a) Concluded

Tunnel condition	Runs	Propeller	Velocity, m/sec	α, deg	β, deg	δ_f, deg	rpm	Sideslip, deg	Power, kW	Thrust, N
Static	126(03)	3B	0	0	20	0	3000	0	24	1121
Static	126(04)	3B	0	0	20	0	4000	0	59	1997
Static	126(05)	3B	0	0	20	0	5000	0	125	3207
Static	95(02)	3BT	0	0	12	0	3000	0	10	569
Static	95(03)	3BT	0	0	12	0	3500	0	17	796
Static	95(04)	3BT	0	0	12	0	4000	0	27	1068
Static	95(05)	3BT	0	0	12	0	4500	0	40	1317
Static	95(06)	3BT	0	0	12	0	5000	0	56	1624
Static	96(03)	3BT	0	0	16	0	3000	0	16	805
Static	96(04)	3BT	0	0	16	0	3500	0	25	1081
Static	96(05)	3BT	0	0	16	0	4000	0	39	1415
Static	96(06)	3BT	0	0	16	0	4500	0	57	1828
Static	96(07)	3BT	0	0	16	0	5000	0	79	2260
Static	104(02)	3BT	0	0	20	0	3000	0	22	1010
Static	104(03)	3BT	0	0	20	0	4000	0	56	1793
Static	104(04)	3BT	0	0	20	0	4500	0	83	2313
Static	104(05)	3BT	0	0	20	0	5000	0	116	2918
Static	105(04)	3BT	0	0	24	0	3000	0	77	2273
Static	105(05)	3BT	0	0	24	0	4500	0	112	2927
Static	64(05)	5BT	0	0	12	0	3000	0	11	592
Static	64(06)	5BT	0	0	12	0	3500	0	19	810
Static	64(07)	5BT	0	0	12	0	4000	0	29	1059
Static	64(08)	5BT	0	0	12	0	4500	0	43	1317
Static	64(09)	5BT	0	0	12	0	5000	0	62	1673
Static	70(05)	5BT	0	0	16	0	3000	0	21	836
Static	70(06)	5BT	0	0	16	0	3500	0	33	1090
Static	70(07)	5BT	0	0	16	0	4000	0	59	1503

TABLE IV.- Continued

(b) Tunnel-operating conditions

Tunnel condition	Runs	Propeller	Velocity, m/sec	α, deg	β, deg	δ_f, deg	rpm	Sideslip, deg	Power, kW	Thrust, N	V/nD
Flow	2(01)	None	25	0	--	0	----	0	0	0	-----
Flow	3(01)	None	29	0	--	0	----	0	0	0	-----
Flow	49(01)	2B	29	0	12	0	1500	0	42	258	0.565
Flow	50(01)	2B	29	0	12	0	2000	0	32	881	.433
Flow	51(01)	2B	29	0	12	0	2500	0	76	1837	.346
Flow	52(01)	2B	29	0	12	0	2700	0	105	2371	.324
Flow	53(01)	2B	27	0	12	0	2700	0	107	2486	.300
Flow	54(01)	2B	25	0	12	0	2700	0	112	2678	.270
Flow	46(01)	2B	29	0	16	0	1500	0	19	565	.570
Flow	47(01)	2B	29	0	16	0	2000	0	47	1575	.442
Flow	48(01)	2B	29	0	16	0	2250	0	92	2126	.390
Flow	30(01)	2B	29	0	24	0	1500	0	48	1214	.575
Flow	31(01)	2B	29	0	24	0	2000	0	128	2393	.483
Flow	37(01)	2B	29	0	20	0	1000	0	73	1392	.581
Flow	118(01)	3B	29	0	12	0	3000	0	6	147	.550
Flow	119(01)	3B	29	0	12	0	4000	0	22	436	.415
Flow	120(01)	3B	29	0	12	0	5000	0	48	867	.238
Flow	122(01)	3B	29	0	16	0	3000	0	12	294	.559
Flow	123(01)	3B	29	0	16	0	4000	0	35	721	.415
Flow	124(01)	3B	29	0	16	0	5000	0	76	1357	.340
Flow	128(01)	3B	29	0	20	0	3000	0	11	463	.558
Flow	129(01)	3B	29	0	20	0	4000	0	53	1050	.420
Flow	130(01)	3B	29	0	20	0	5000	0	114	1877	.341
Flow	132(01)	3B	29	0	24	0	3000	0	29	649	.560
Flow	133(01)	3B	29	0	24	0	4000	0	78	1414	.425
Flow	134(01)	3B	29	0	24	0	4500	0	117	1939	.379

TABLE IV.- Concluded

(b) Concluded

Tunnel condition	Runs	Propeller	Velocity, m/sec	α, deg	β, deg	δ_f, deg	rpm	Sideslip, deg	Power, kW	Thrust, N	V/nD
Flow	91(01)	3BT	29	0	12	0	3000	0	7	147	0.555
Flow	92(01)	3BT	29	0	12	0	4000	0	22	436	.422
Flow	93(01)	3BT	29	0	12	0	4500	0	34	618	.375
Flow	94(01)	3BT	29	0	12	0	5000	0	50	841	.335
Flow	97(01)	3BT	29	0	16	0	2000	0	12	276	.558
Flow	98(01)	3BT	29	0	16	0	4000	0	34	694	.420
Flow	99(01)	3BT	29	0	16	0	5000	0	76	1272	.335
Flow	100(01)	3BT	29	0	20	0	3000	0	18	423	.558
Flow	101(01)	3BT	29	0	20	0	4000	0	51	952	.420
Flow	102(01)	3BT	29	0	20	0	4500	0	75	1317	.378
Flow	103(01)	3BT	29	0	20	0	5000	0	111	1761	.340
Flow	107(01)	3BT	29	0	24	0	3000	0	28	600	.558
Flow	108(01)	3BT	29	0	24	0	4000	0	75	1303	.420
Flow	109(01)	3BT	29	0	24	0	4500	0	111	1757	.374
Flow	111(01)	3BT	29	0	28	0	3000	0	38	769	.560
Flow	112(01)	3BT	29	0	28	0	4000	0	100	1646	.429
Flow	66(01)	5BT	29	0	12	0	3000	0	8	165	.556
Flow	67(01)	5BT	29	0	12	0	4000	0	25	463	.420
Flow	68(01)	5BT	29	0	12	0	4500	0	40	658	.376
Flow	69(01)	5BT	29	0	12	0	5000	0	57	859	.340
Flow	72(01)	5BT	29	0	16	0	3000	0	14	280	.552
Flow	73(01)	5BT	29	0	16	0	3500	0	24	485	.481
Flow	74(01)	5BT	29	0	16	0	4000	0	40	694	.421
Flow	75(01)	5BT	29	0	16	0	4500	0	58	988	.380
Flow	77(01)	5BT	29	0	16	0	5000	0	84	1348	.345
Flow	82(01)	5BT	29	0	24	0	3000	0	33	632	.560
Flow	83(01)	5BT	29	0	24	0	4000	0	84	1415	.426
Flow	86(01)	5BT	29	0	32	0	3500	0	104	1704	.494
Flow	89(01)	5BT	29	0	36	0	3000	0	92	1383	.568
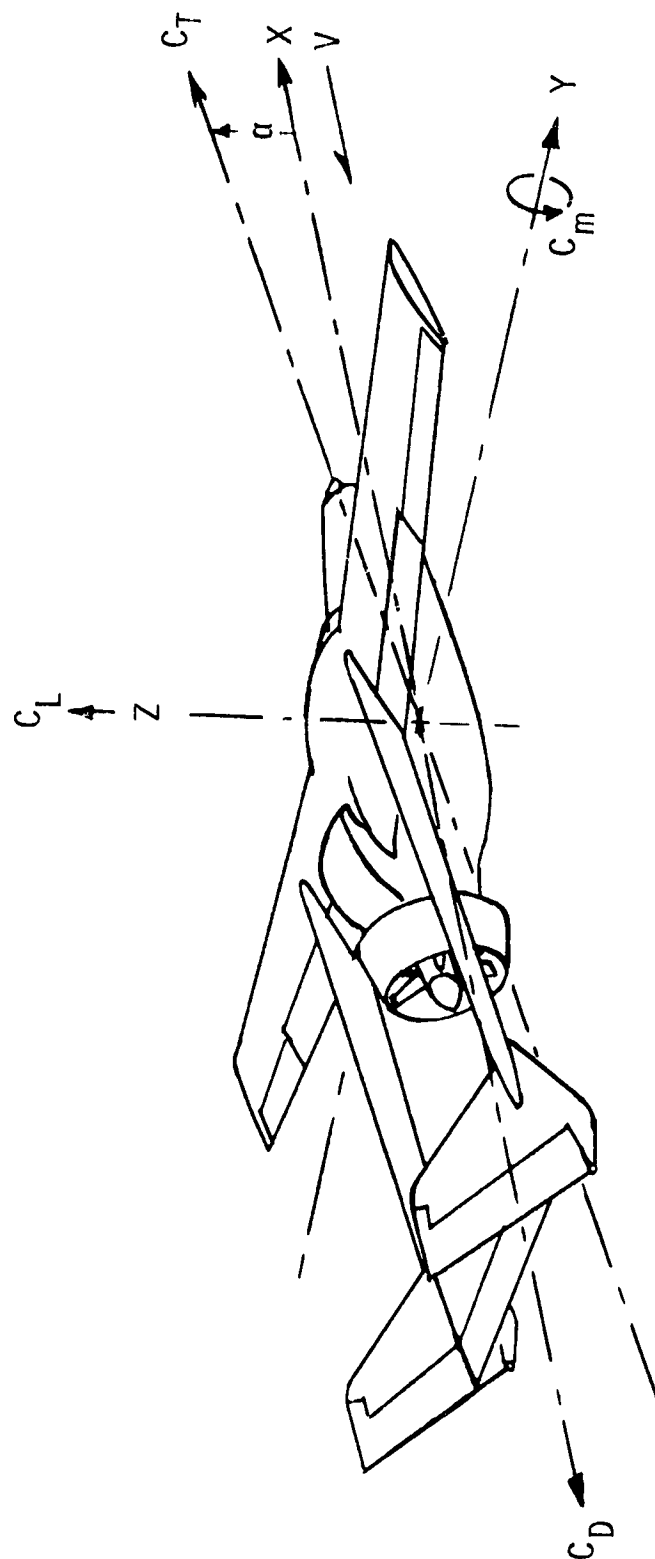
Figure 1.- System of stability axes and positive sense of angles, forces, and moments.
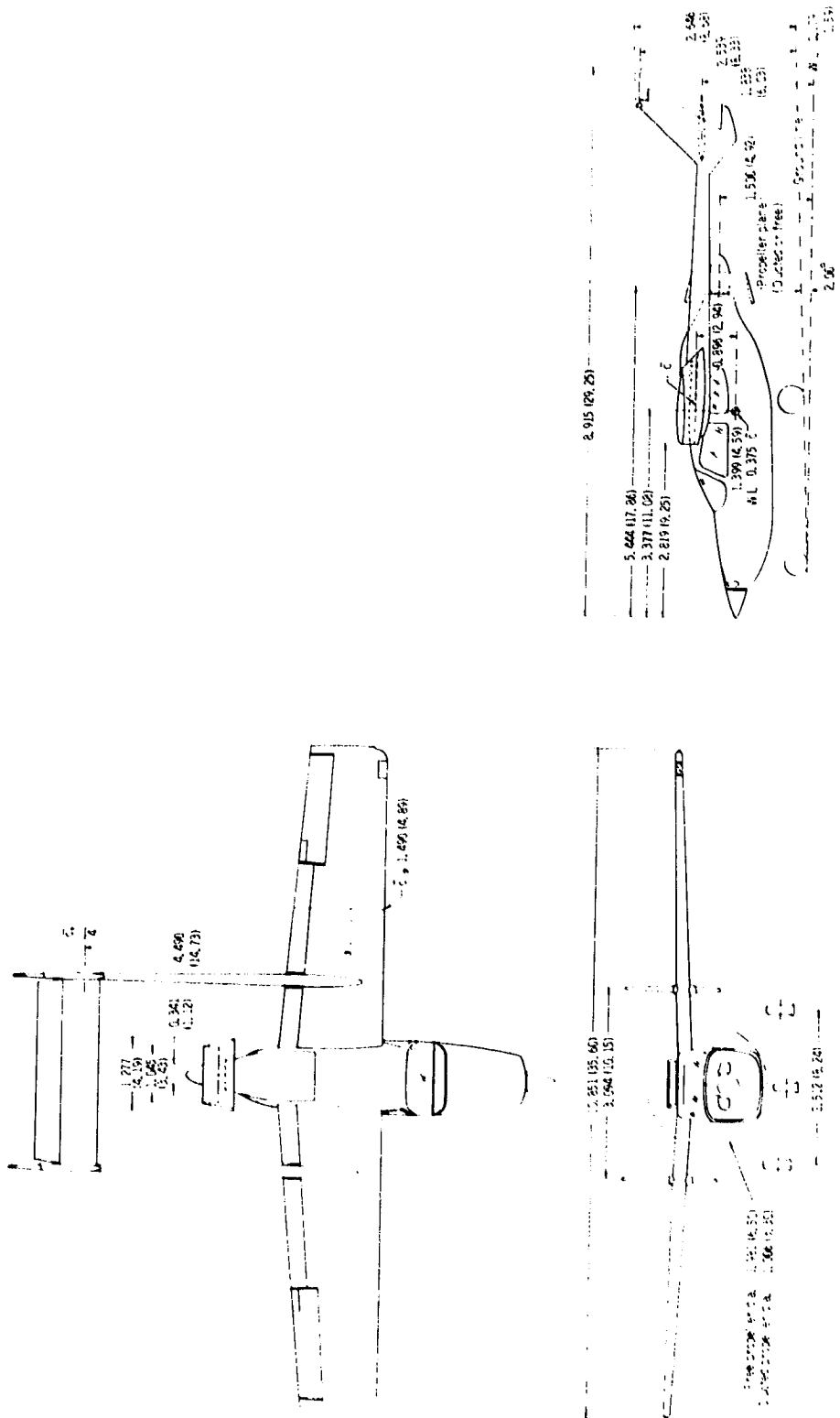
Figure 2.— Geometric characteristics of test airplane. All dimensions in meters (feet). Measurements made in conventional units.
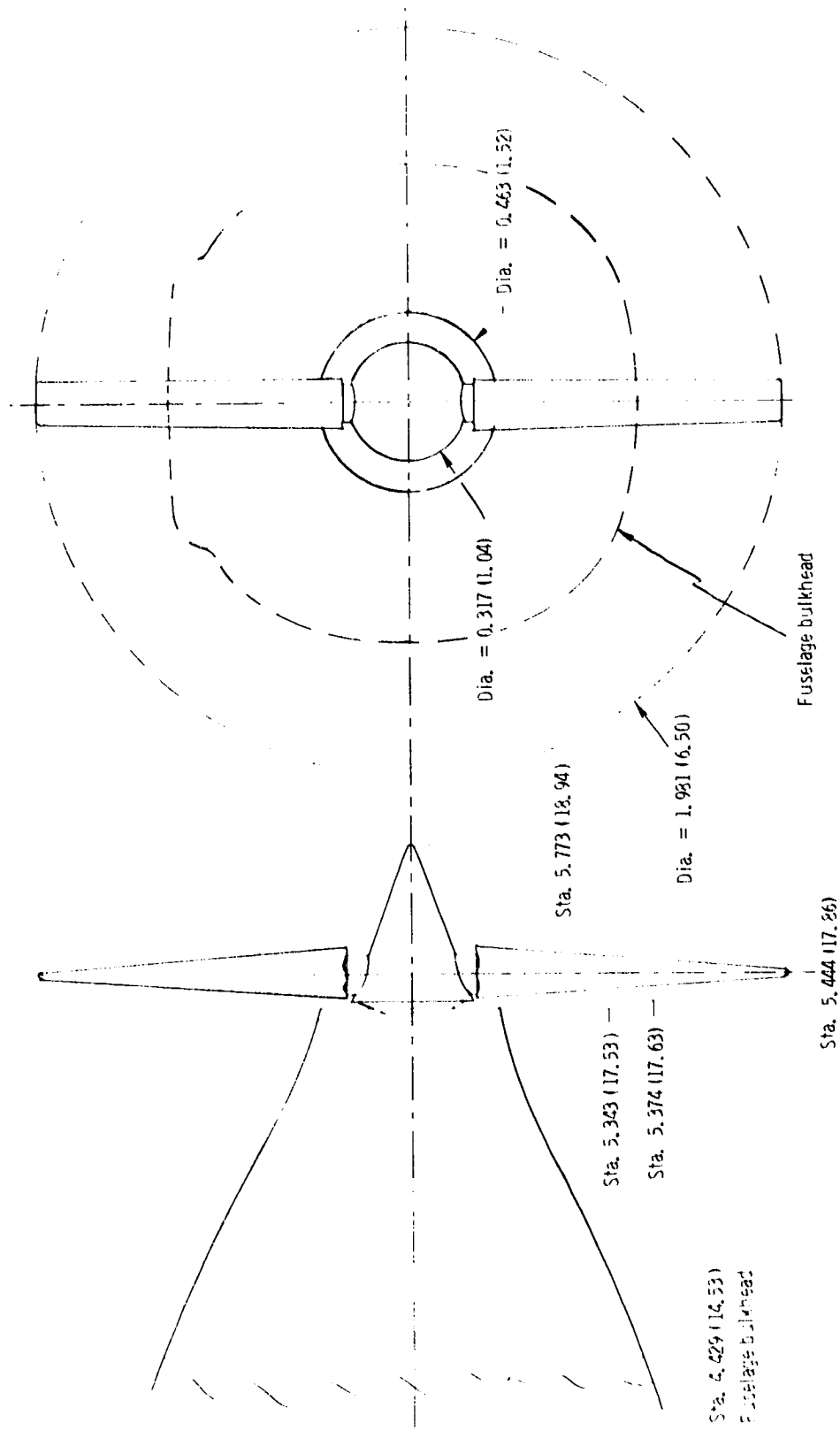
Figure 3.- Geometric arrangement of test propellers. All dimensions in meters (feet). Measurements made in conventional units.

(a) 2-blade free propeller.

22

Dia. = 0.463 (1.52)

Dia. = 0.341 (1.12)

Dia. = 1.015 (3.33)

Dia. = 1.277 (4.19)

Fuselage bulkhead

Sta. 5.977 (19.61)
Propeller dia. = 1.006 (3.30)

Sta. 5.444 (17.86)
Propeller plane

Sta. 5.700 (18.70)

Sta. 5.252 (17.23)

Sta. 5.343 (17.53)

Sta. 5.188 (17.02)

Sta. 4.429 (14.53)
Fuselage bulkhead
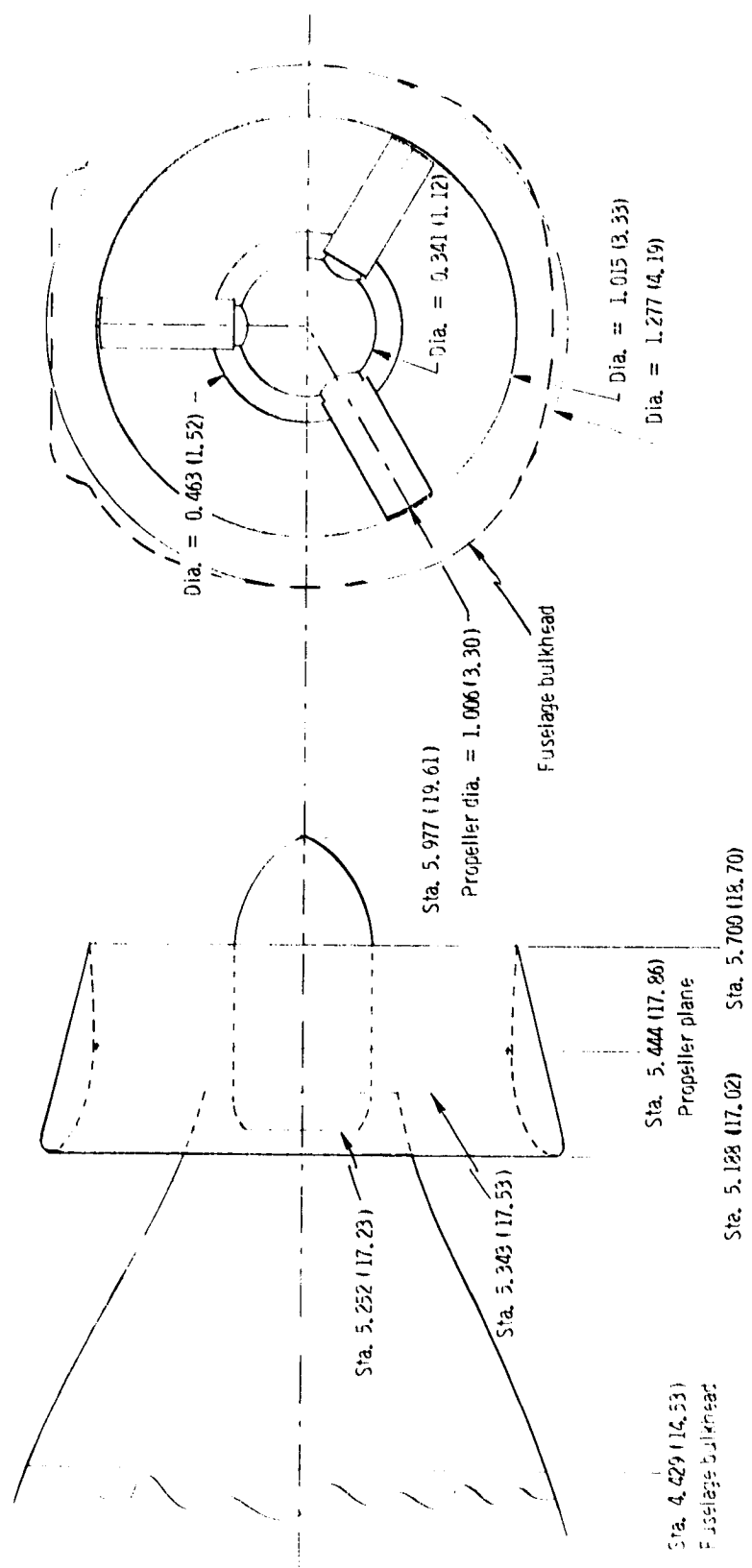
(b) Shrouded 3-blade propeller arrangement.

Figure 3.- Continued.

23

Dia. = 1.015 (3.33)

Dia. = 1.277 (4.19)

Dia. = 0.463 (1.52)

Dia. = 0.341 (1.12)

Propeller dia. 1.006 (3.30)

Fuselage bulkhead

Sta. 5.977 (19.61)

Sta. 5.444 (17.86) Propeller plane

Sta. 5.700 (18.70)

Sta. 5.252 (17.23)

Sta. 5.188 (17.02)

Sta. 5.343 (17.53)

Sta. 4.429 (14.53) Fuselage bulkhead
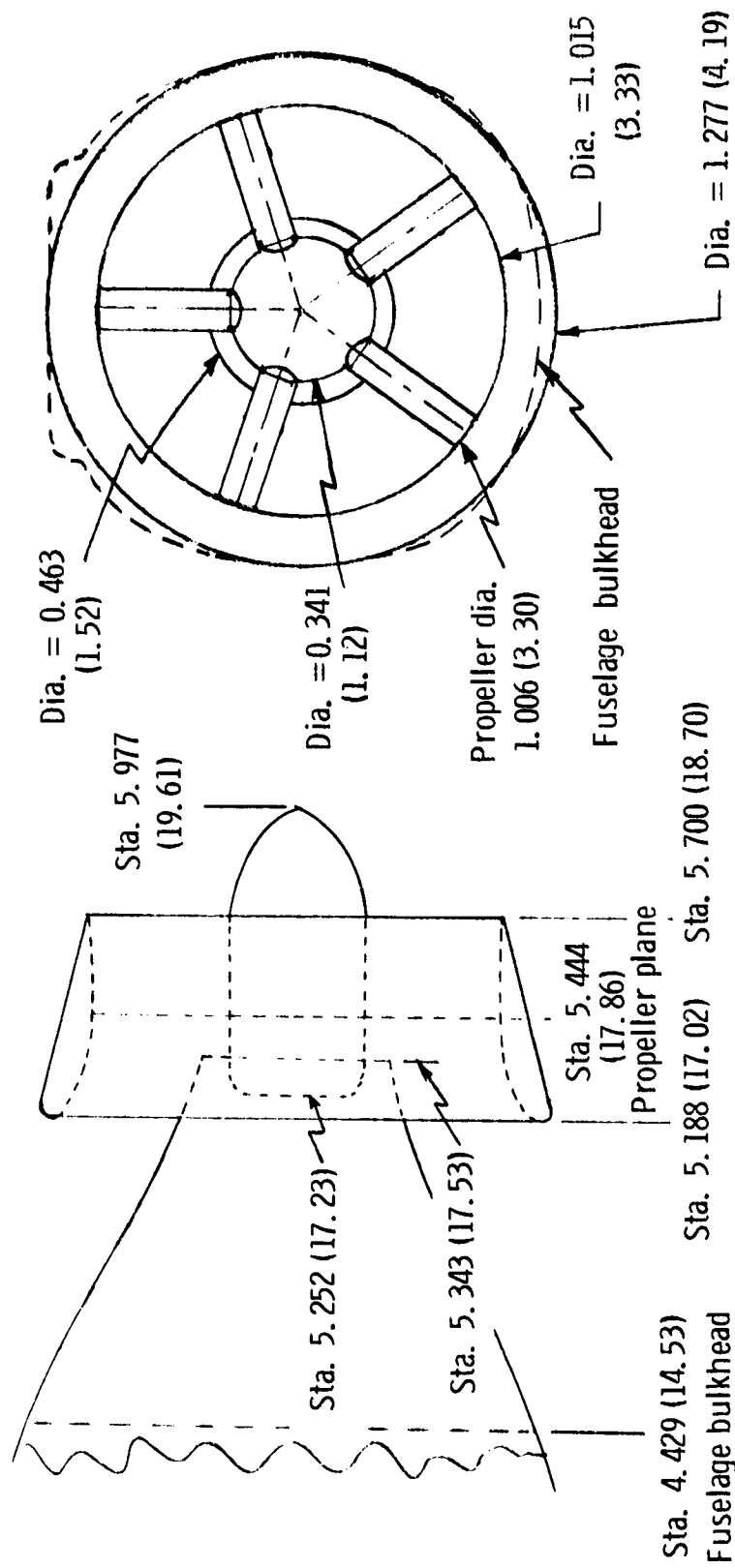
(c) Shrouded 5-blade propeller arrangement.

Figure 3.- Concluded.
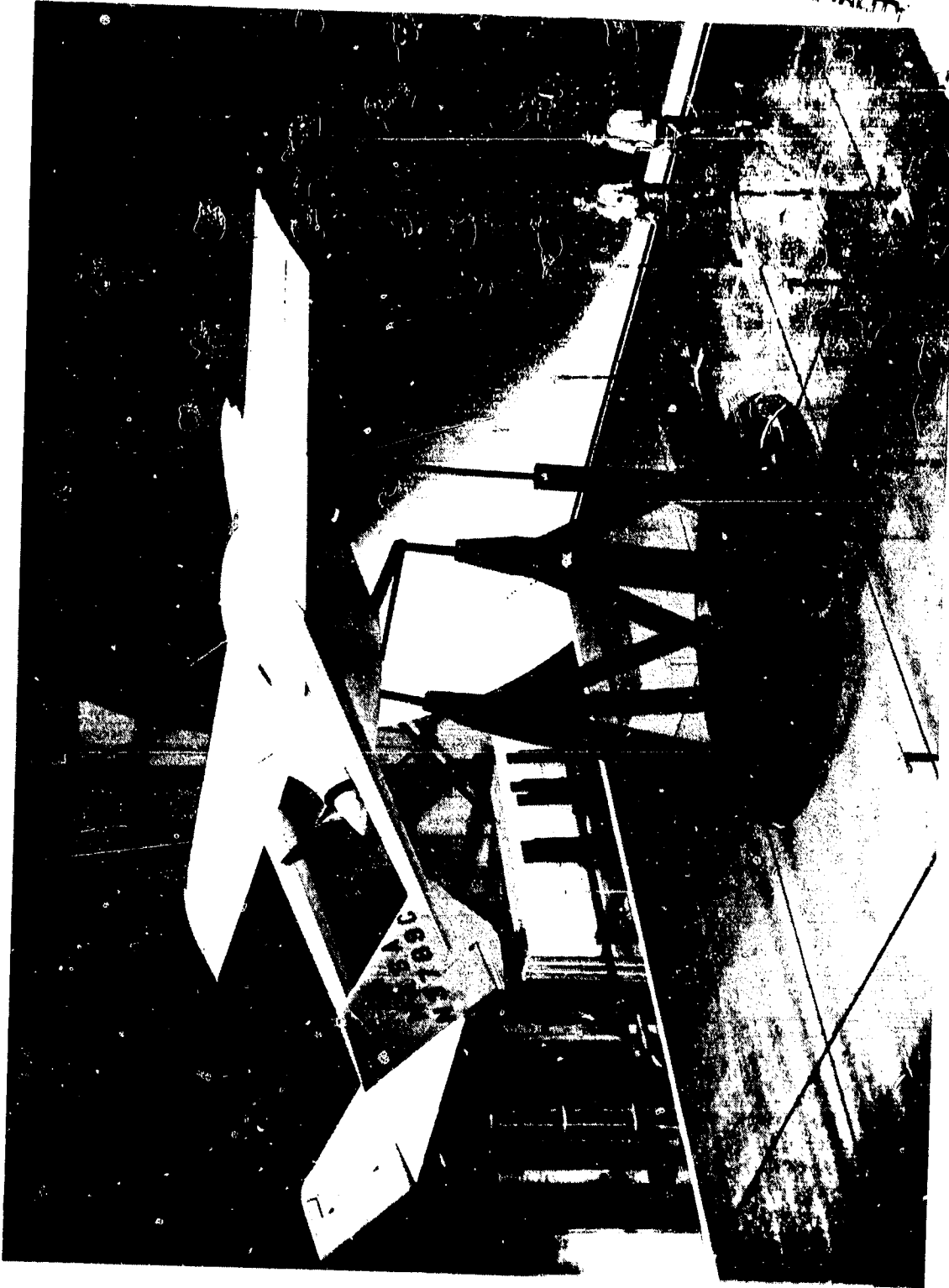
L-74-4534

(a) Three-quarter rear view with free propeller installed.

Figure 4.- Airplane mounted for tests in Langley Full-Scale Tunnel. Microphone array on ground board.
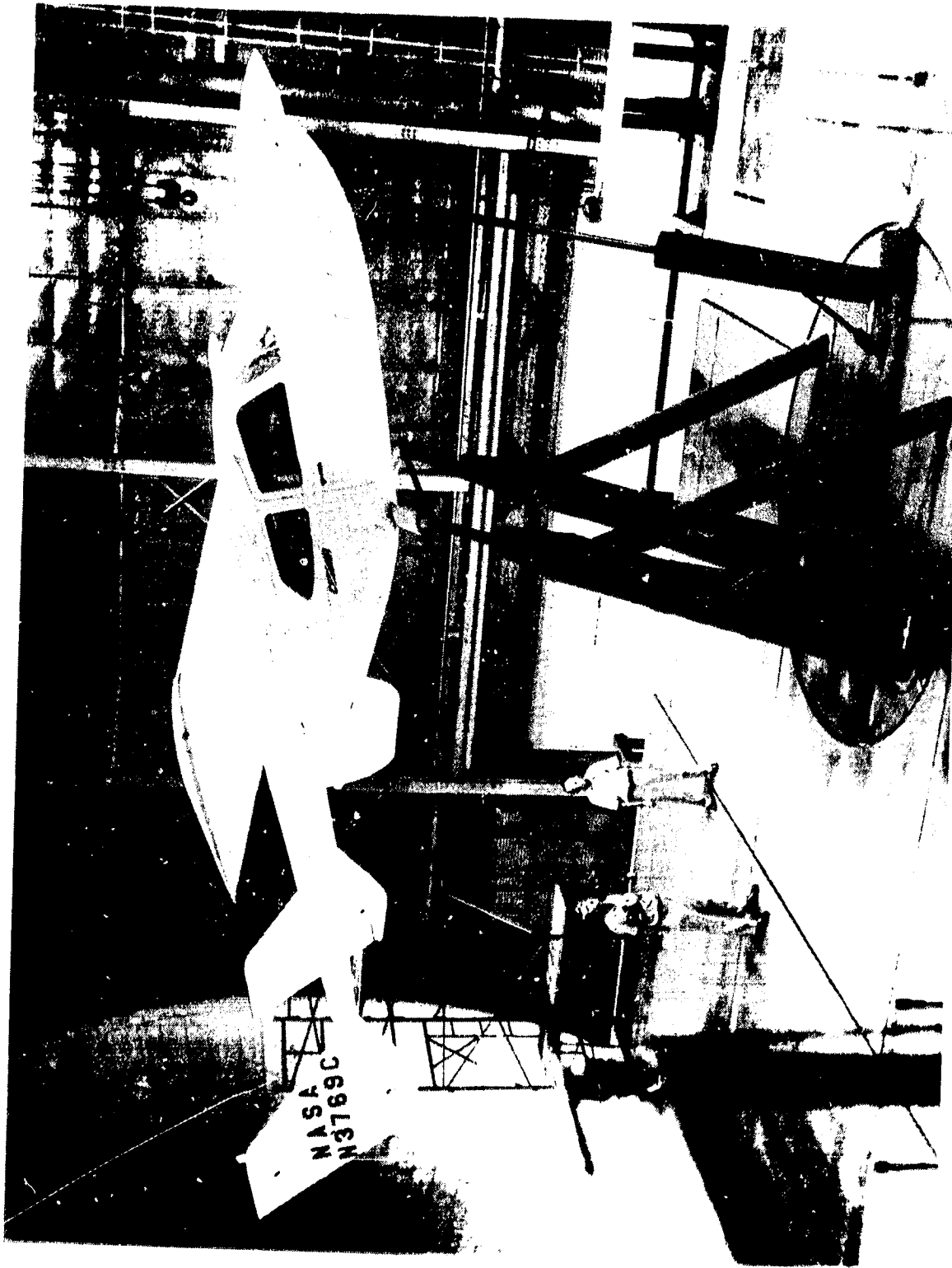
(b) Side view with shrouded propeller installed.

Figure 4.- Continued.

L-74-4683

26
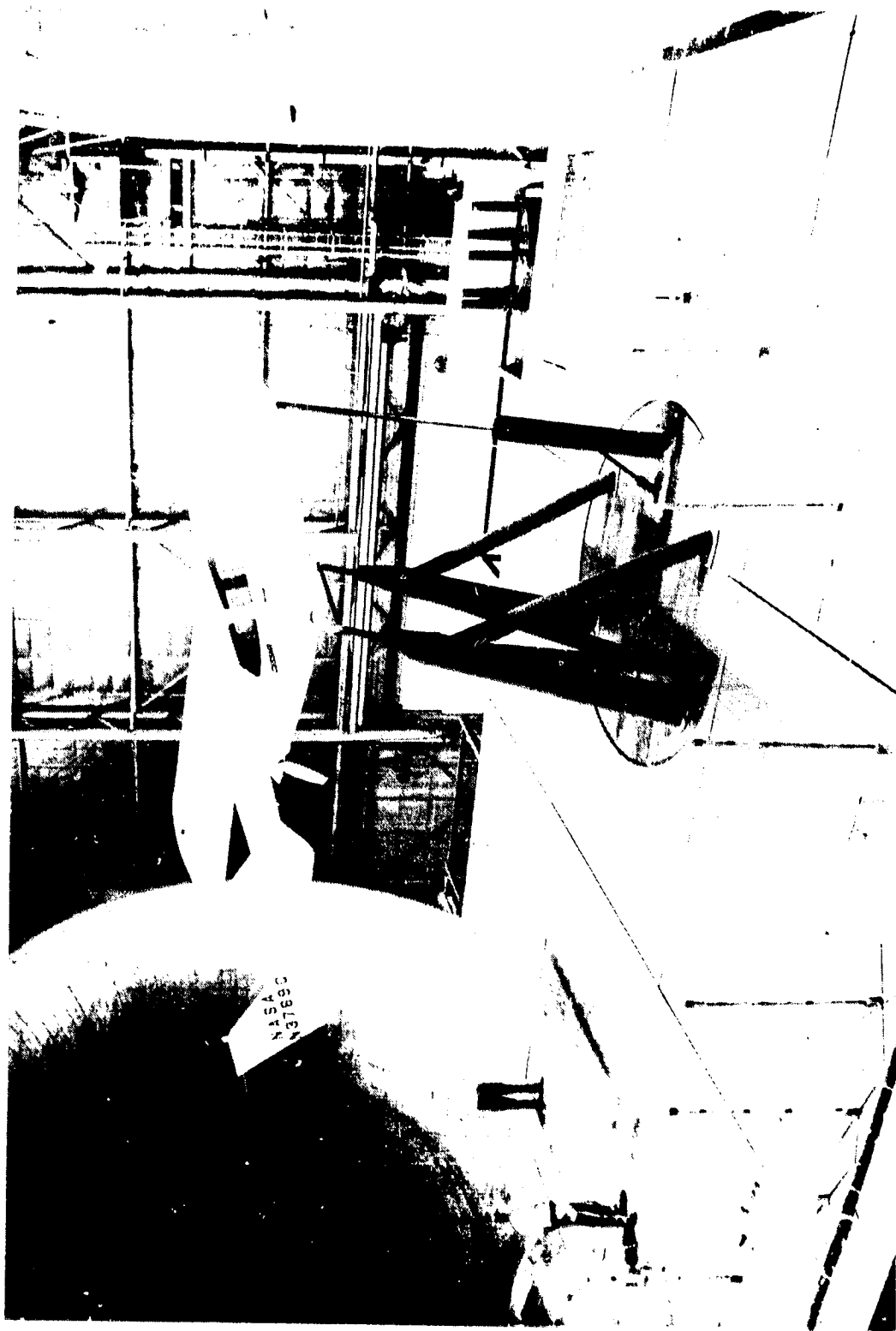
(c) Test airplane and microphone array.

Figure 4.- Concluded.

L-74-4507
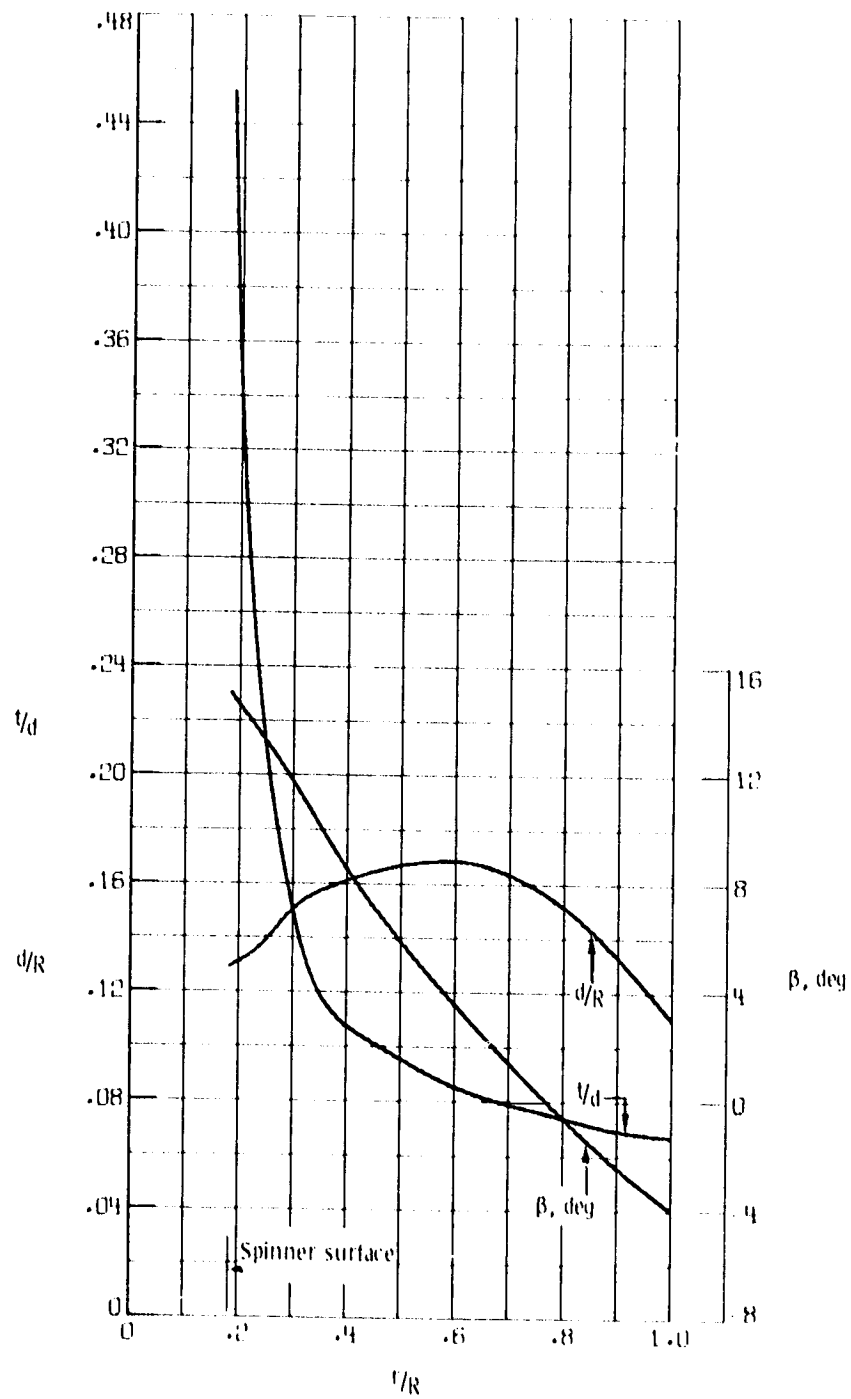
(a) Free propeller.

Figure 5.- Blade-form curves for test propellers
(NACA 16-series airfoil sections).
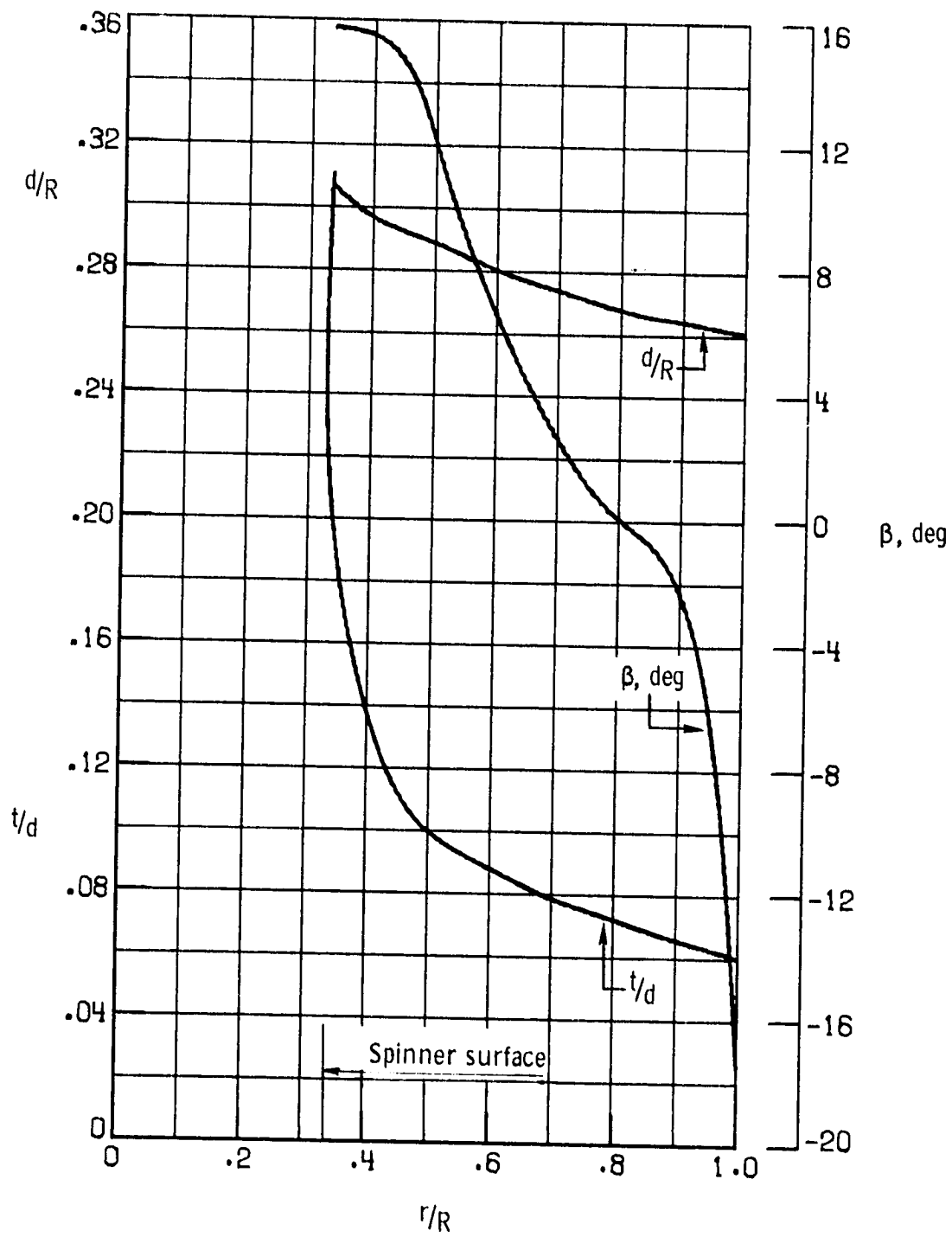
(b)   3-blade, twisted-tip propeller.

Figure 5.- Continued.
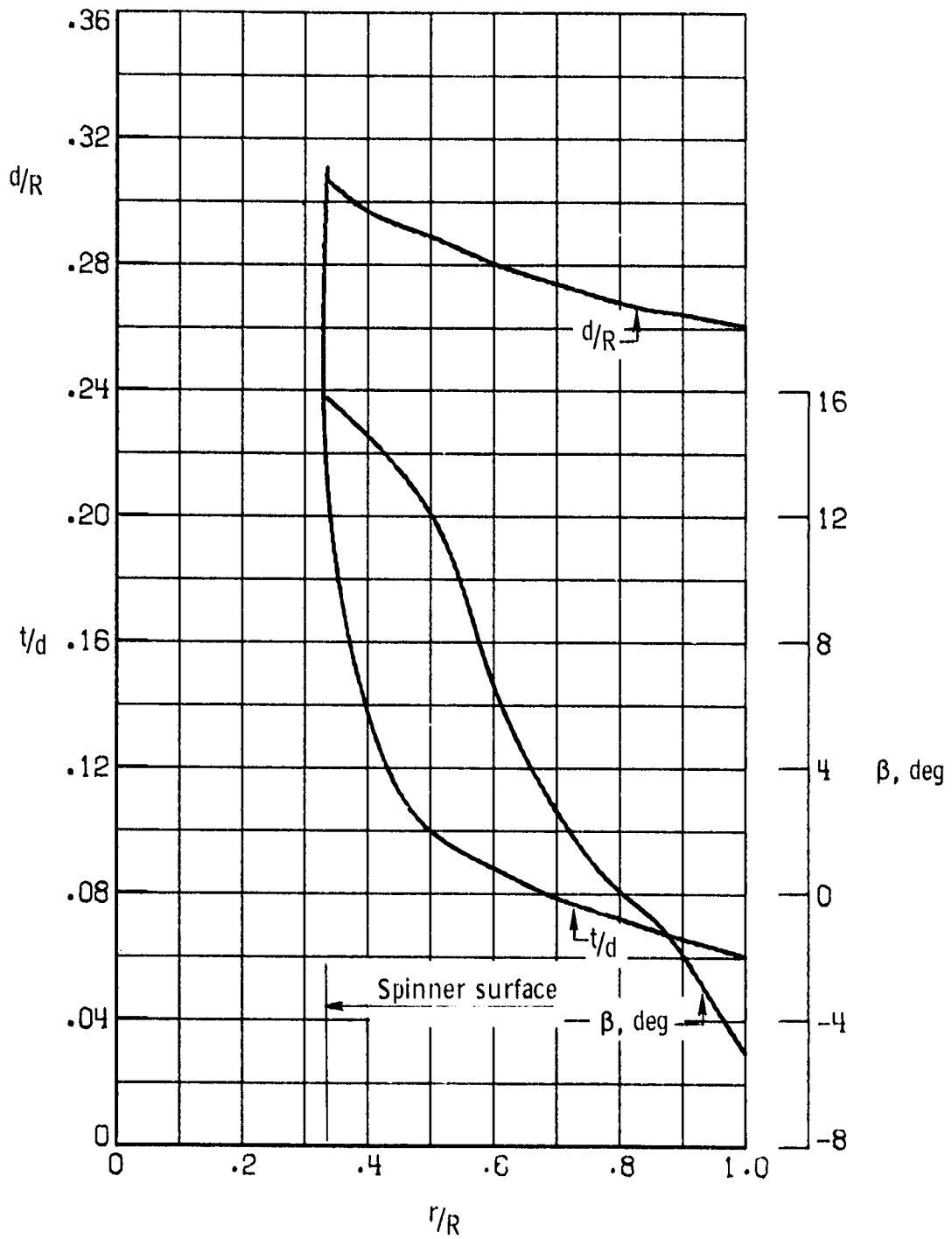
(c) 3-blade, normal-tip propeller.

Figure 5.- Continued.
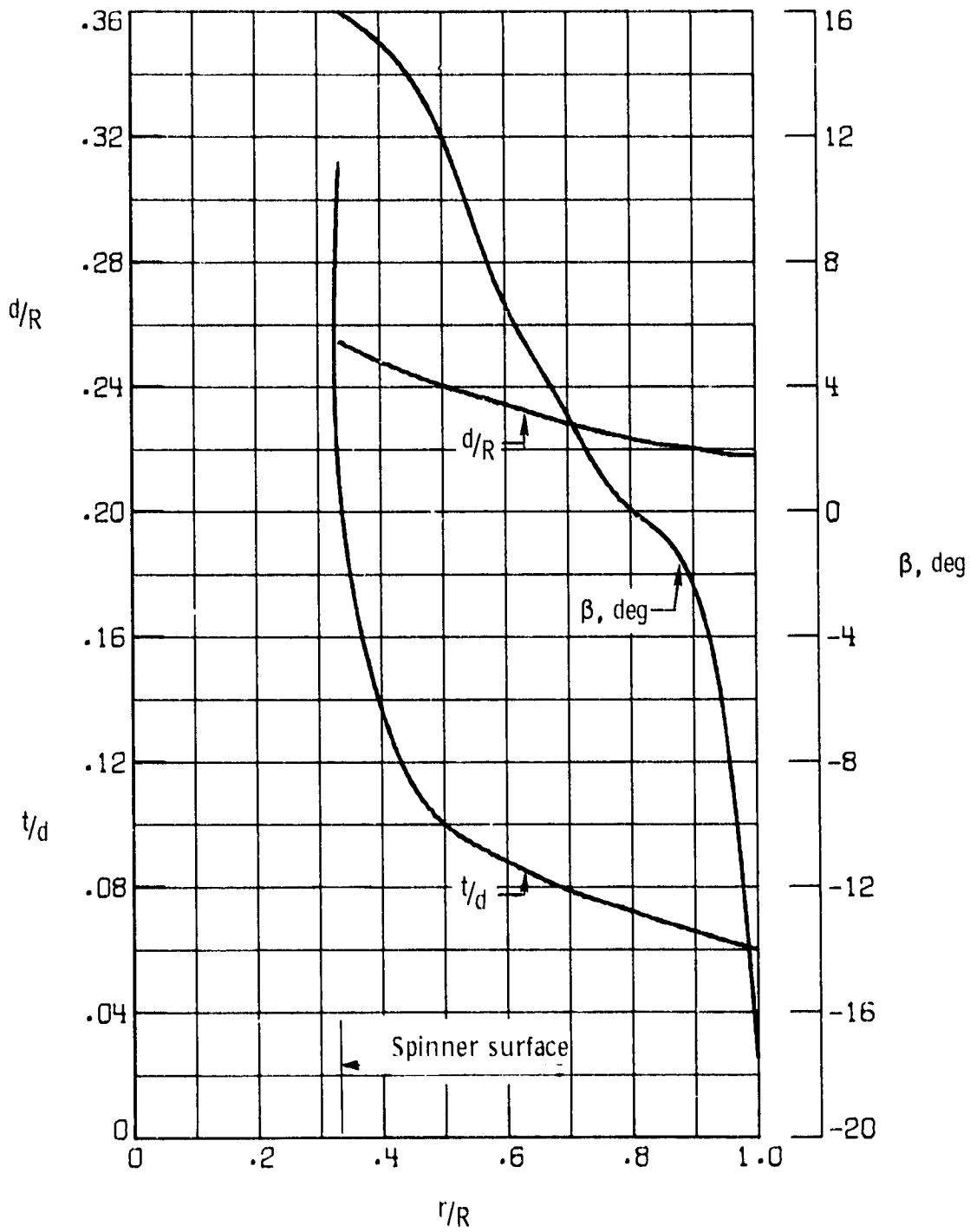
(d)   5-blade propeller.

Figure 5.- Concluded.

MICROPHONE	ζ, deg	ξ, deg	MICROPHONE	ζ, deg	ξ, deg
1	0	30	7	100	99
2	20	35	8	120	116
3	40	43	9	140	132
4	60	64	10	160	145
5	80	81	11	180	150
6	90	90			
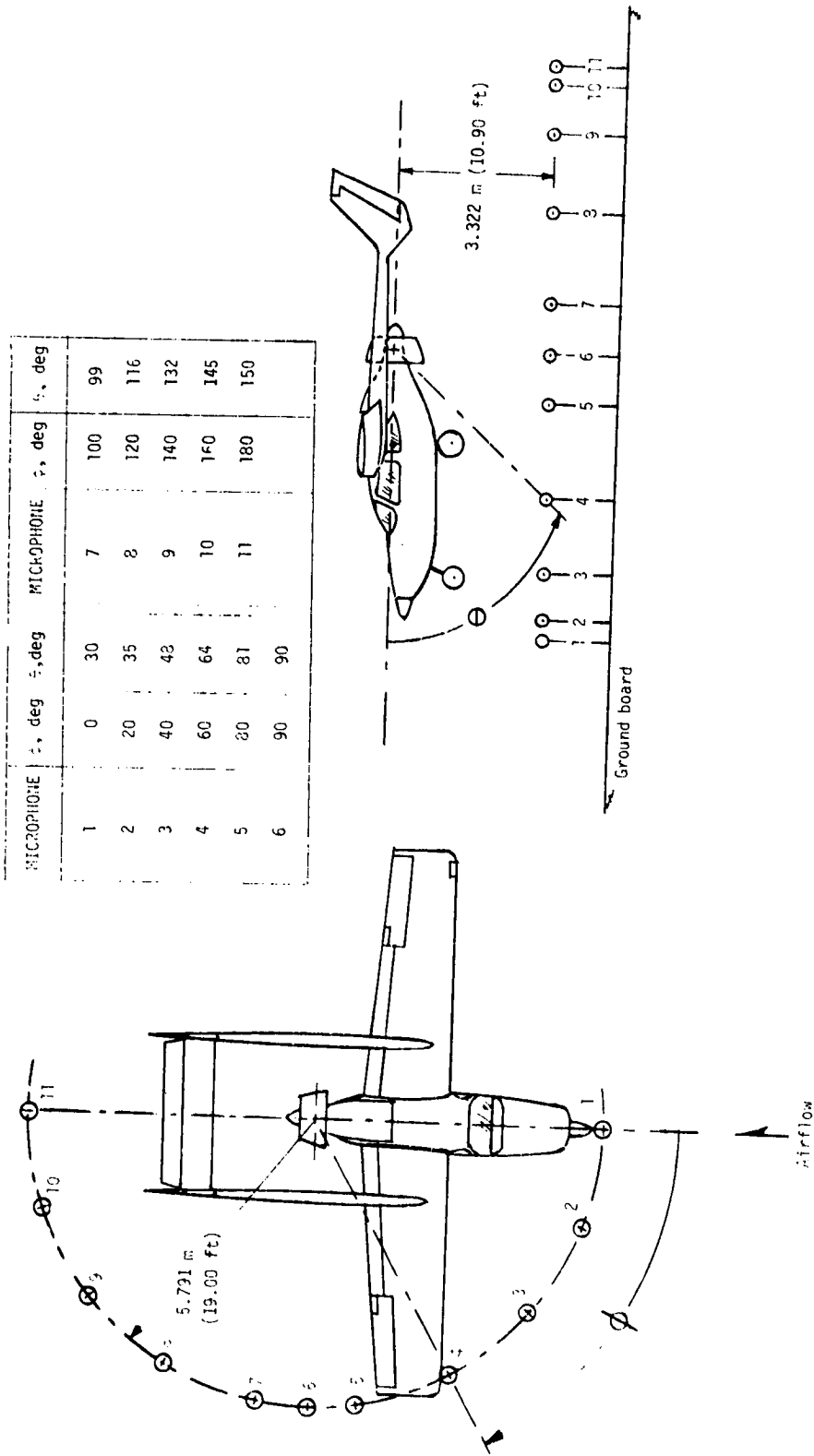
Figure 6.- Plan view and side view of airplane and microphone array showing microphone locations.
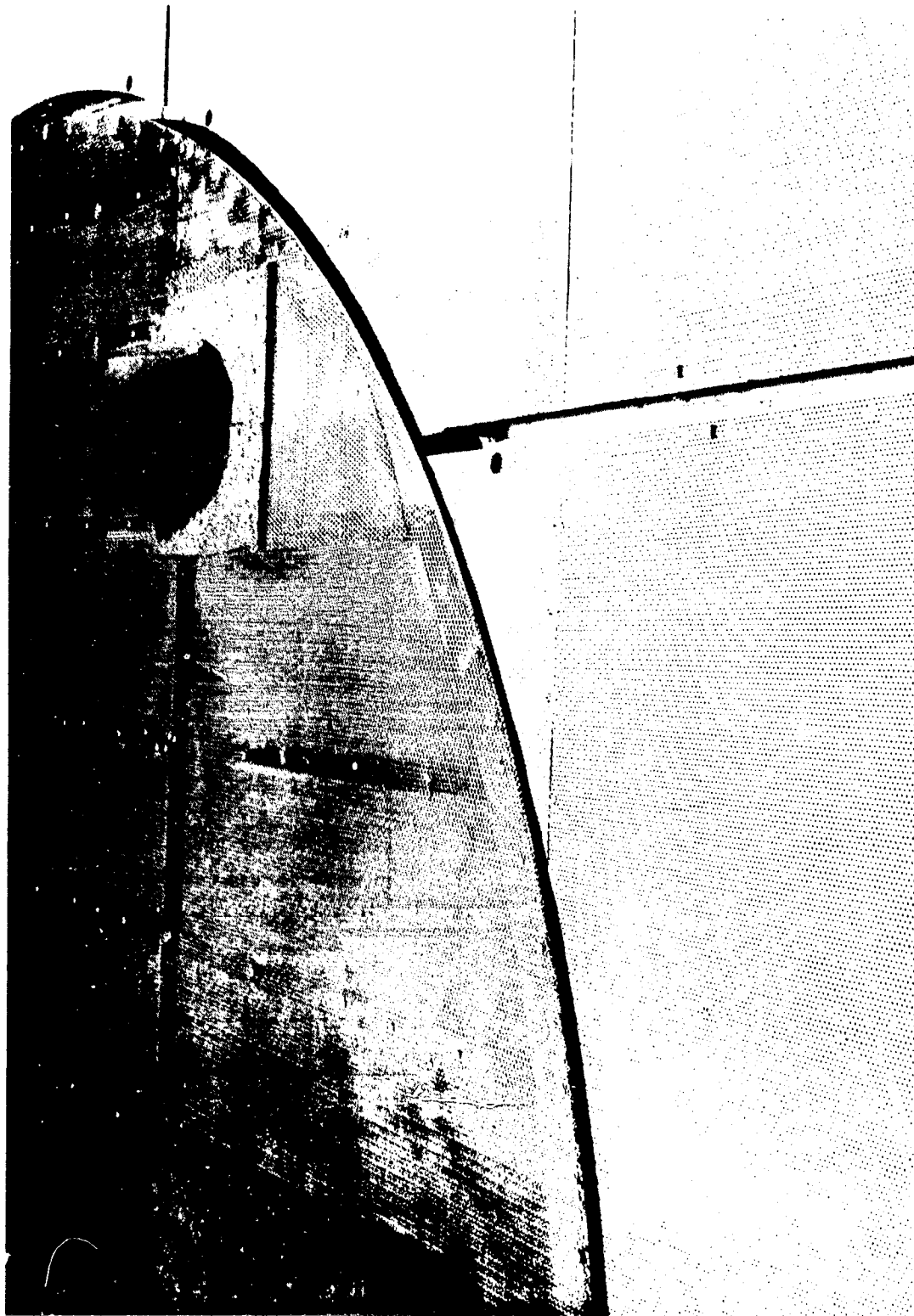
Figure 7.- Photograph of foot of airplane mounting strut with absorption wrapping and acoustic ground board.

L-74-4508

33
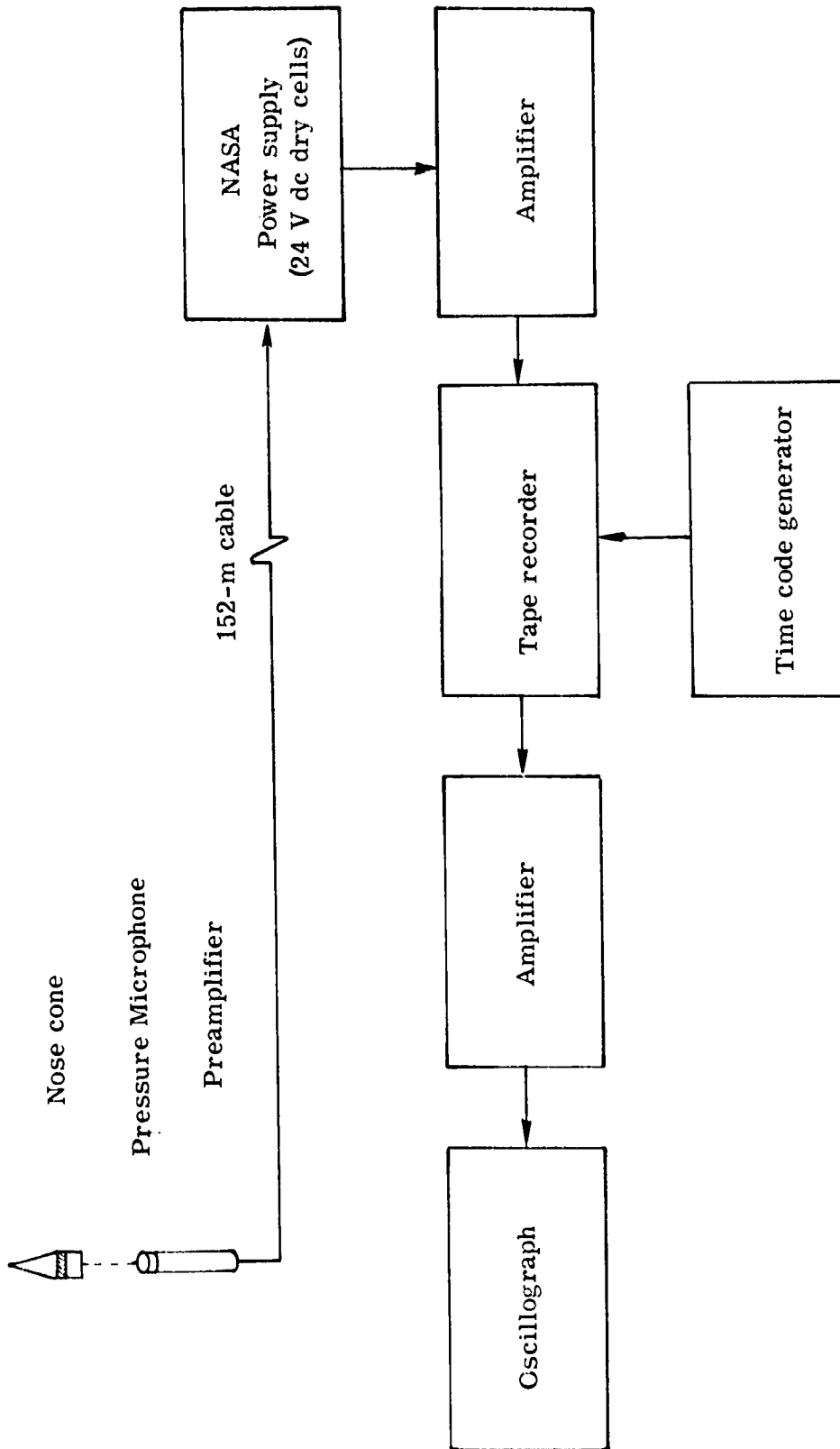
Figure 8.– Instrumentation block diagram for acoustic measurements.
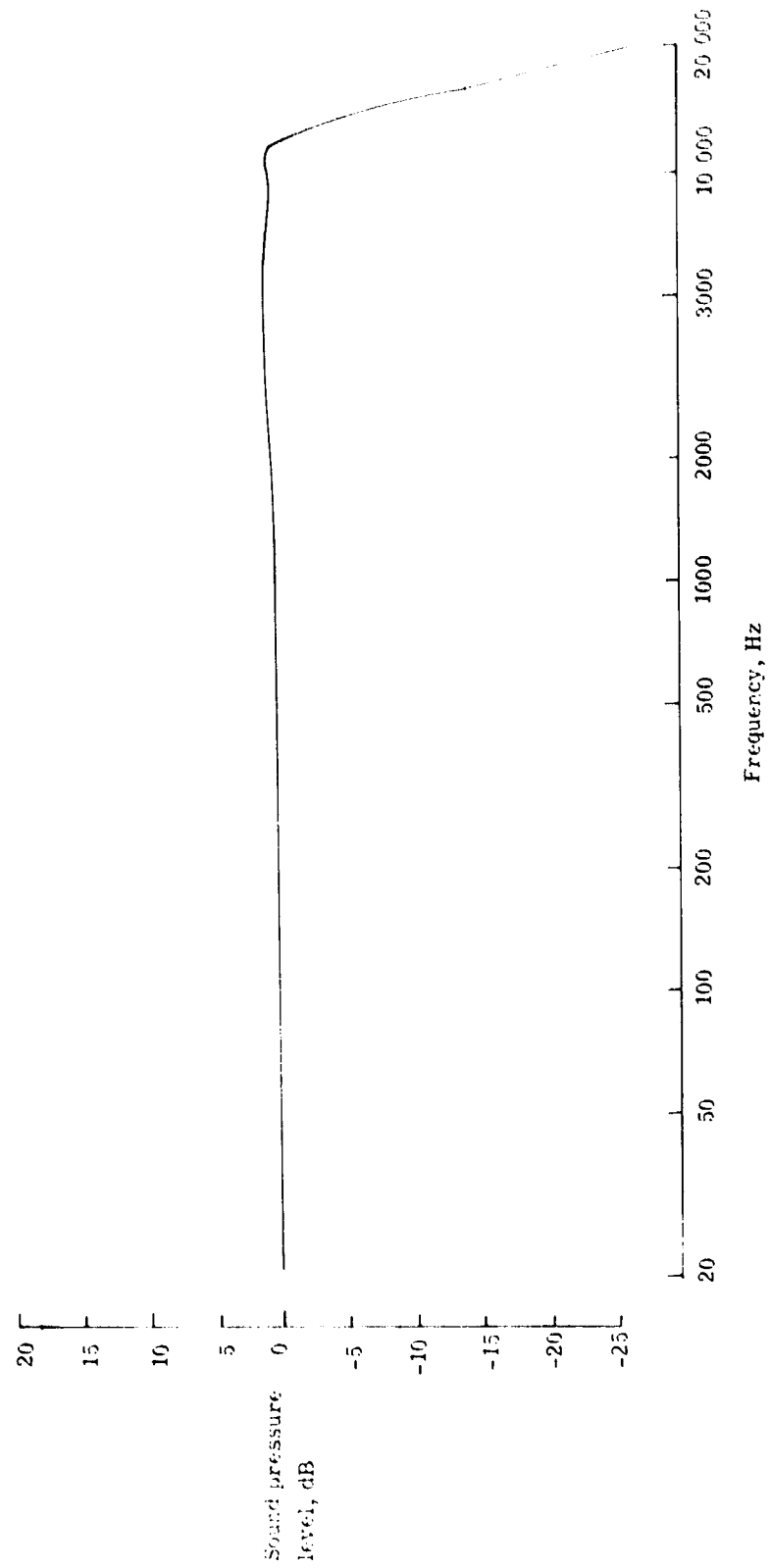
Figure 9.- Typical system-frequency response.
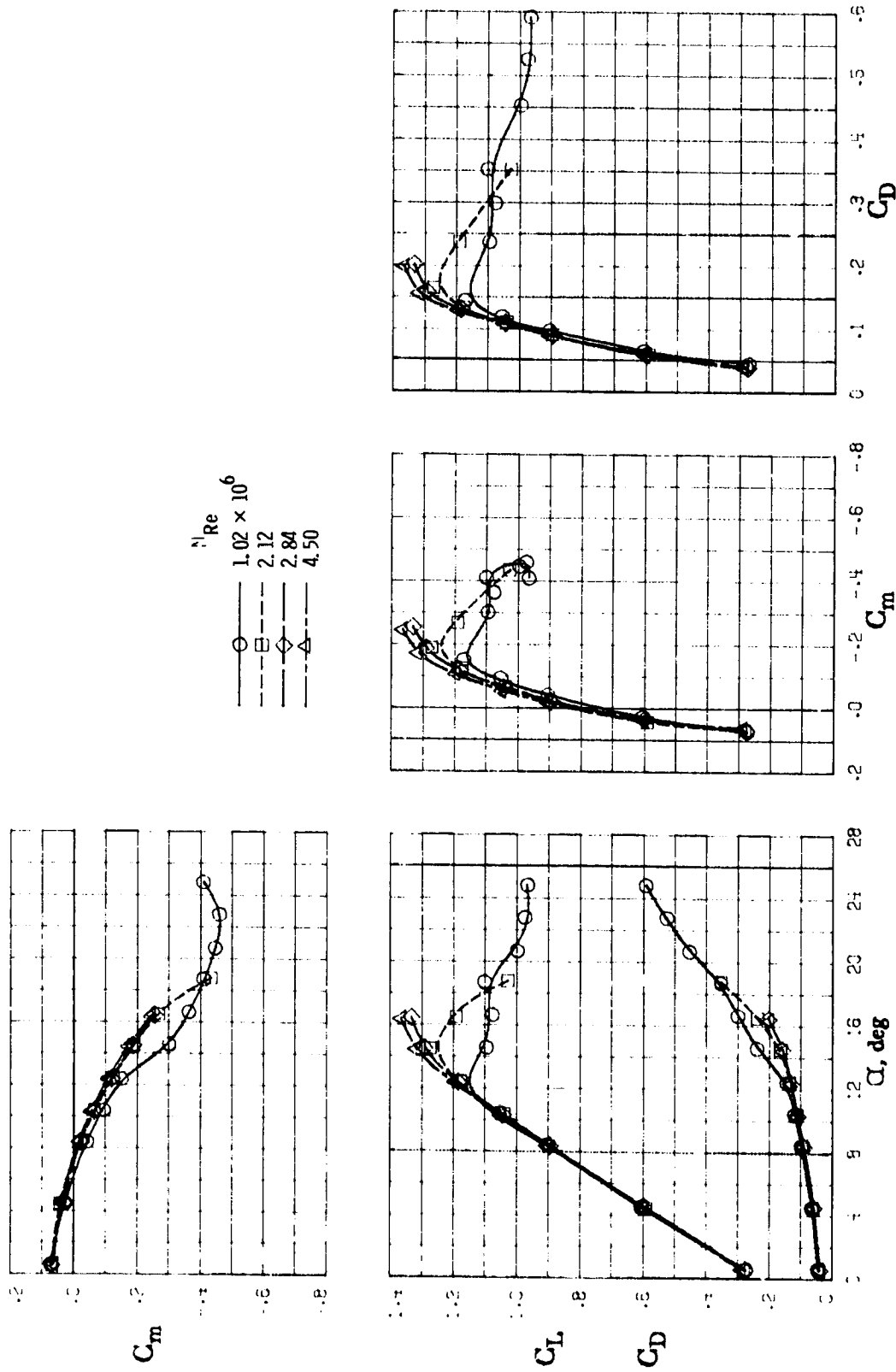
Figure 10.- Effects of Reynolds number on aerodynamic characteristics with propeller removed. $\delta_f = 0°$.

36
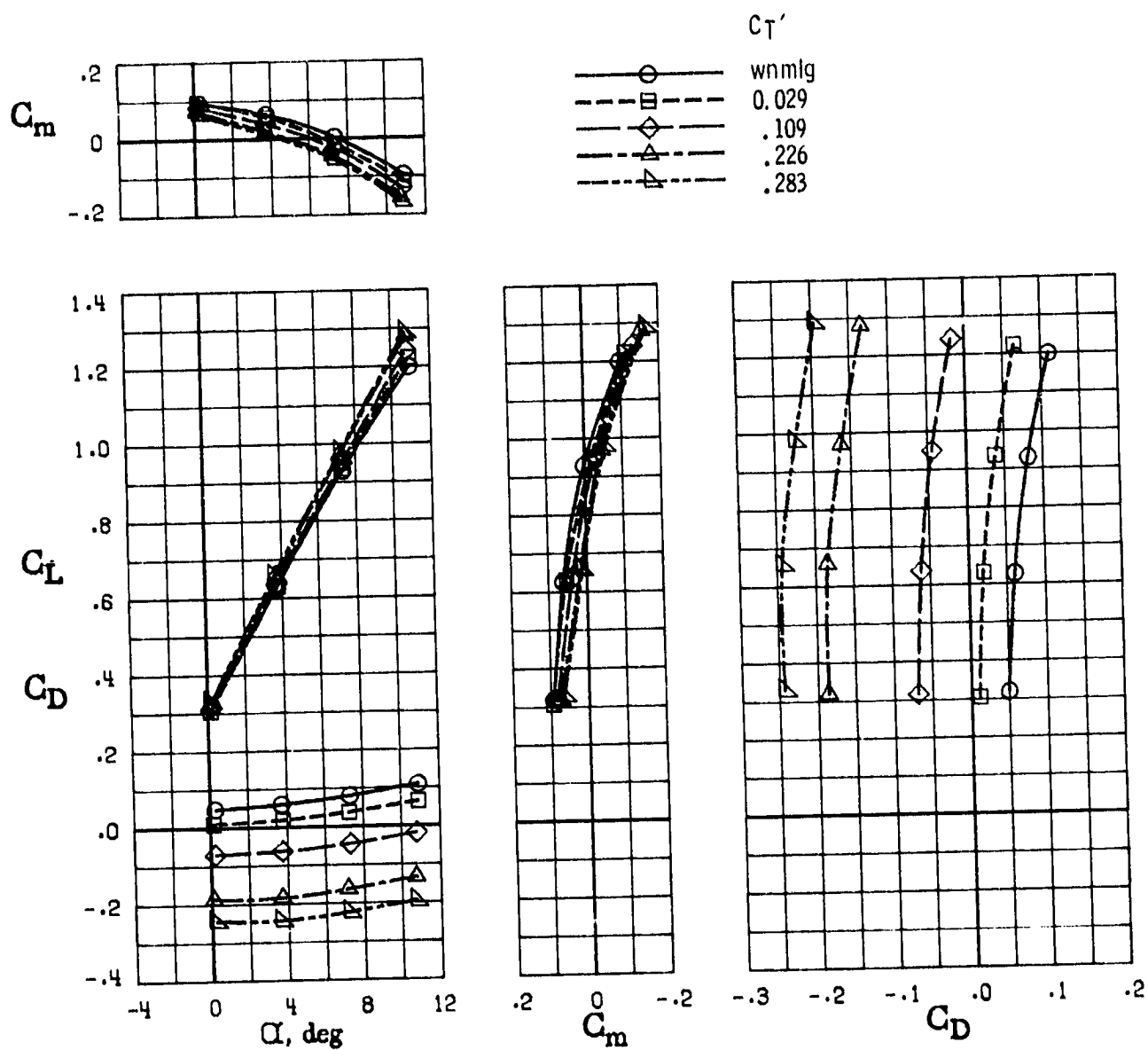
(a) $\beta = 12°$.

Figure 11.- Aerodynamic characteristics of airplane with free propeller operating. $\delta_f = 0°$; $N_{Re} = 2.84 \times 10^6$.
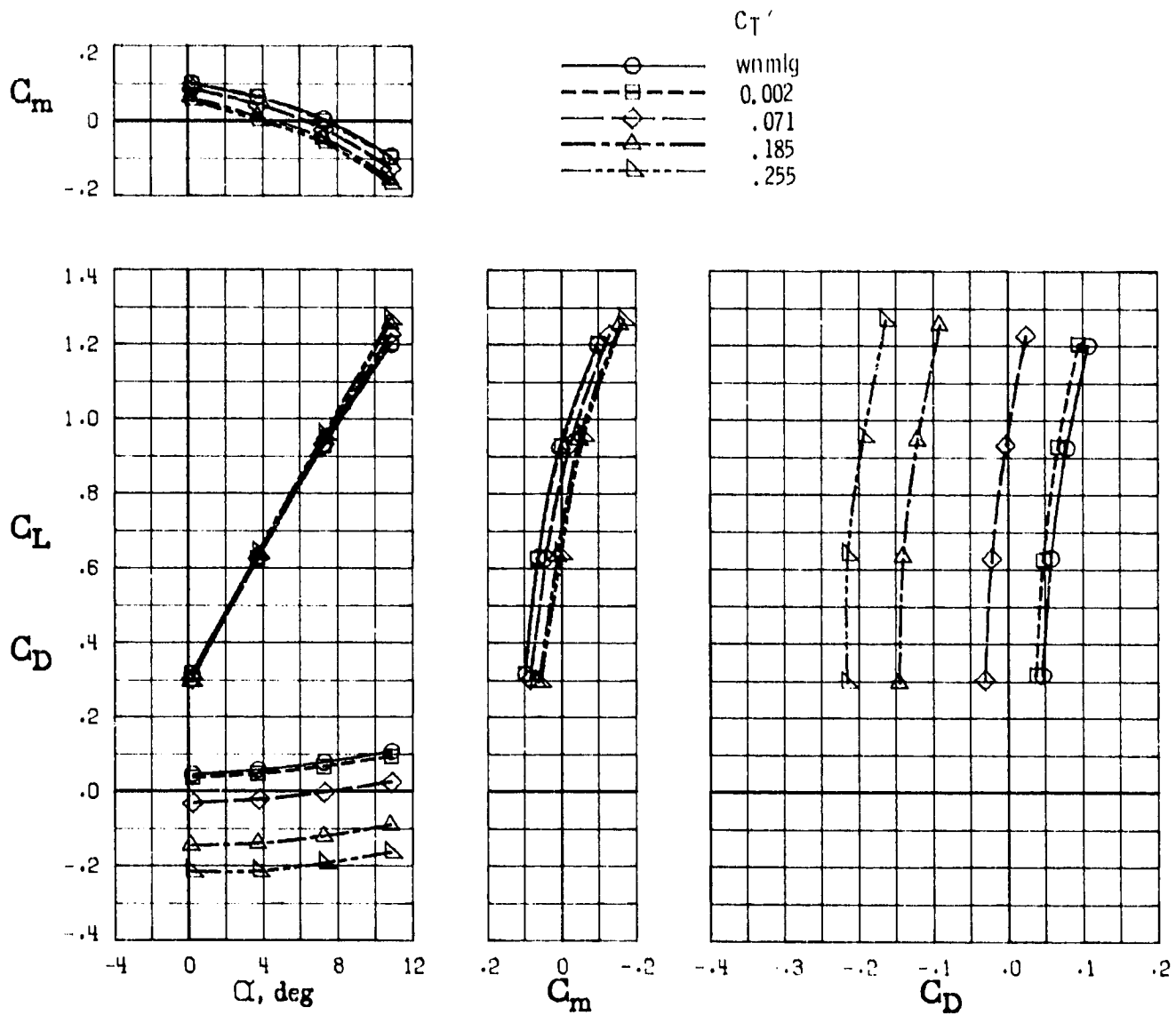
(b) $\beta = 16°$.

Figure 11.- Continued.
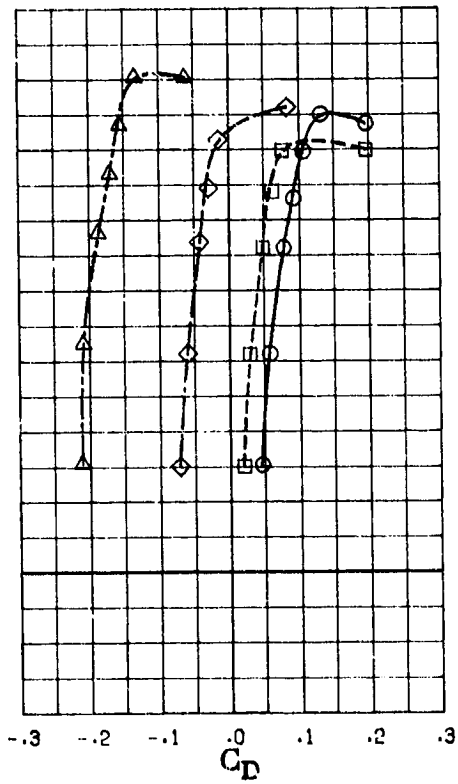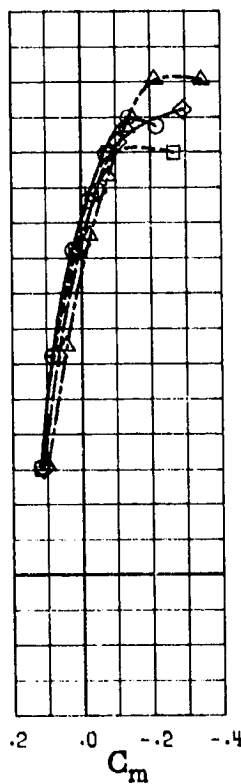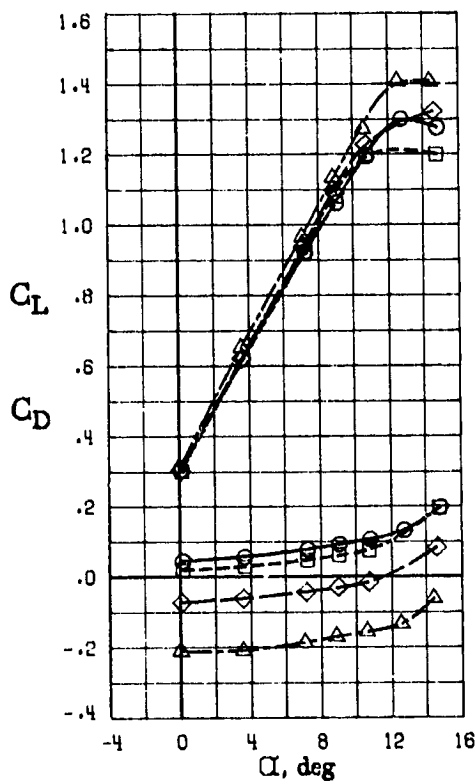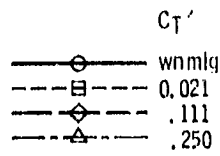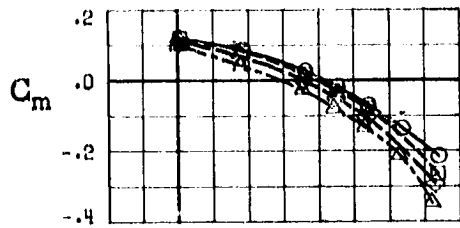
(c)   β = 20°.

Figure 11.- Continued.
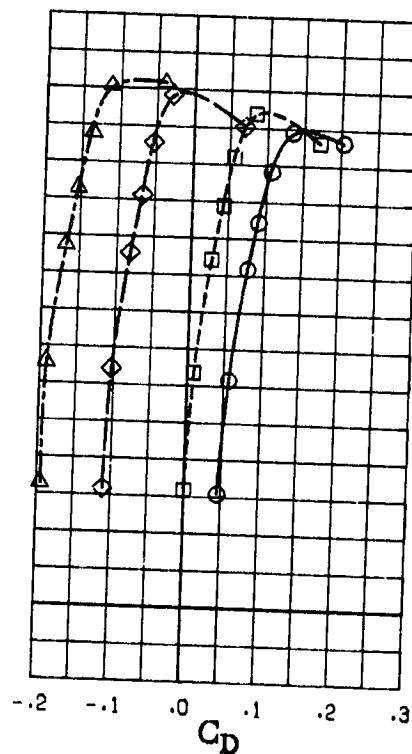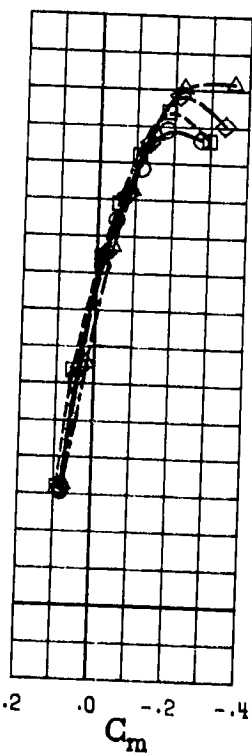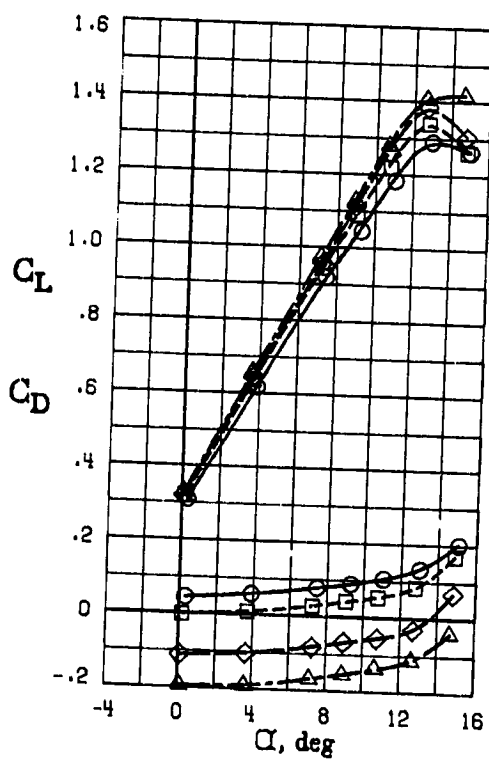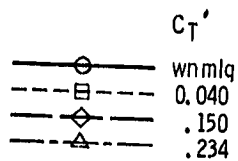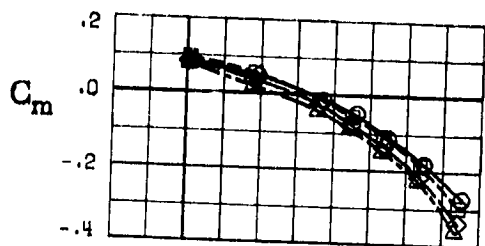
(d) $\beta = 24°$.

Figure 11.- Continued.
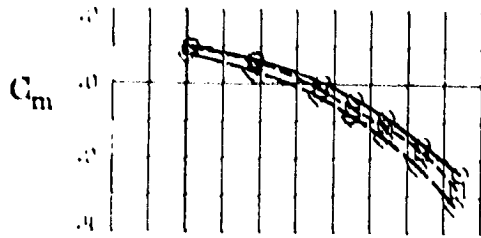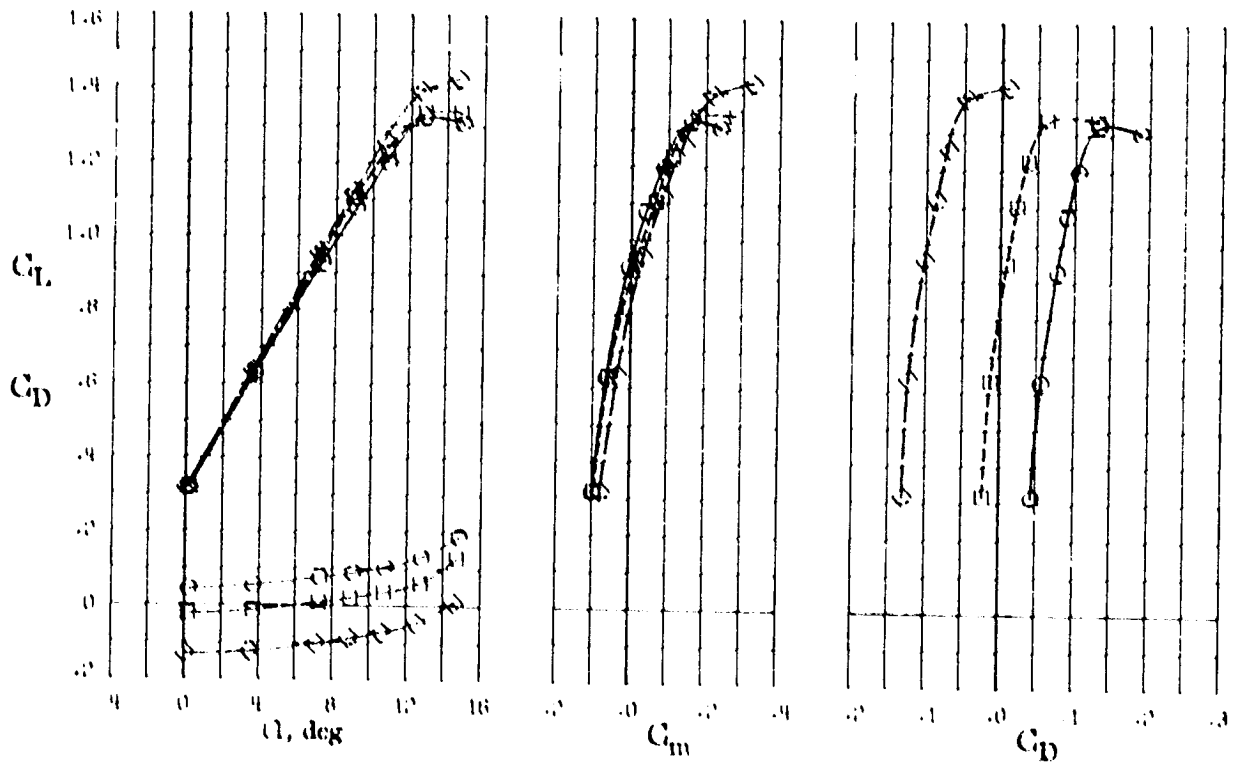
(e) δ = 28°.

Figure 11. Concluded.

(a) $\beta = 12^{o}$.
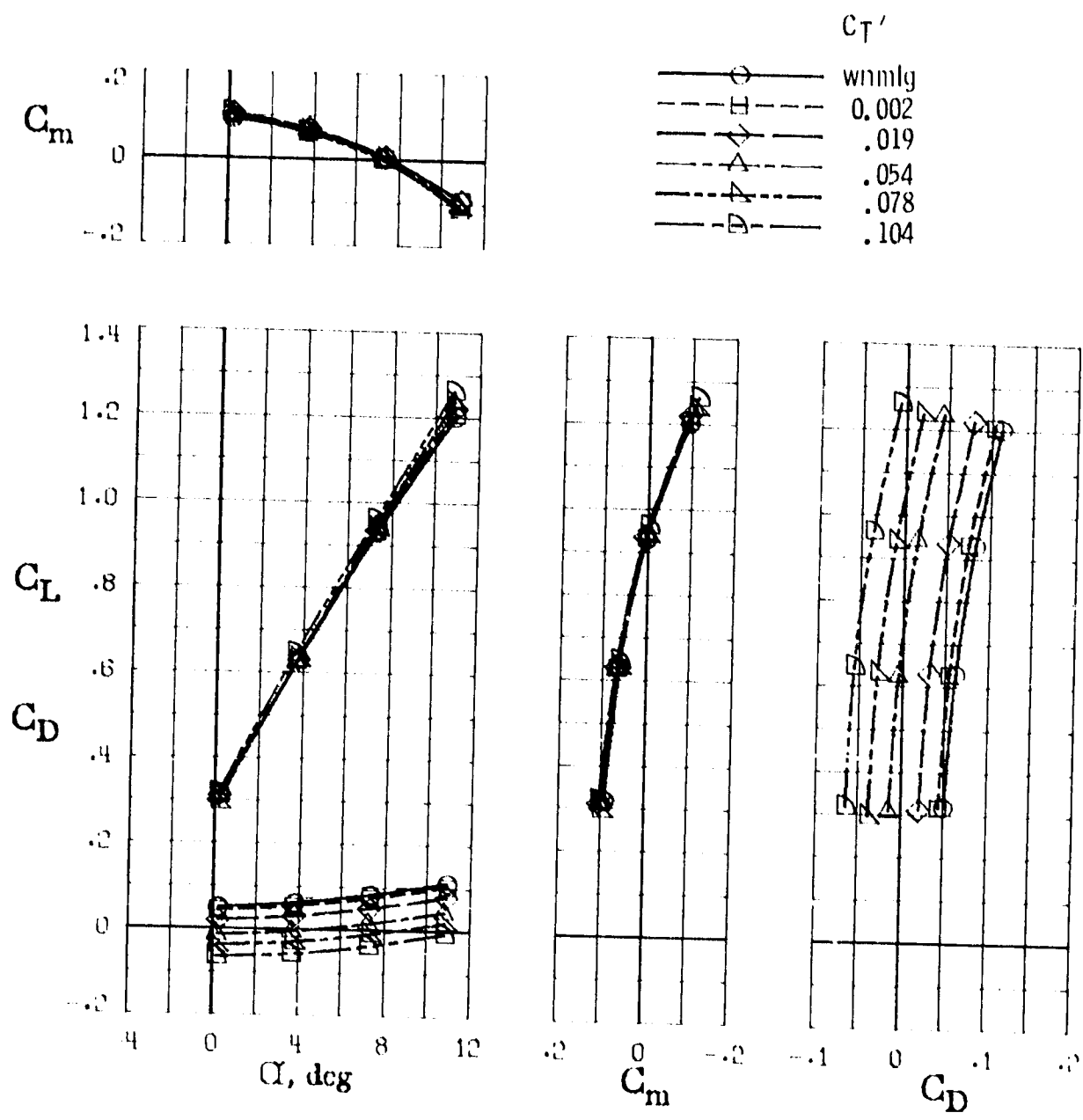
Figure 12.- Aerodynamic characteristics of airplane with 3-blade, unloaded-tip, shrouded propeller operating. $\delta_f = 0^{o}$.

42
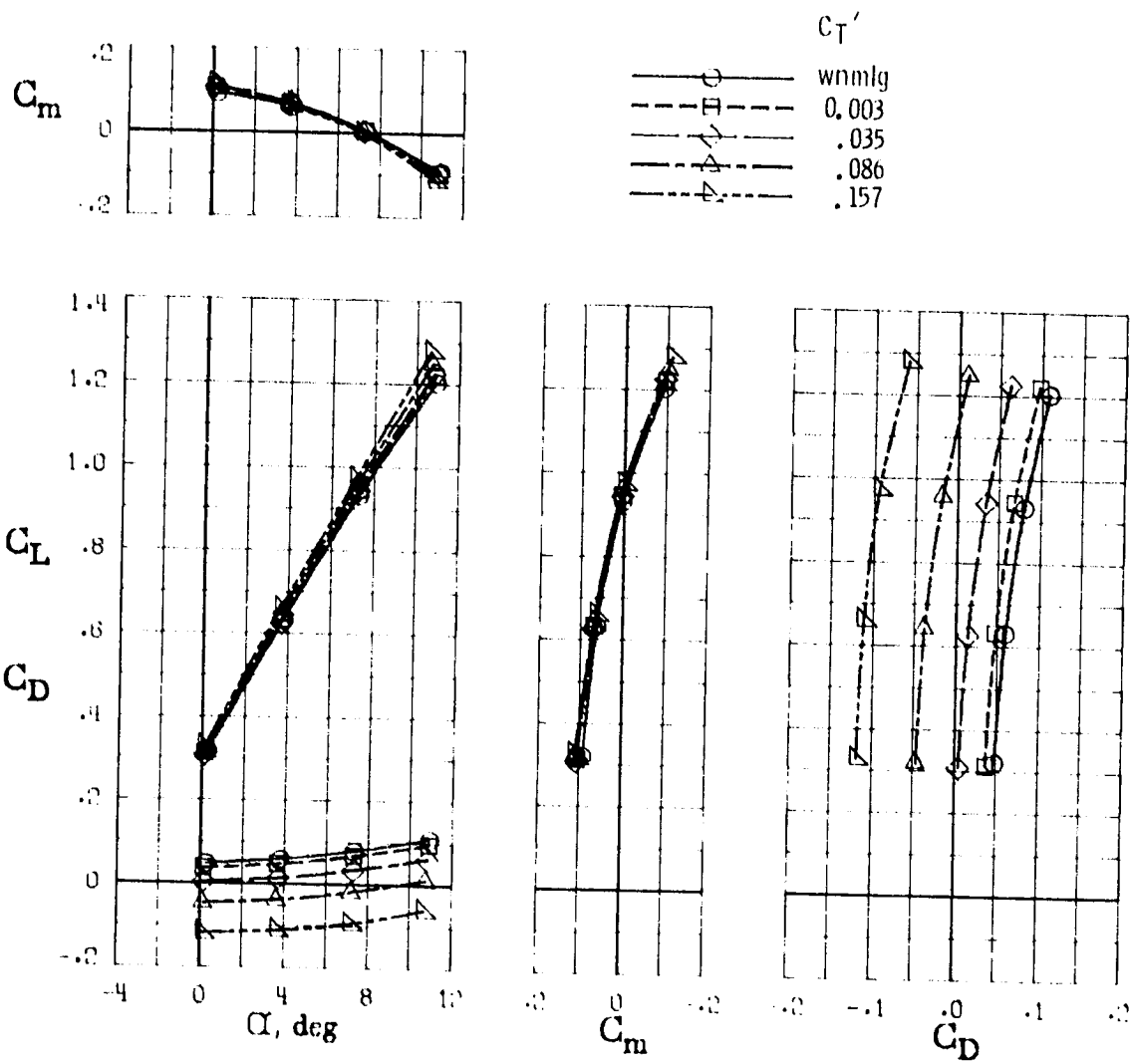
(b) $\beta = 16^{\circ}$.

Figure 12.- Continued.
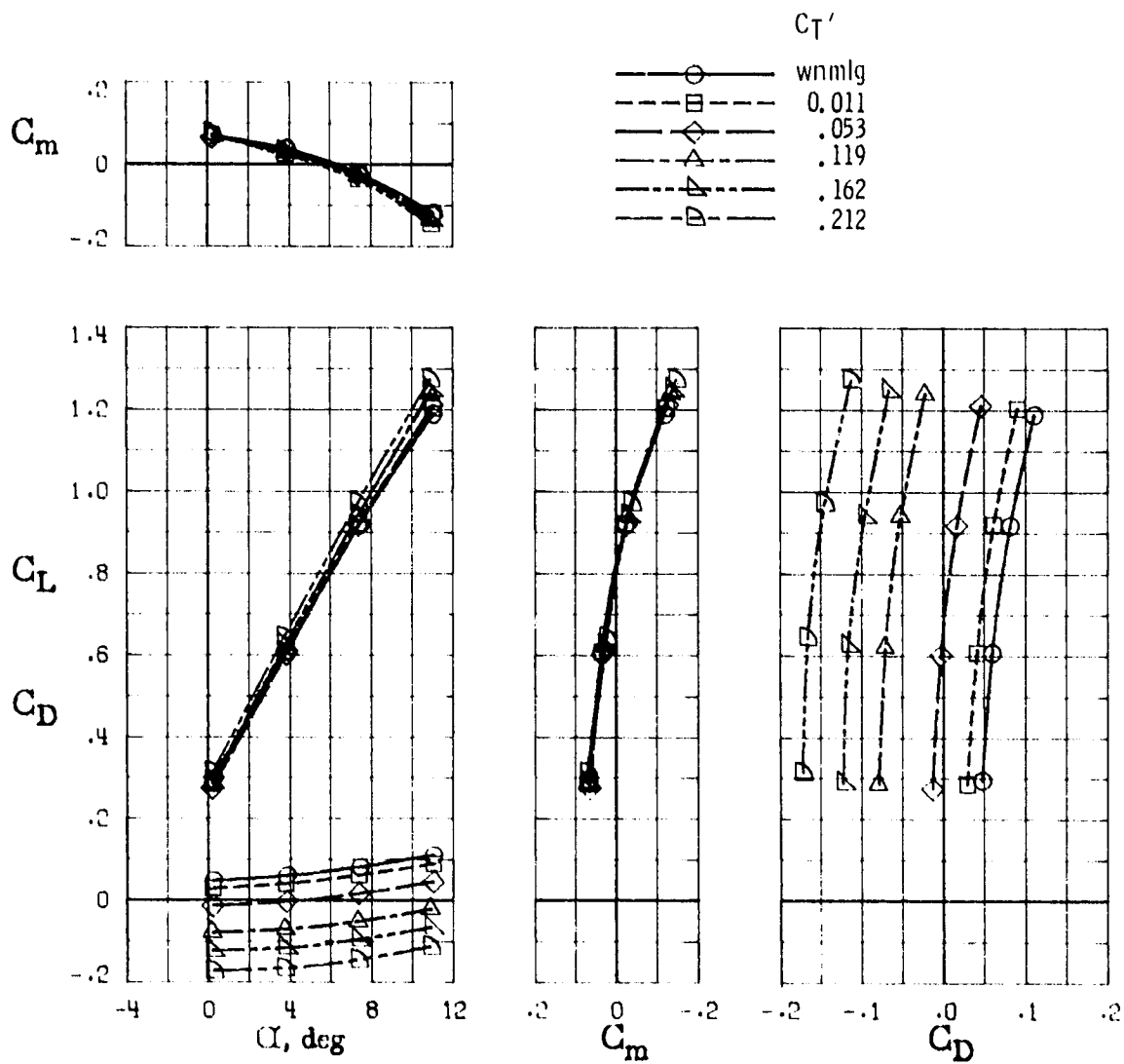
(c) $\beta = 20^{\circ}$.

Figure 12.- Continued.
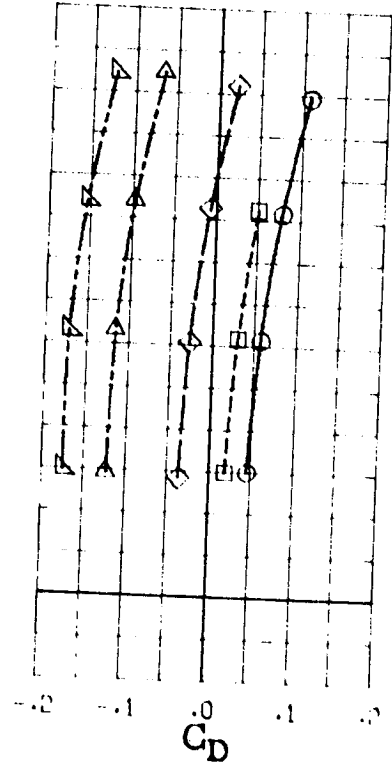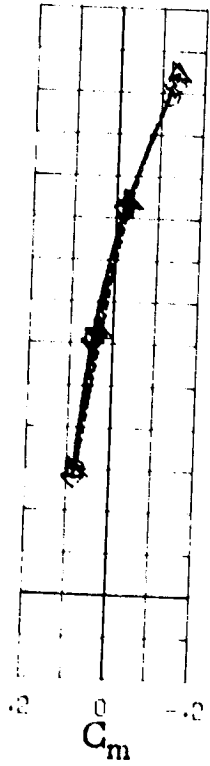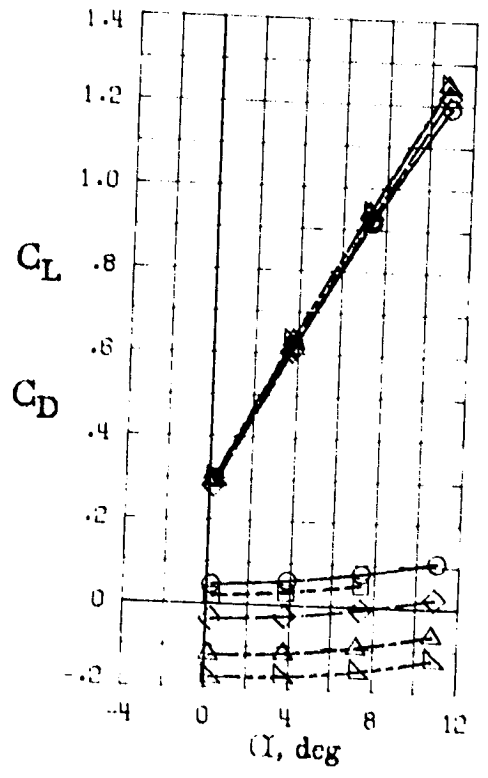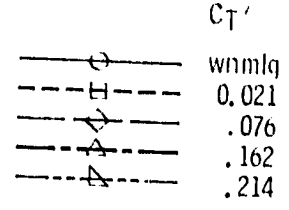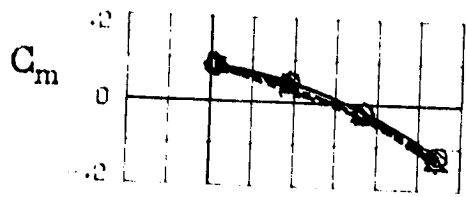
(d) $\beta = 24°$.

Figure 12.- Continued.
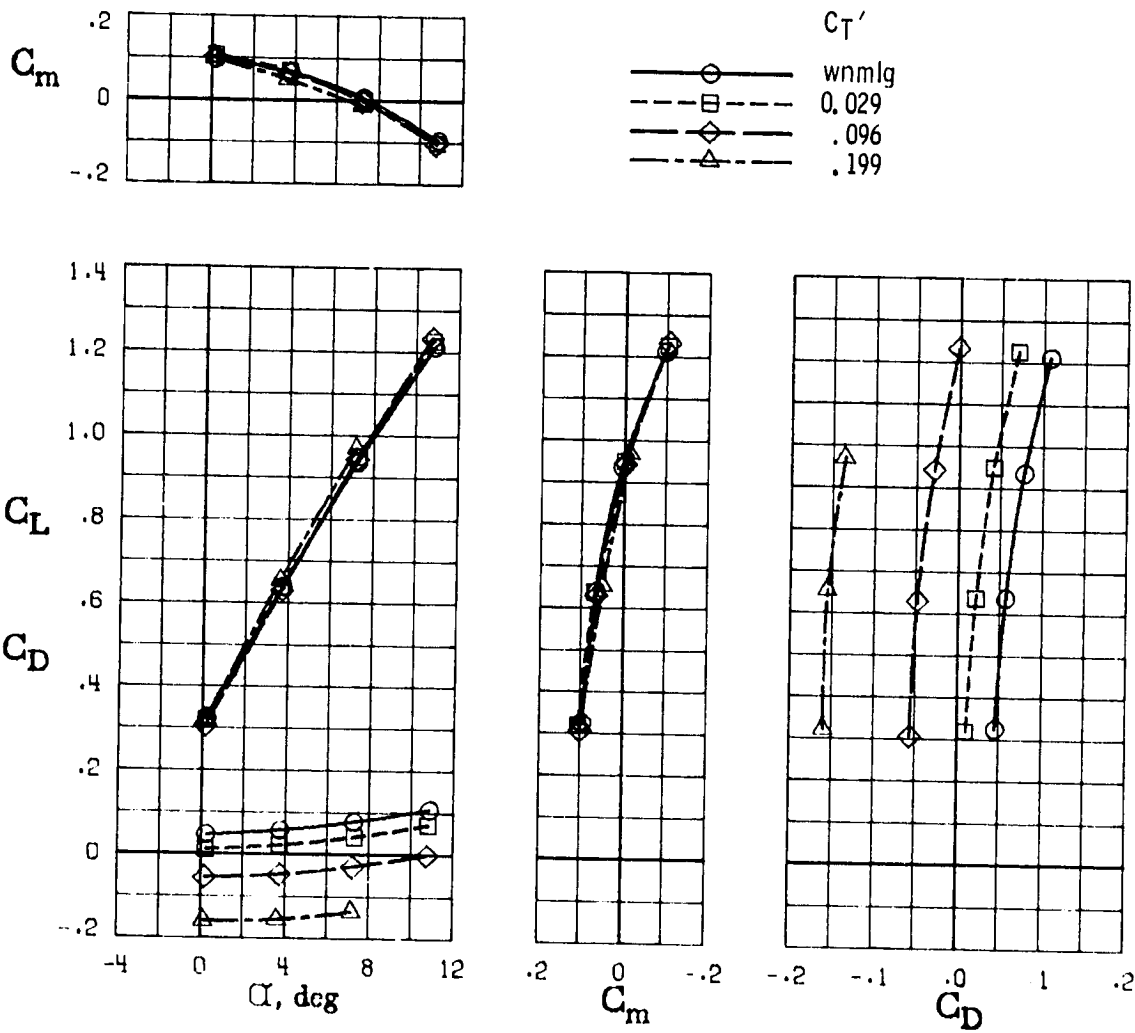
(e) $\beta = 28^\circ$.

Figure 12.- Continued.
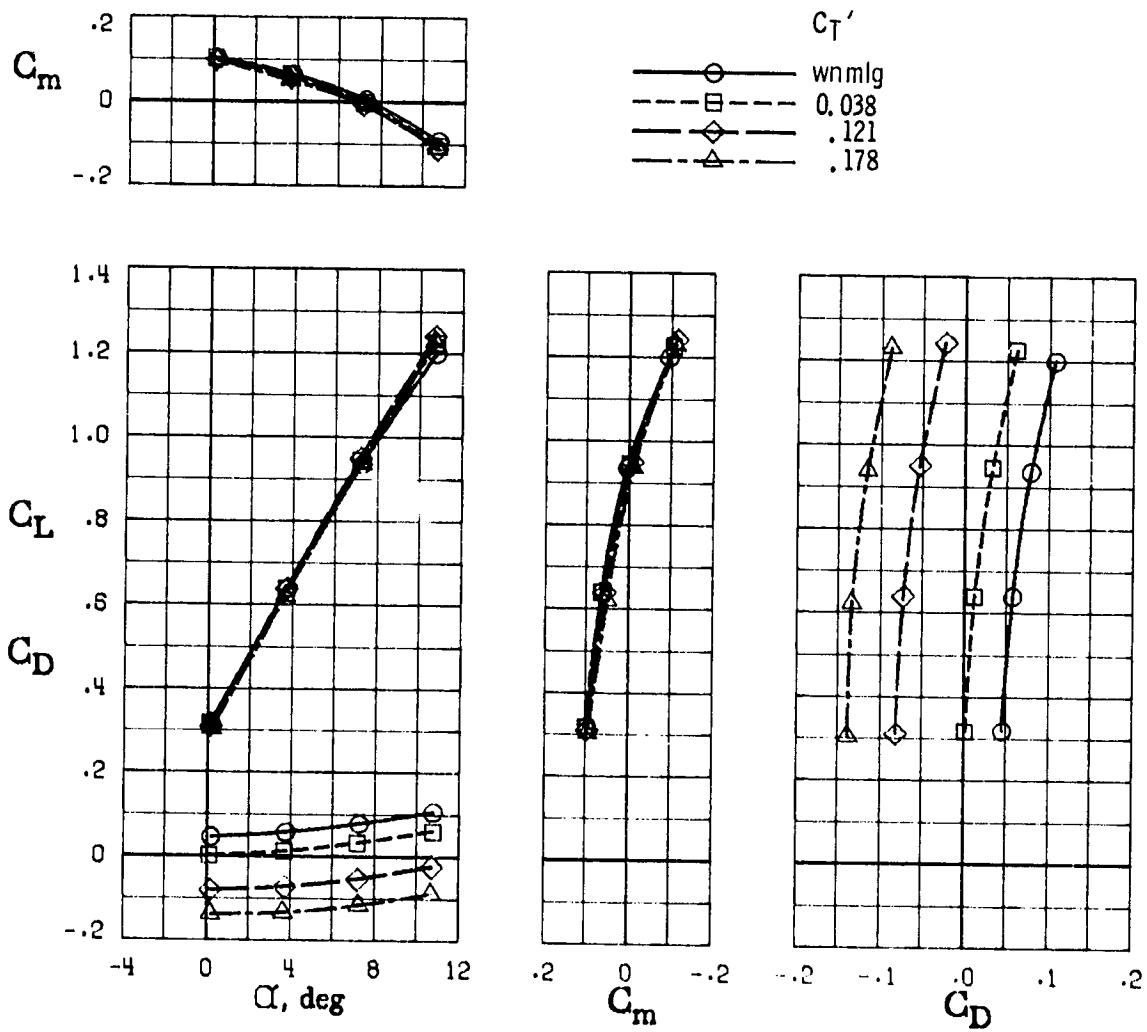
(f) $\beta = 32°$.

Figure 12.- Concluded.
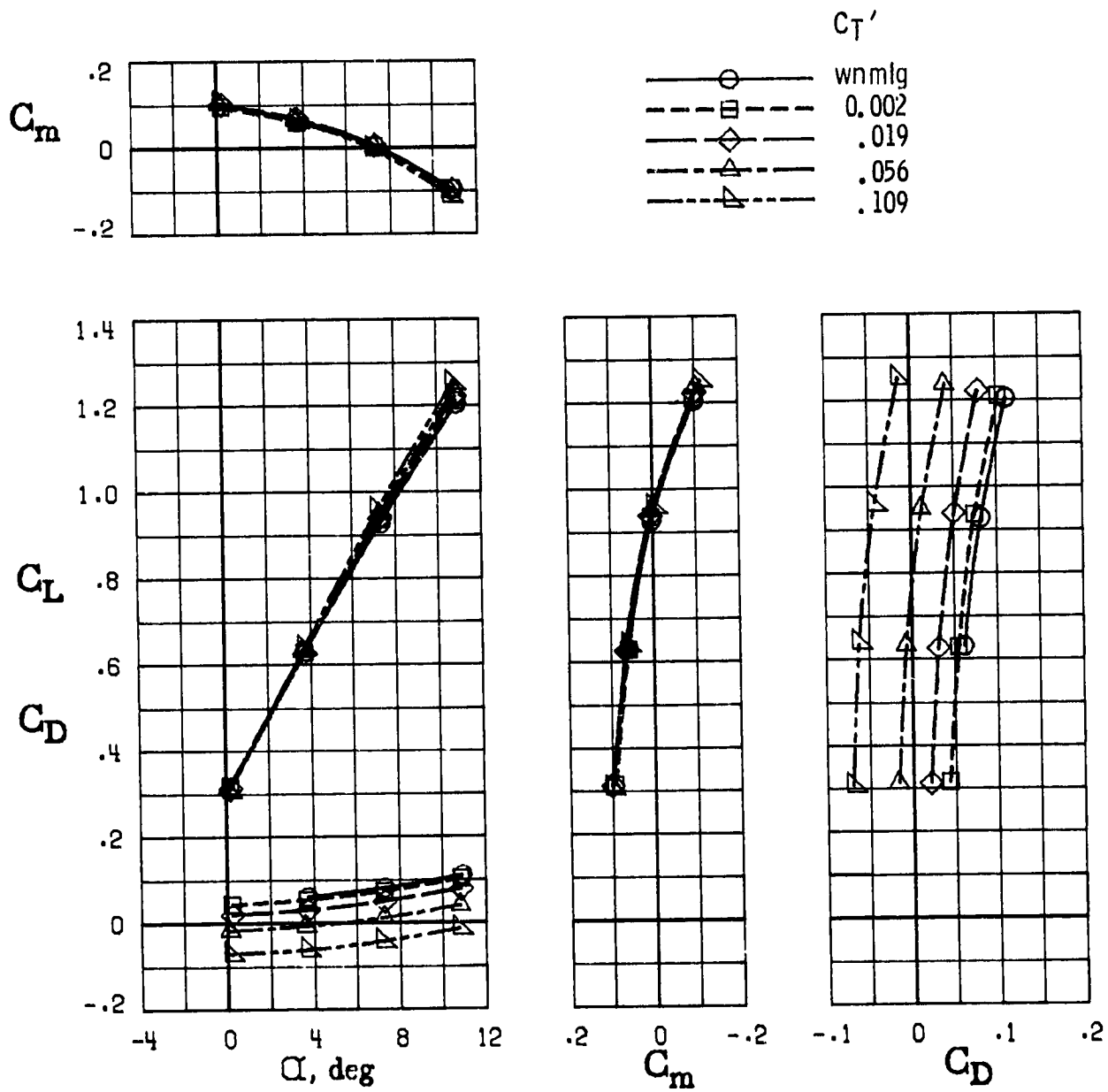
(a) $\beta = 12^\circ$.

Figure 13.- Aerodynamic characteristics of airplane with 3-blade, normal-tip, shrouded propeller operating. $\delta_f = 0^\circ$.

48

(b) $\beta = 16^{o}$.

Figure 13.- Continued.

49
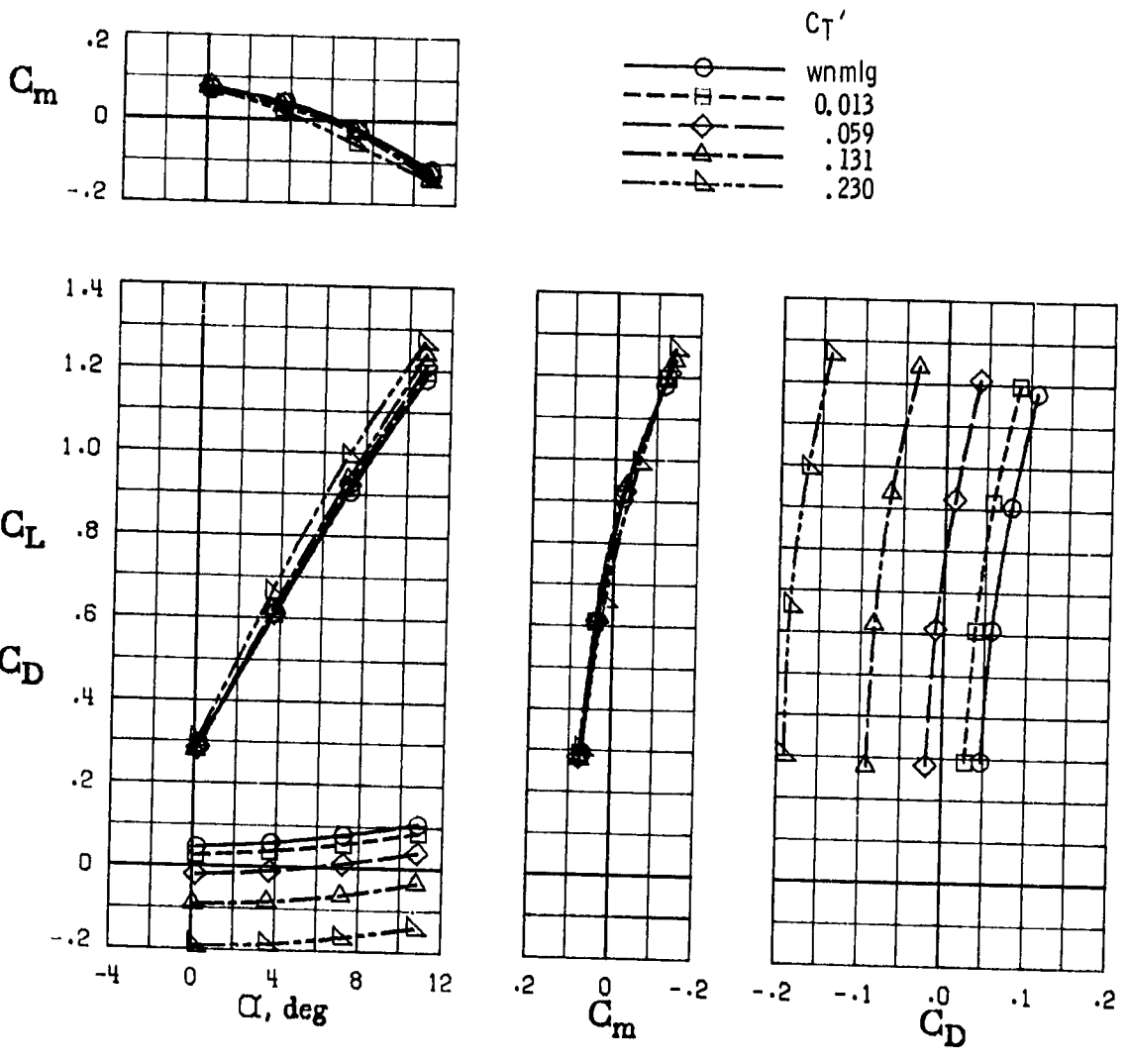
(c) $\beta = 20^\circ$.

Figure 13.- Continued.

50
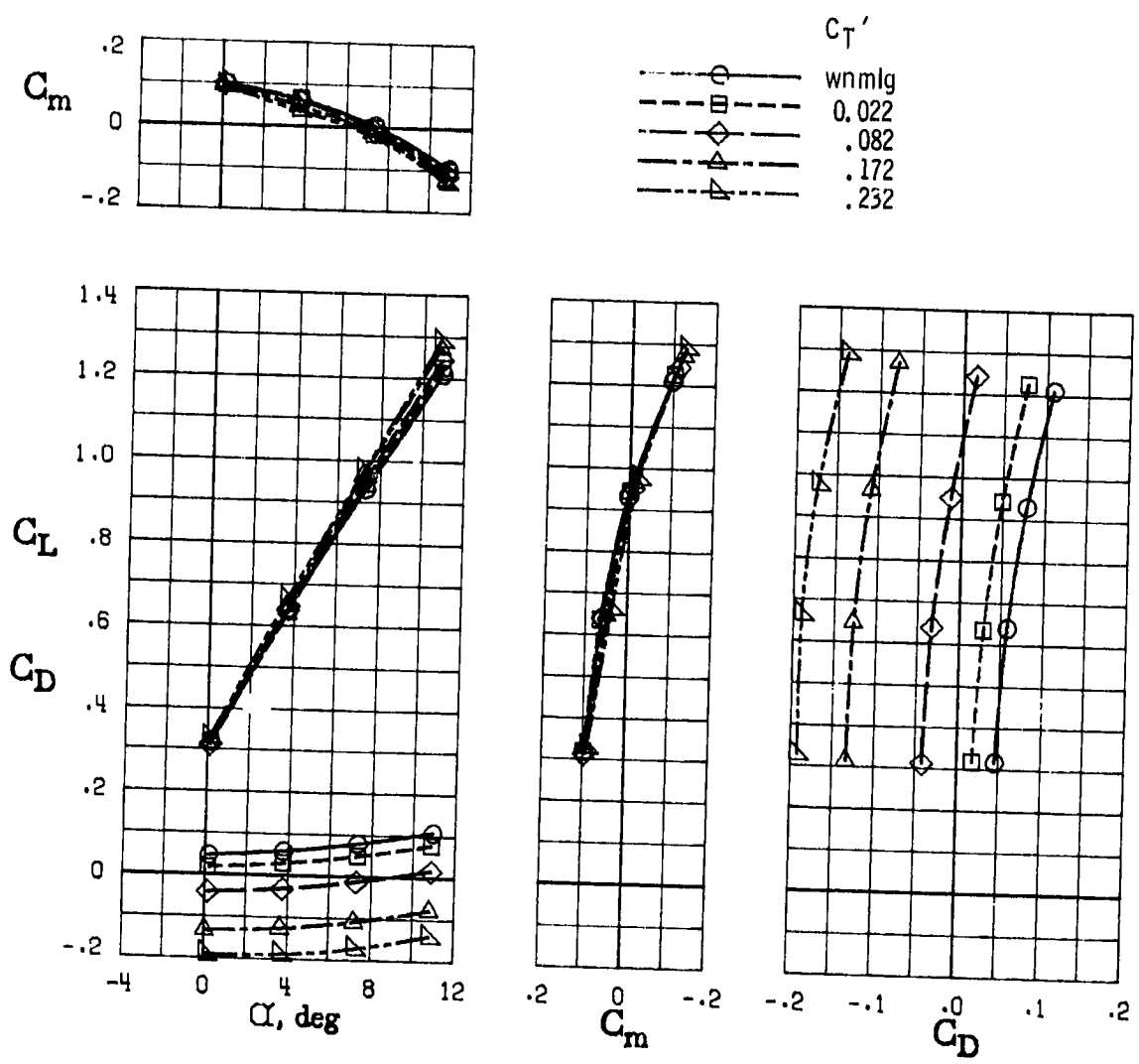
(d) β = 24°.

Figure 13.- Continued.
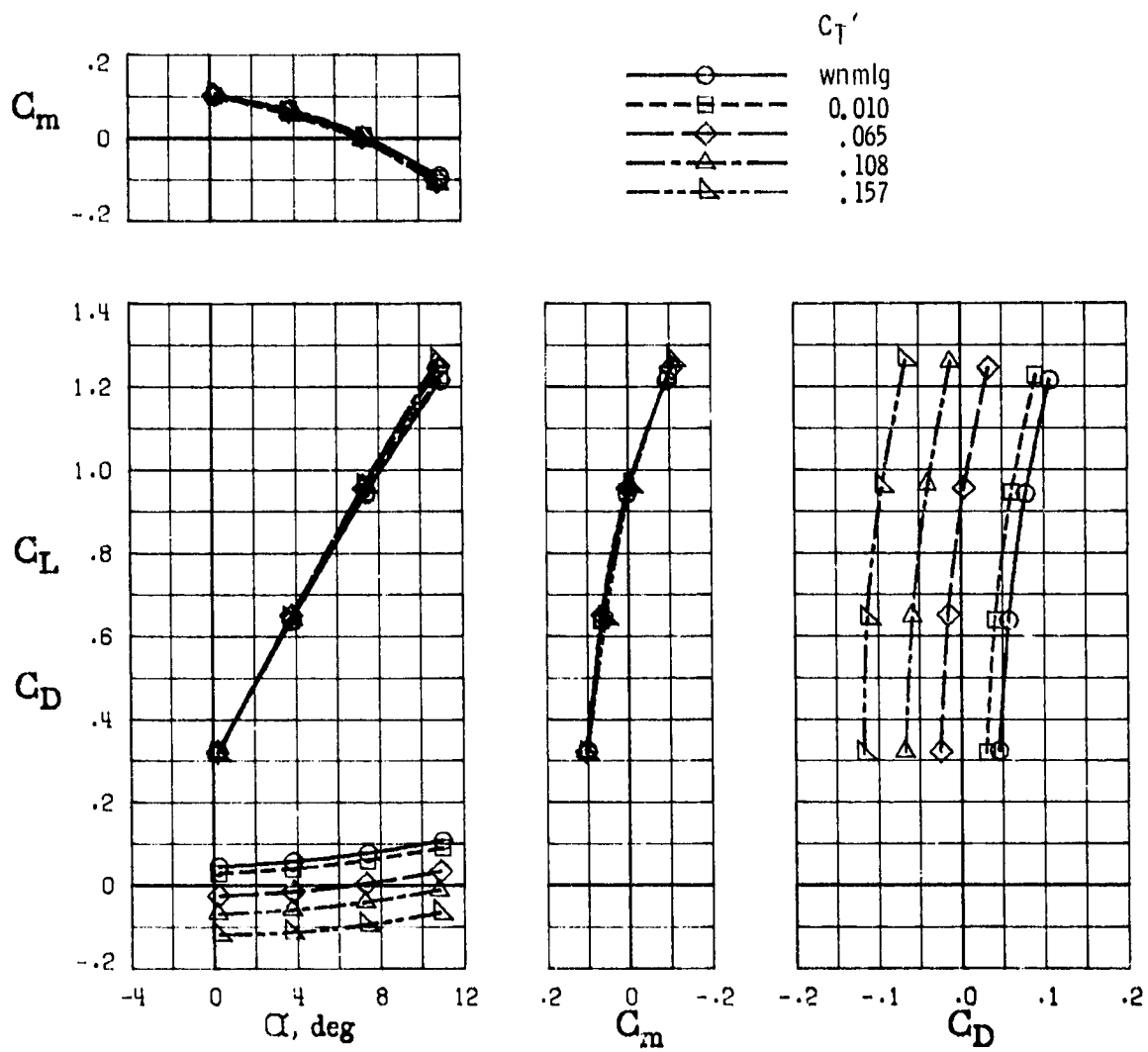
(e) β = 28°.

Figure 13.- Continued.
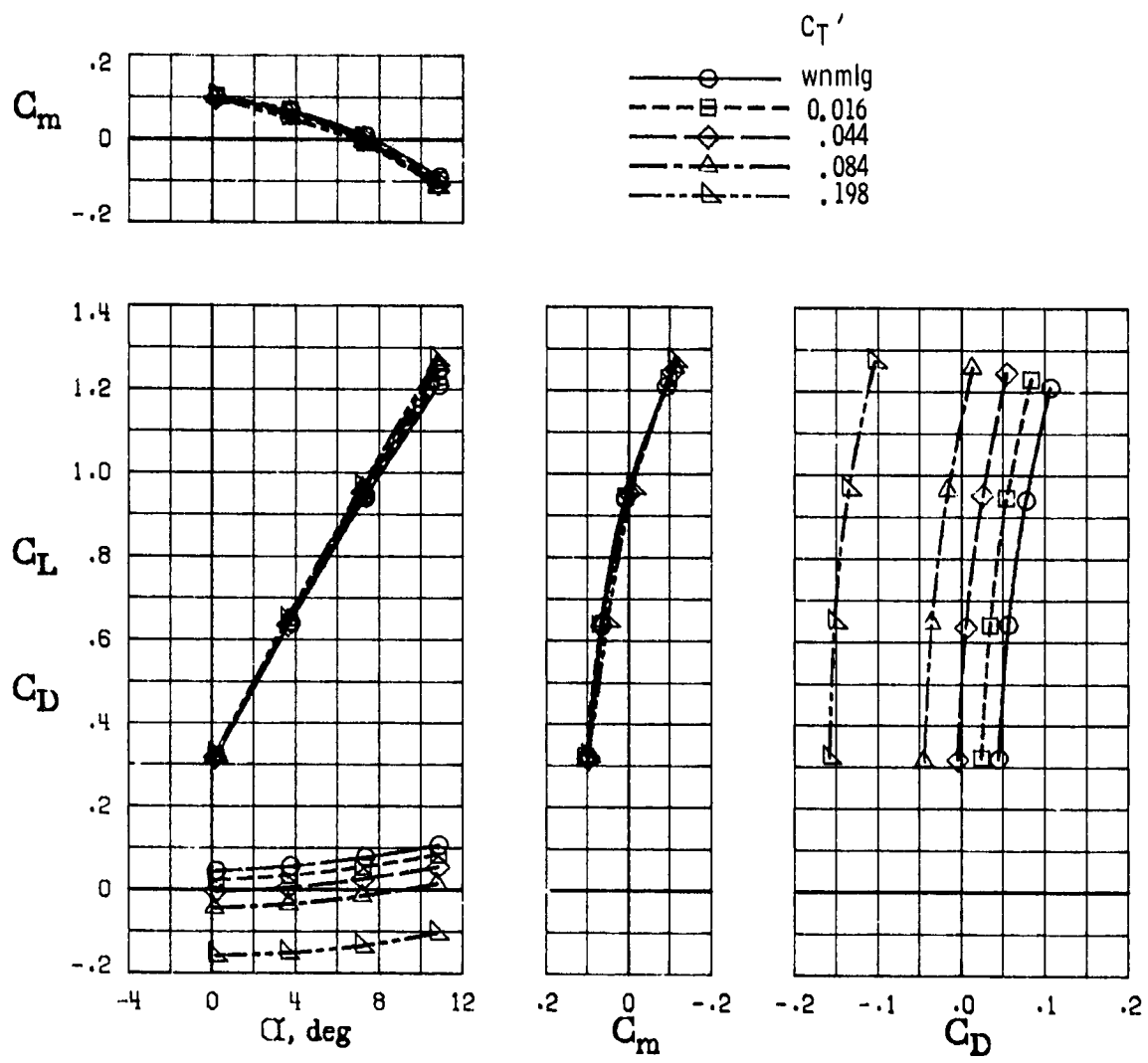
(f)   β = 32°.

Figure 13.- Continued.
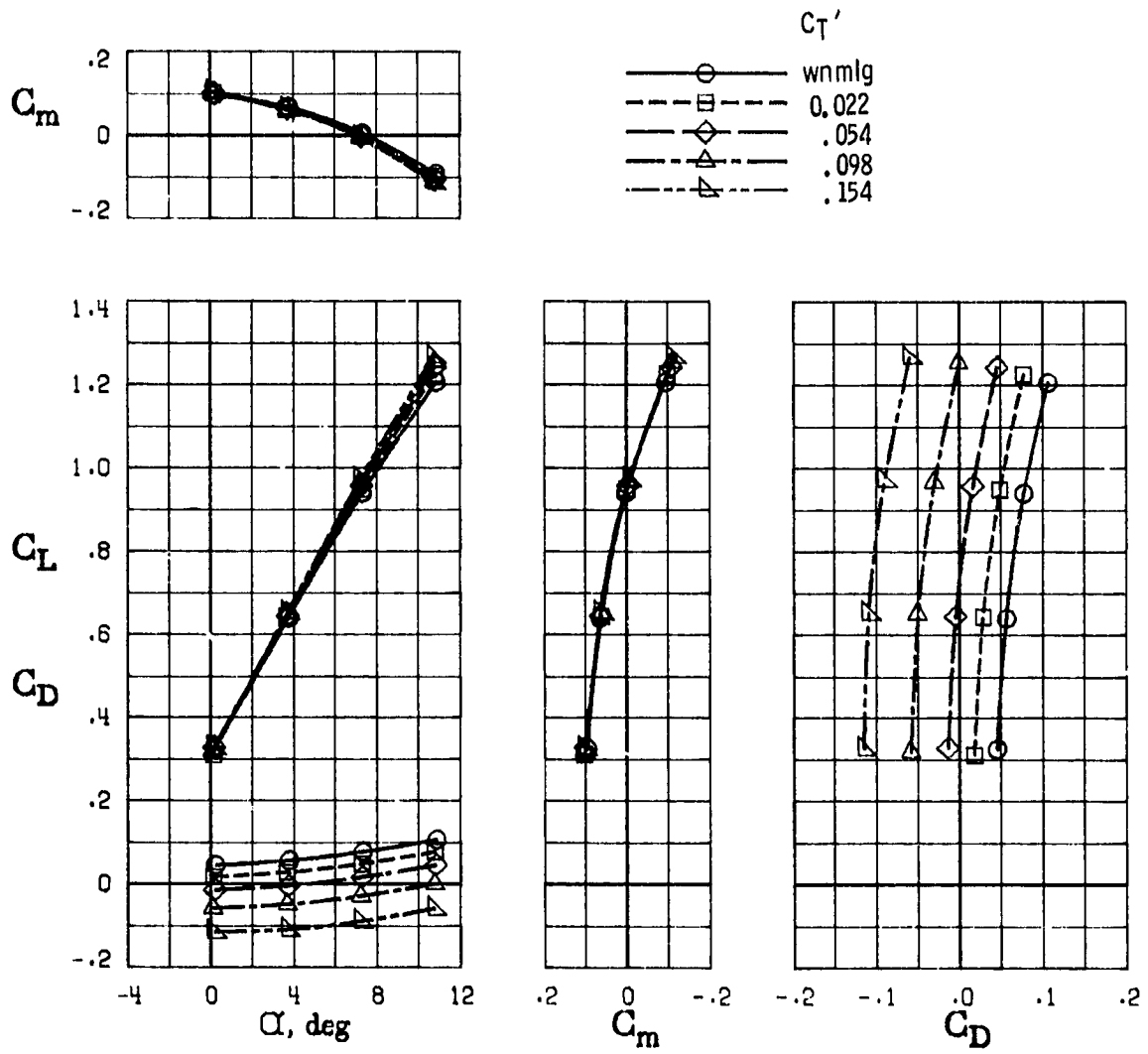
(g) β = 36°.

Figure 13.- Concluded.

(a) $\beta = 16^o$.
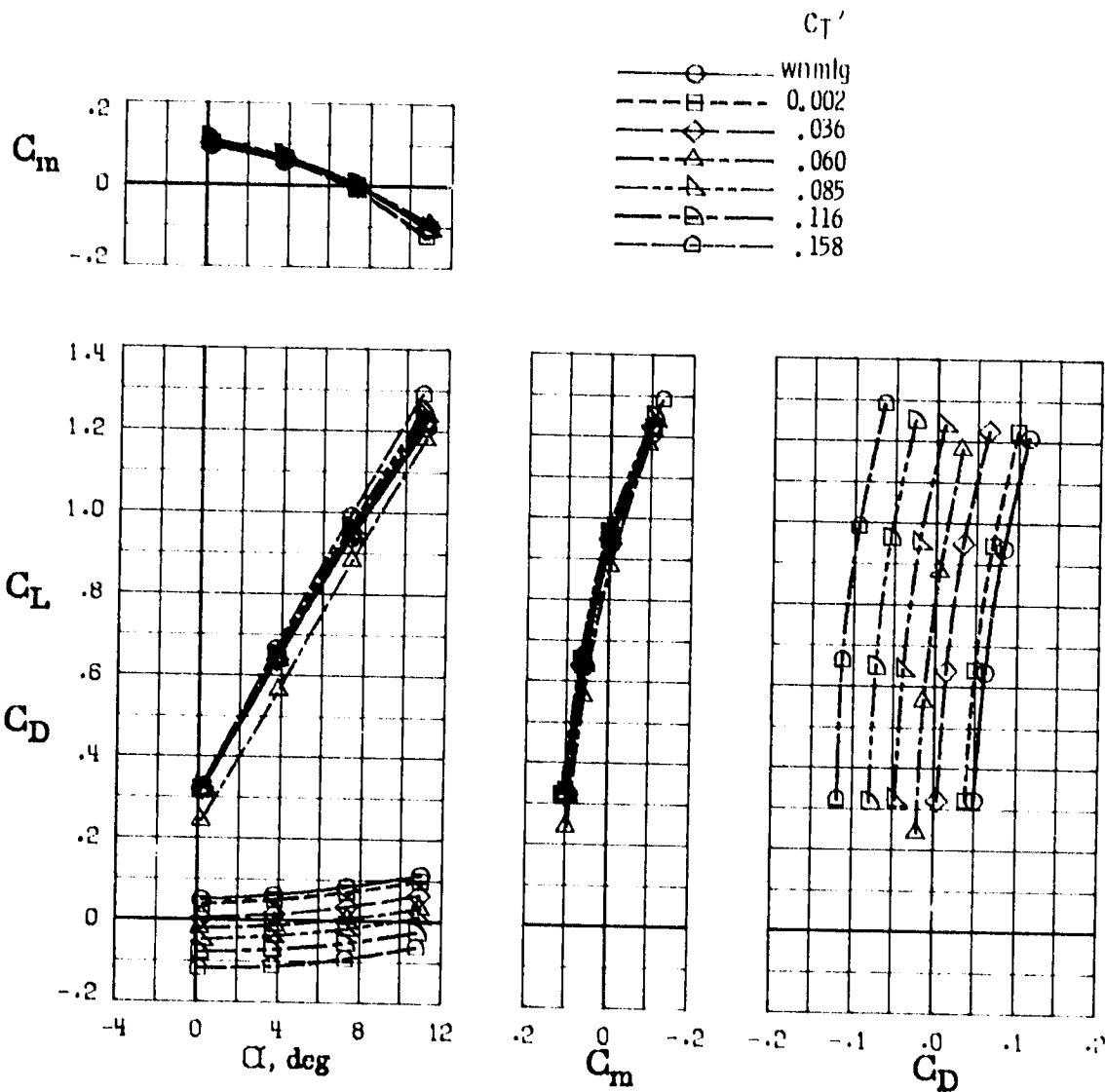
Figure 14.- Aerodynamic characteristics of airplane with 5-blade, unloaded-tip, shrouded propeller operating. $\delta_f = 0^o$.
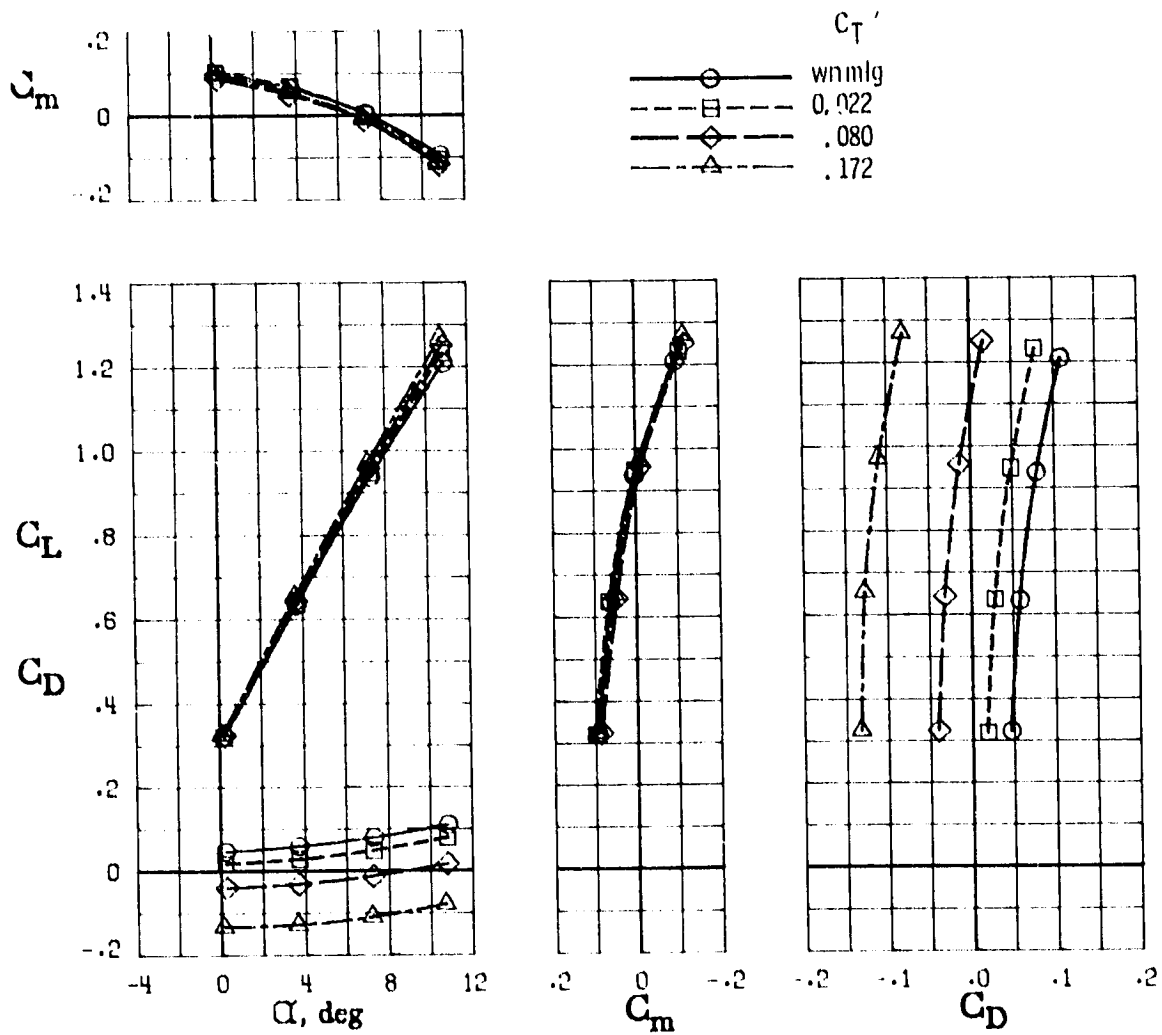
(b) β = 24°.

Figure 14.- Continued.

(c) $\beta = 32^{o}$.
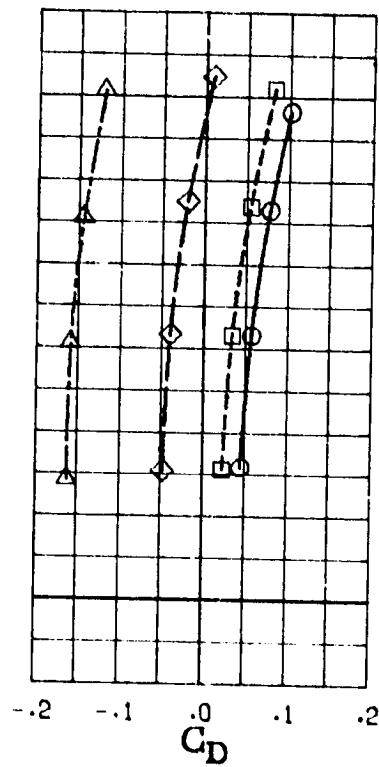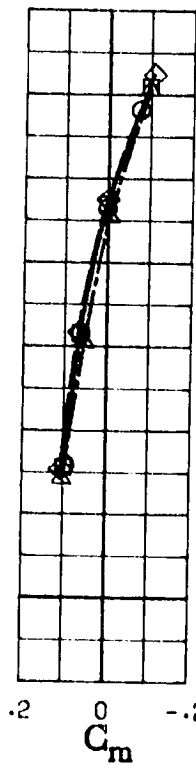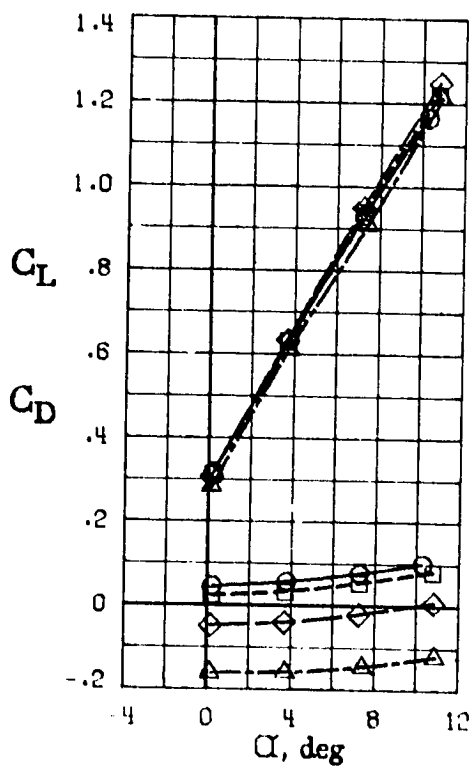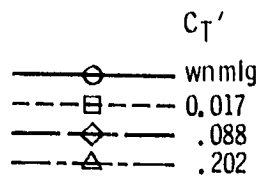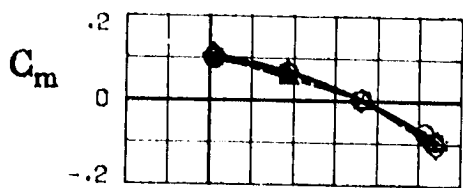
Figure 14 - Continued.
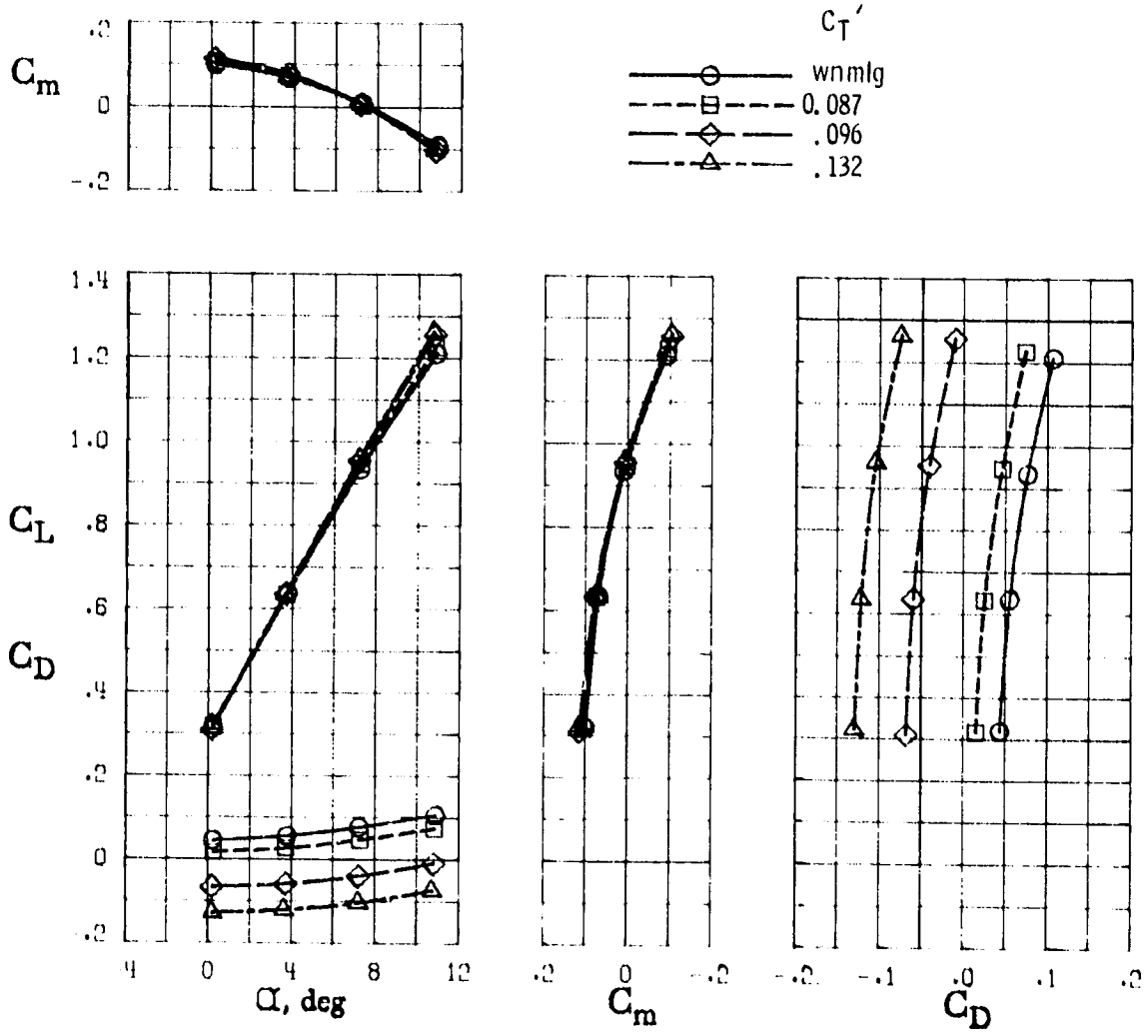
(d) $\beta = 36°$.

Figure 14.- Concluded.
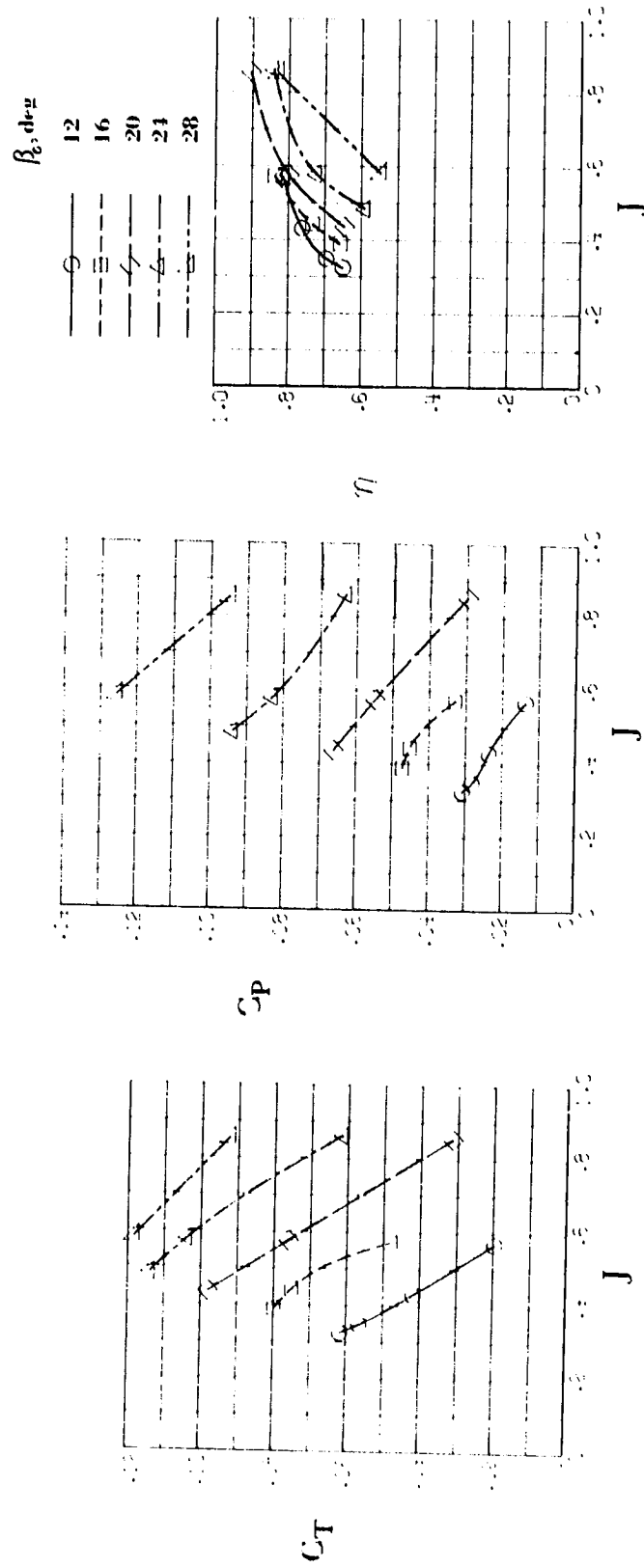
(a) $\alpha = 0°$.

Figure 15.- Aerodynamic characteristics of free propeller. $\delta_f = 0°$.
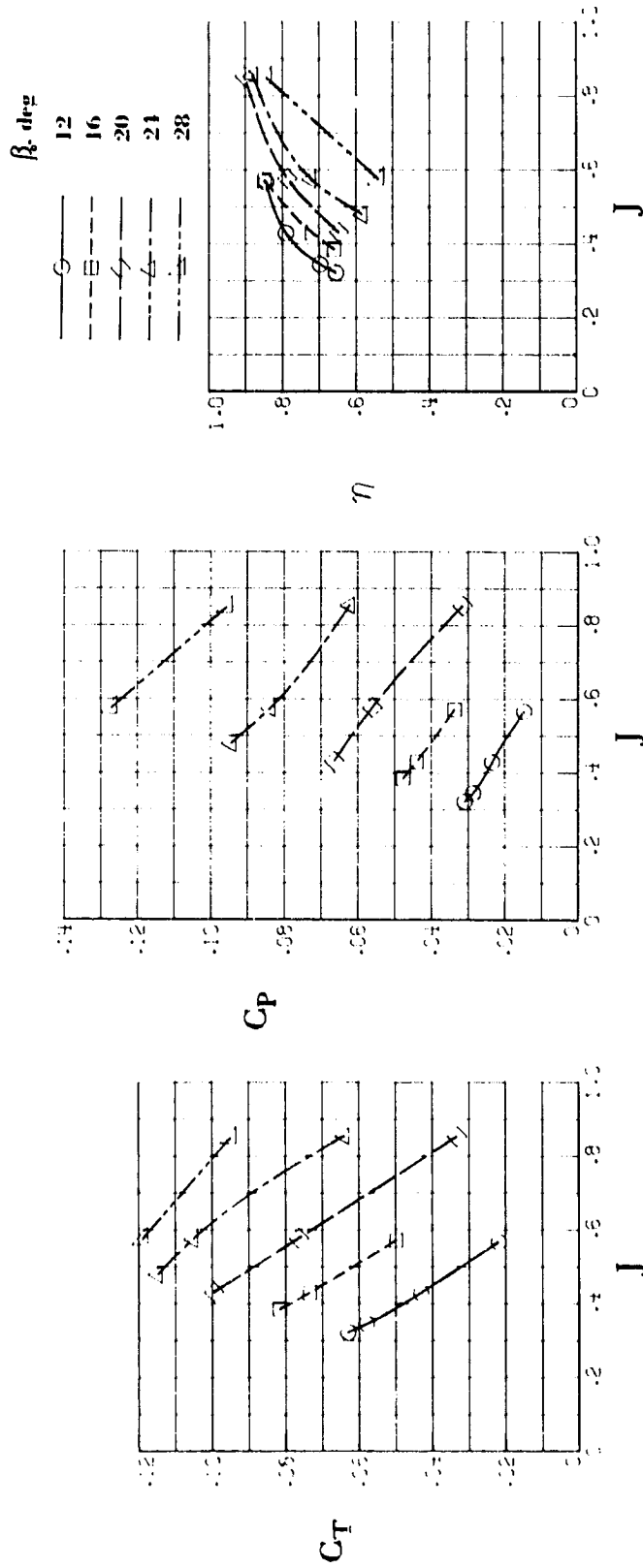
(b) α = 4°.

Figure 15.- Continued.

(c) α = 8°.
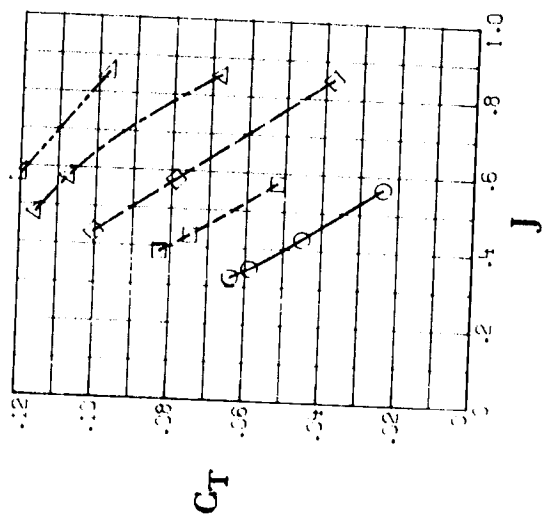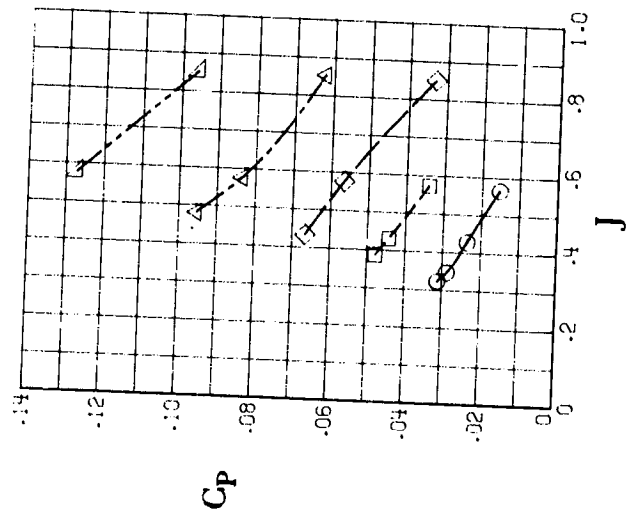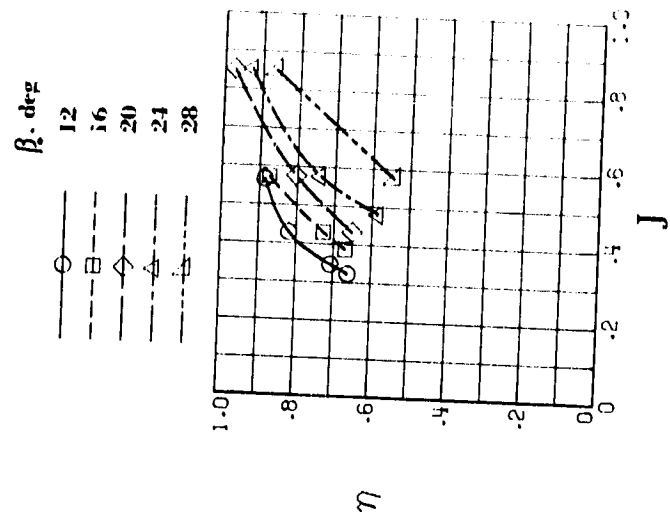
Figure 15.- Continued.

(d) $\alpha = 12°$.
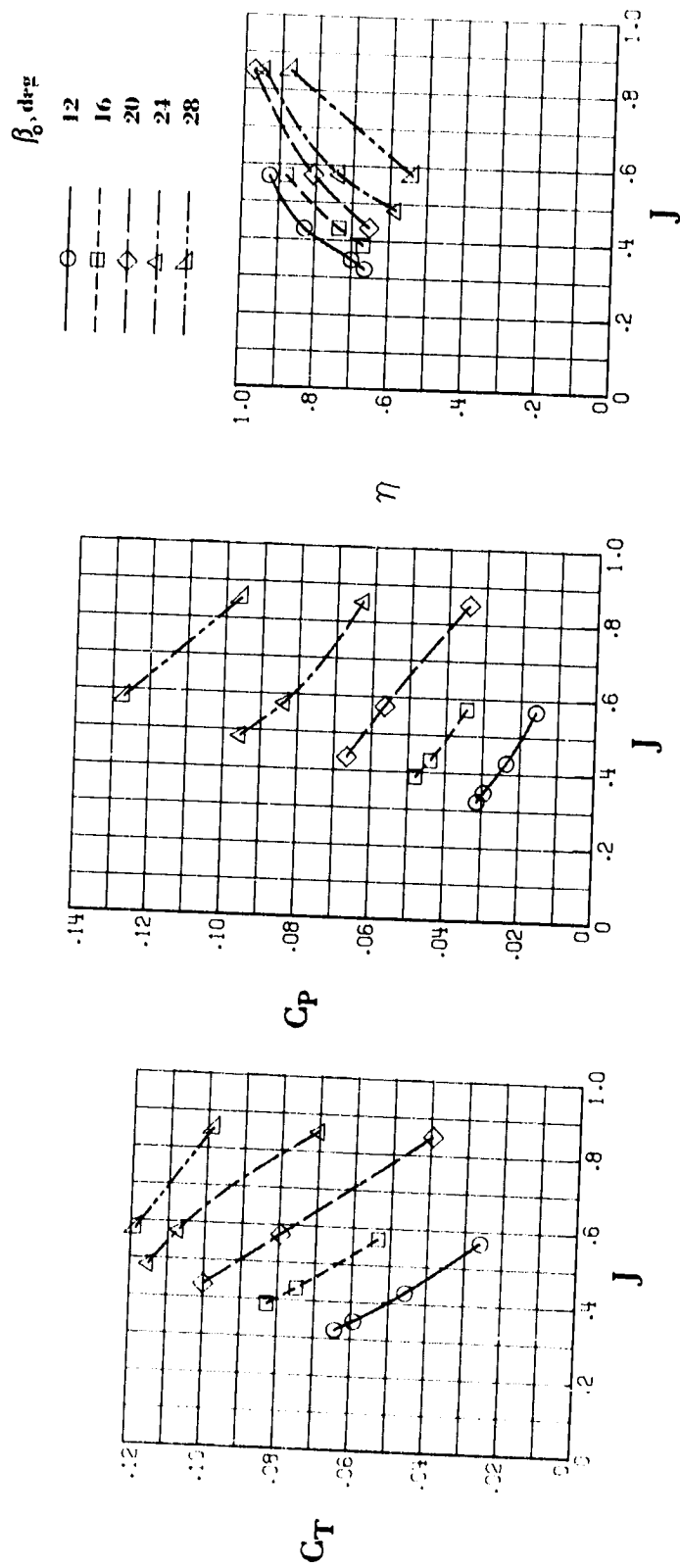
Figure 15.- Concluded.
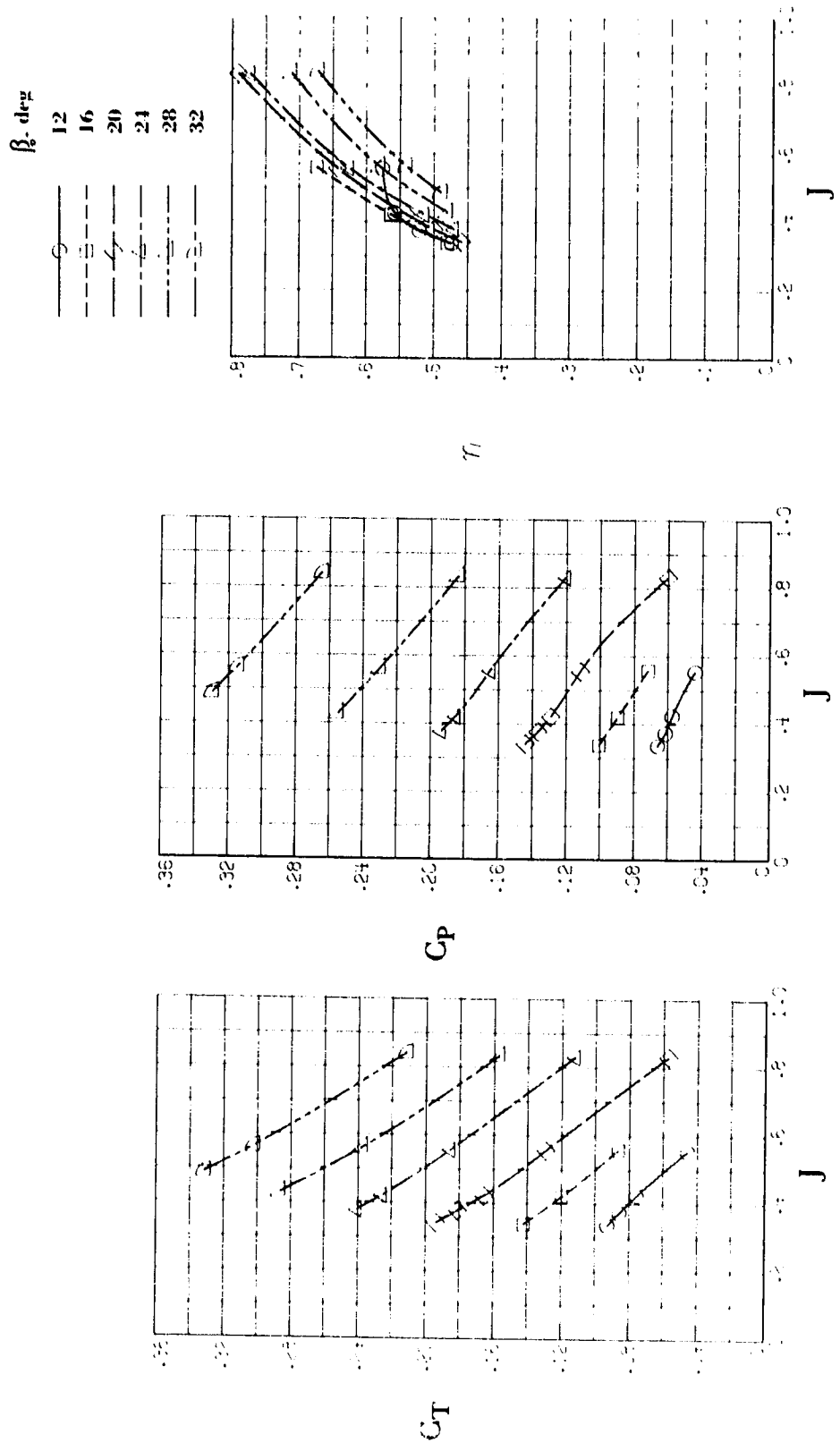
Figure 16.- Aerodynamic characteristics of 3-blade, shrouded propeller with unloaded tip. $\delta_f = 0^o$.

(a) $\alpha = 0^o$.

63
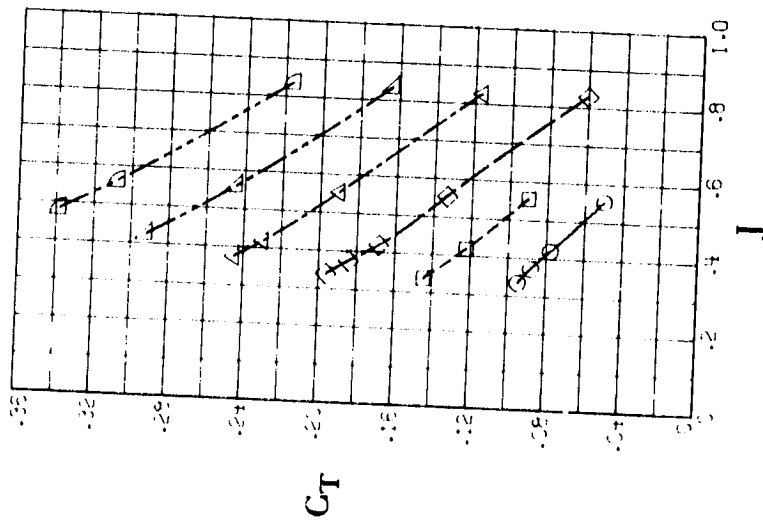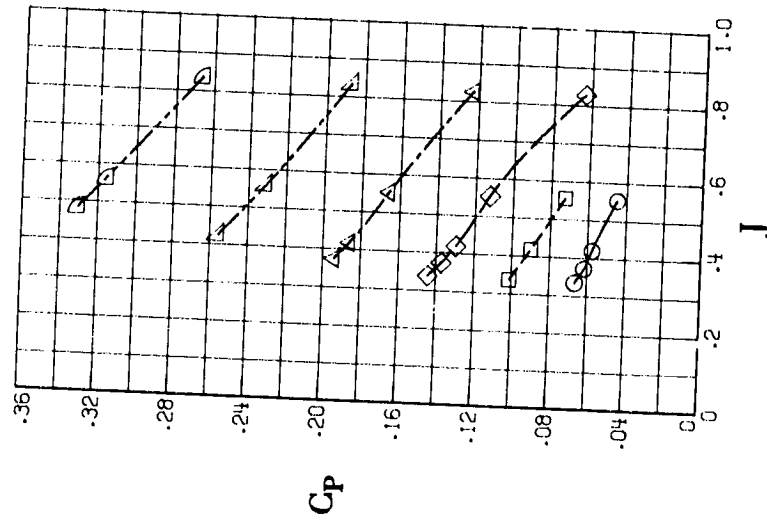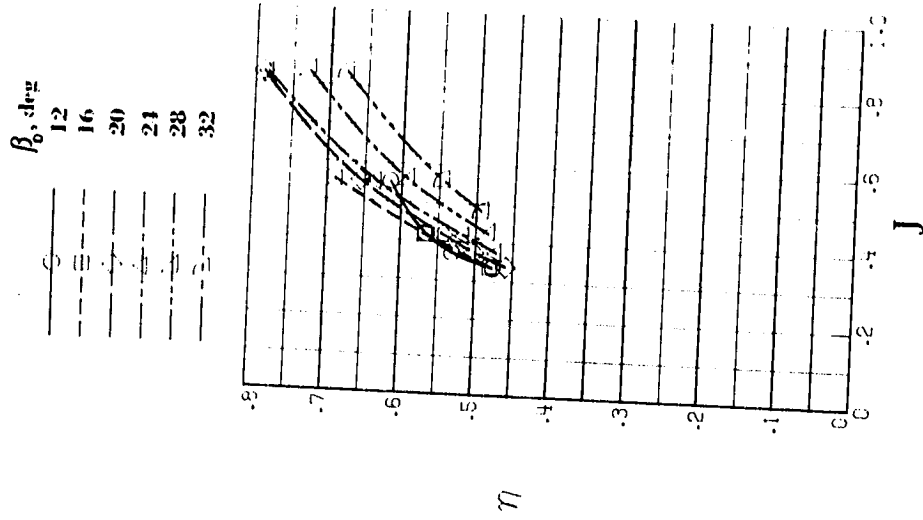
(b) $\alpha = 4^{\circ}$.

Figure 16.- Continued.

64
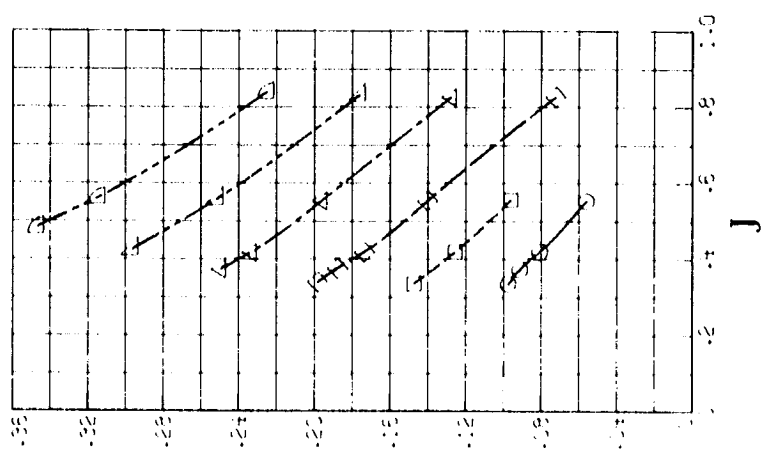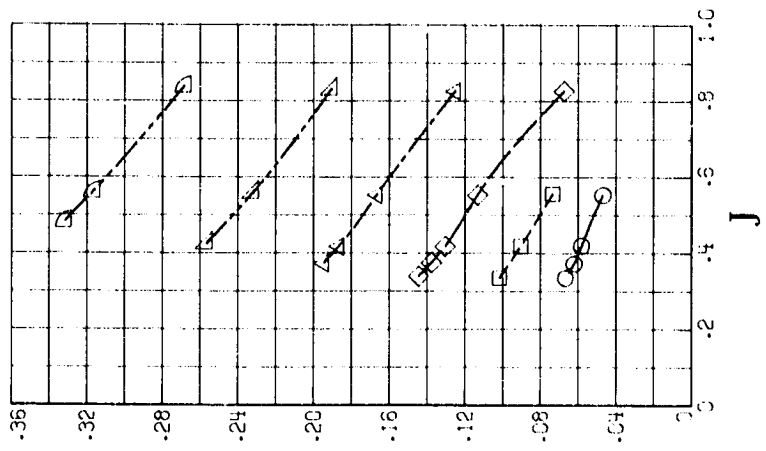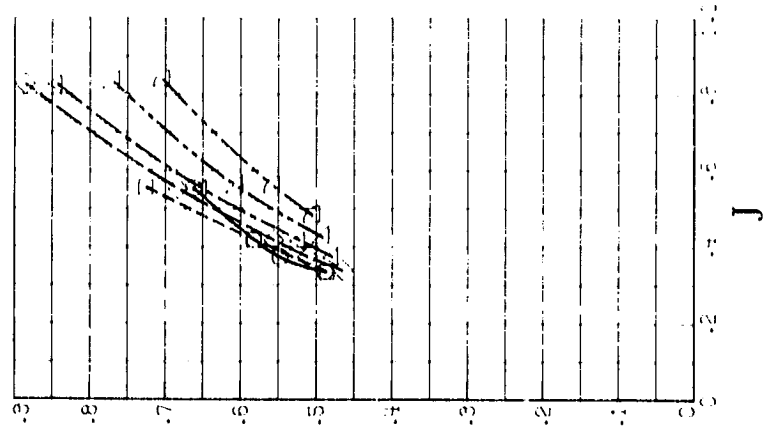
(c) α = 8°.

Figure 16.- Continued.

65

β_0, deg

	12
	16
	20
	24
	28
	32

(d) $\alpha = 12^c$.
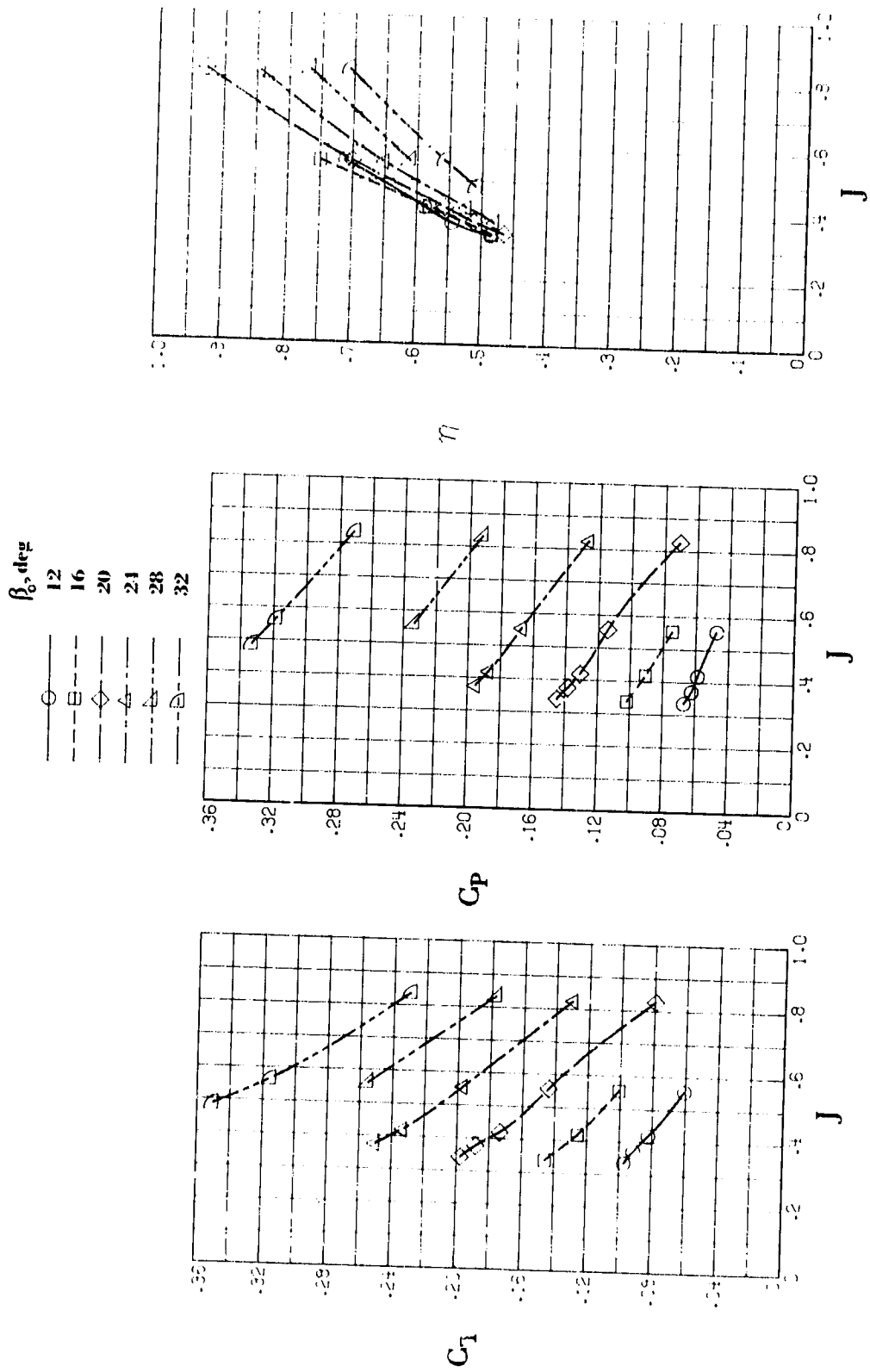
Figure 16.- Concluded.
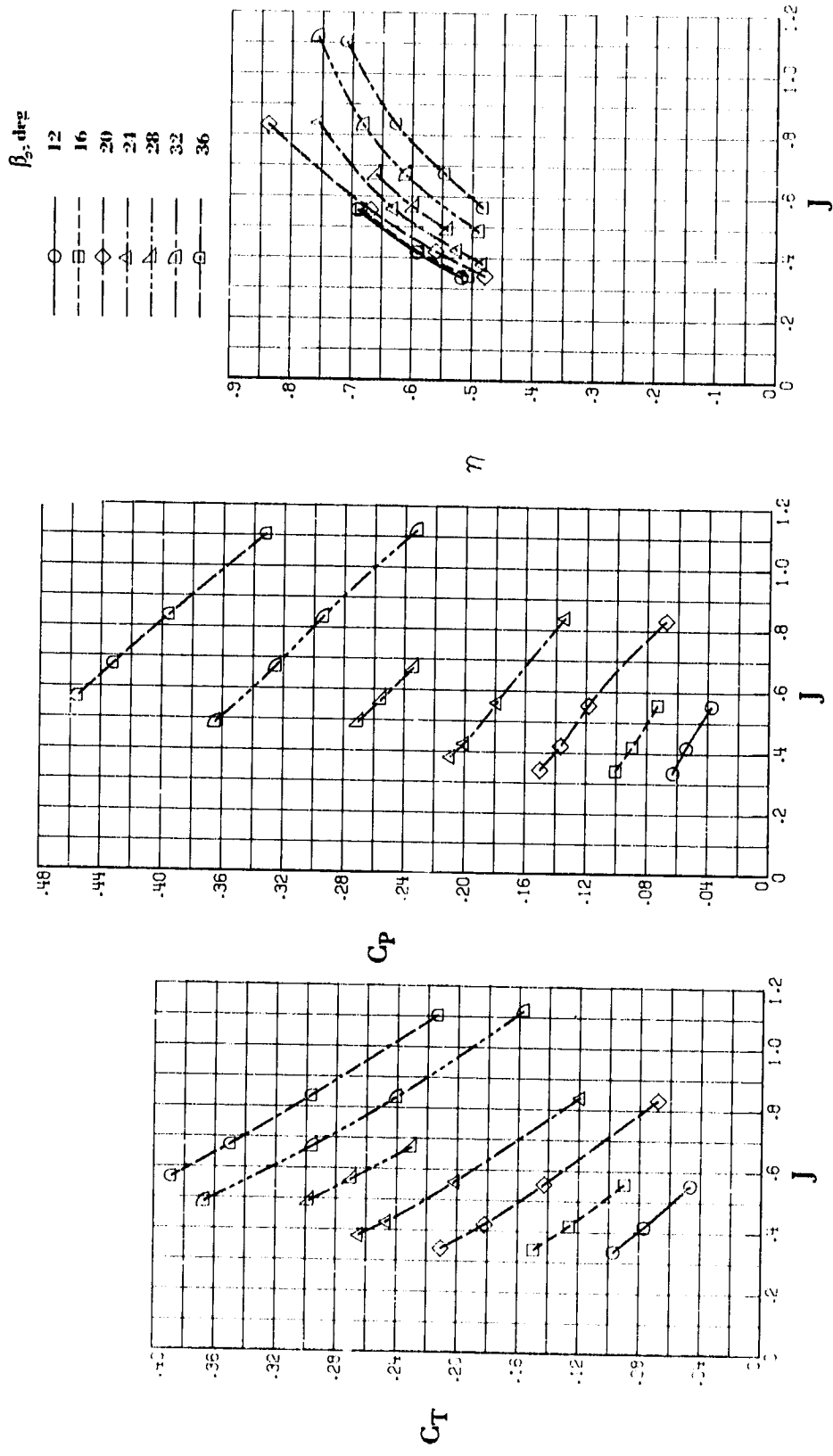
Figure 17.- Aerodynamic characteristics of 3-blade, shrouded propeller with normal tip. $\delta_f = 0^o$.

(a) $\alpha = 0^o$.
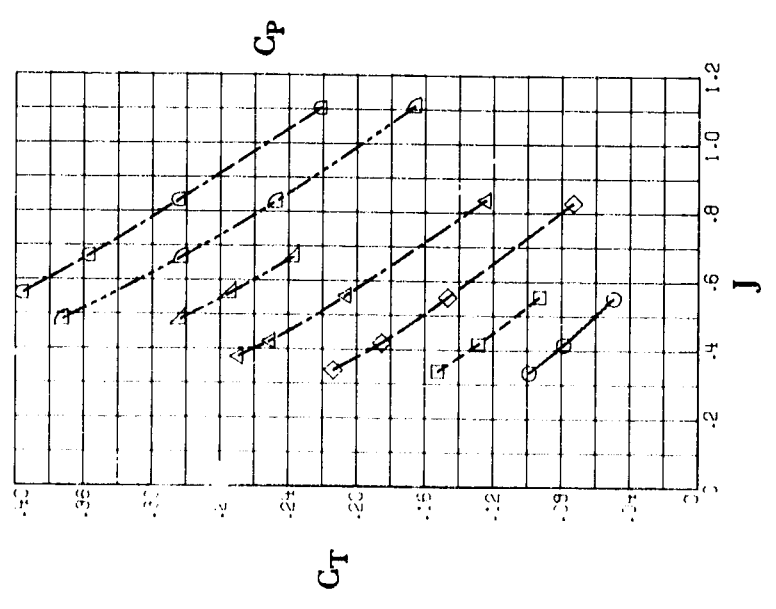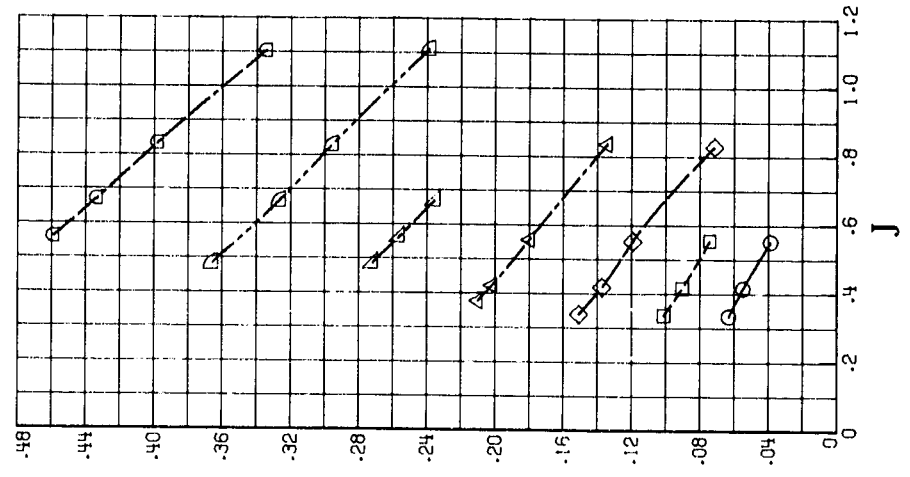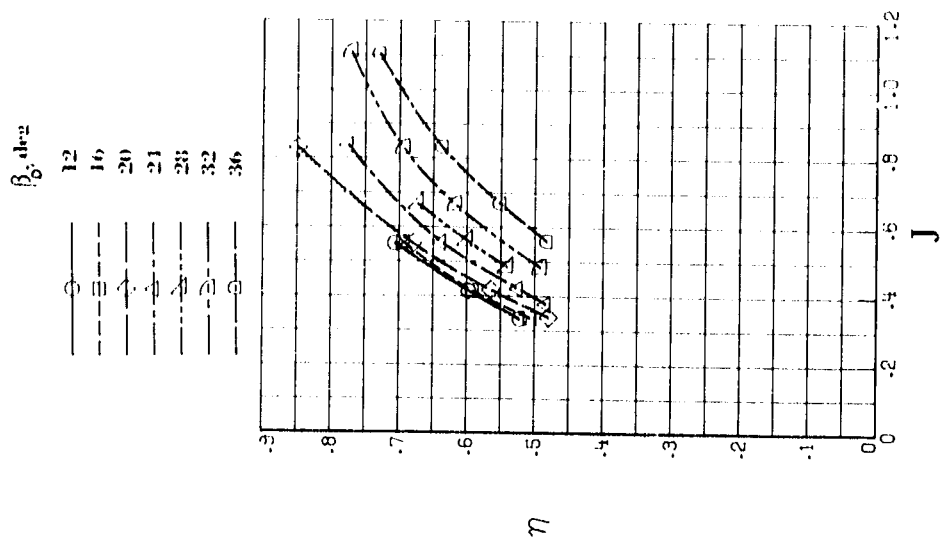
(b) $\alpha = 4°$.

Figure 17.– Continued.
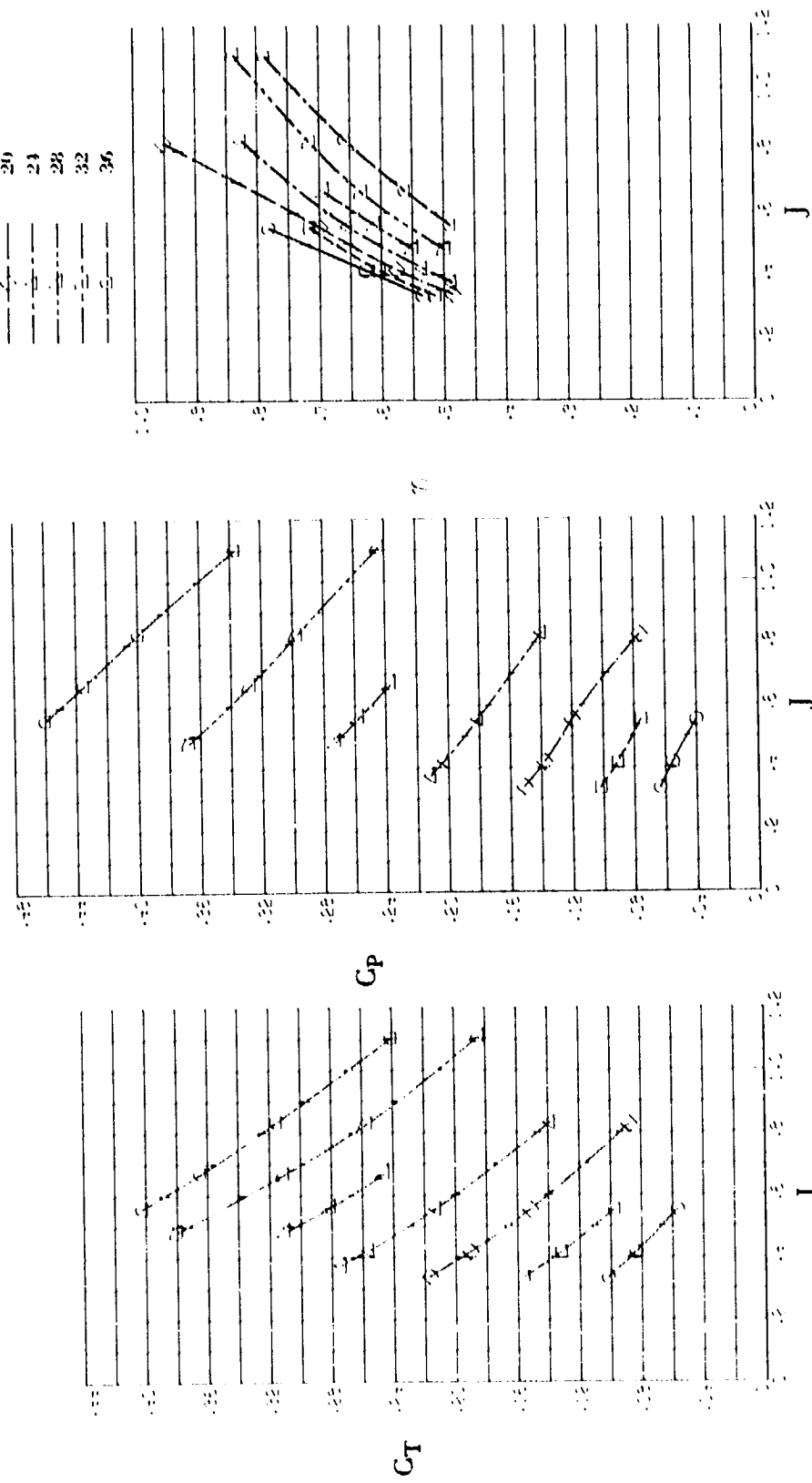
(c) $\alpha = 8^\circ$.

Figure 17.- Continued.

69

(d) $\alpha = 12°$.
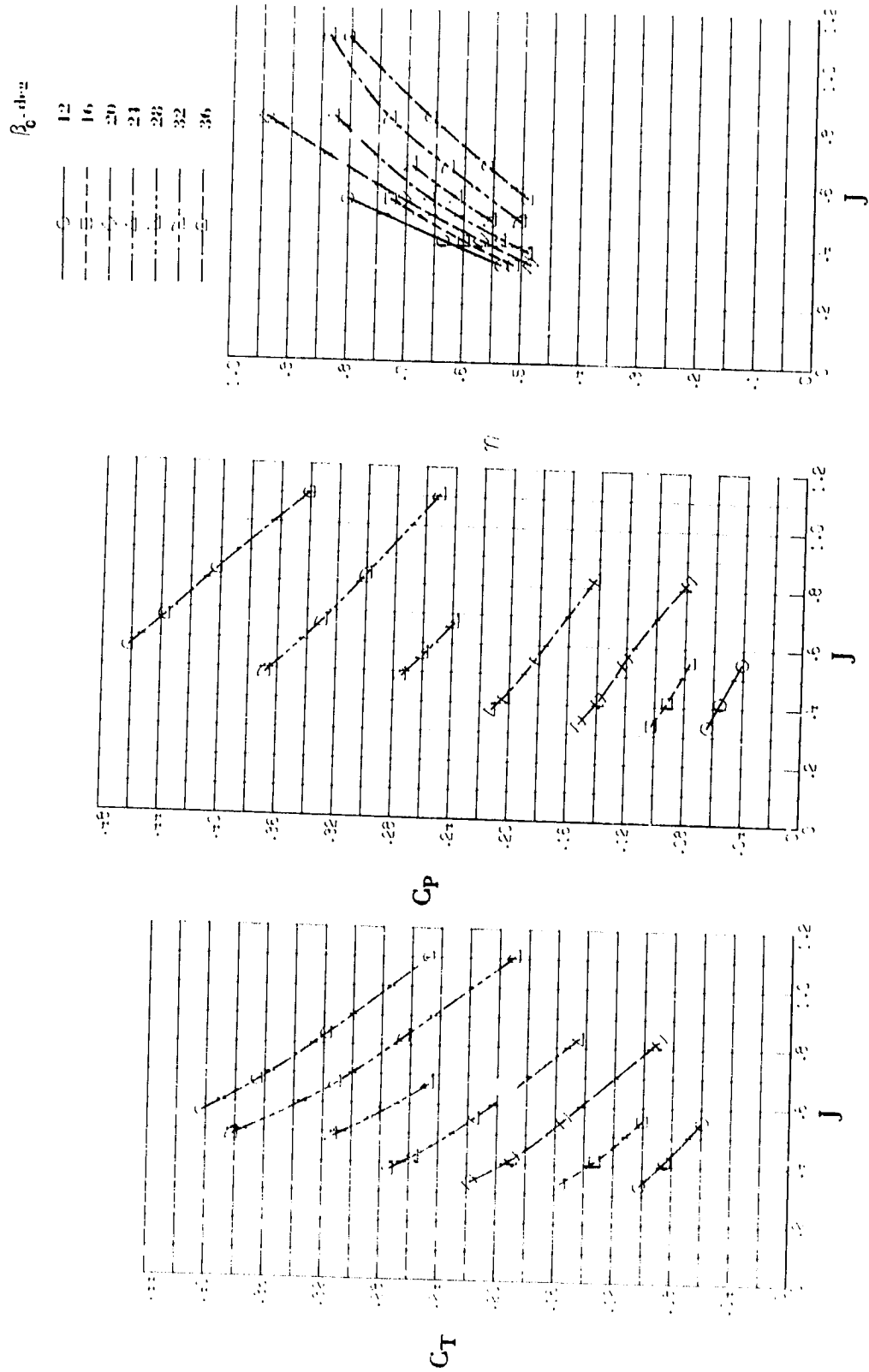
Figure 17.- Concluded.
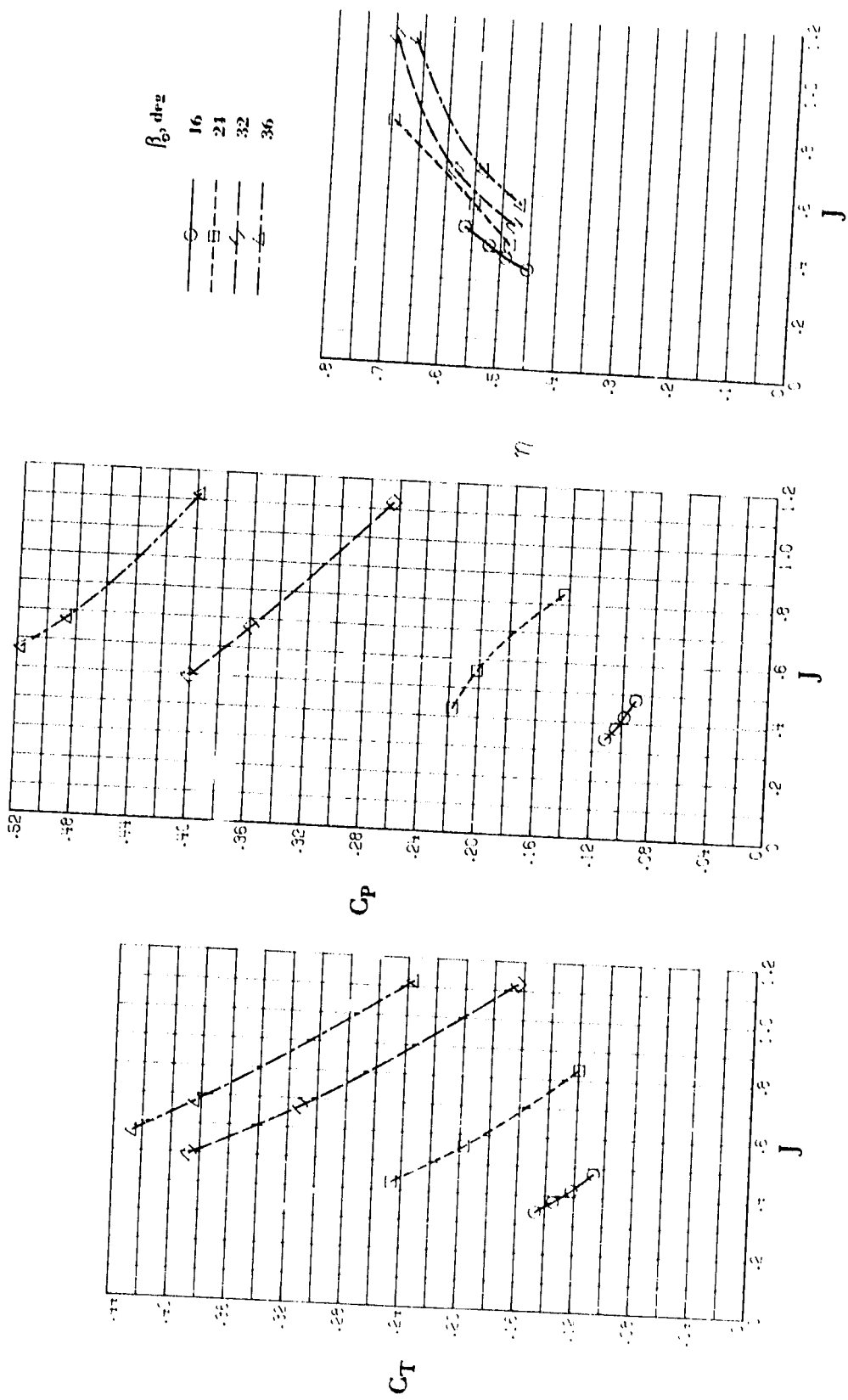
Figure 18.— Aerodynamic characteristics of 5-blade, shrouded propeller with unloaded tip. $\delta_f = 0^\circ$.

(a) $\alpha = 0^\circ$.

71

(b) α = 4°.
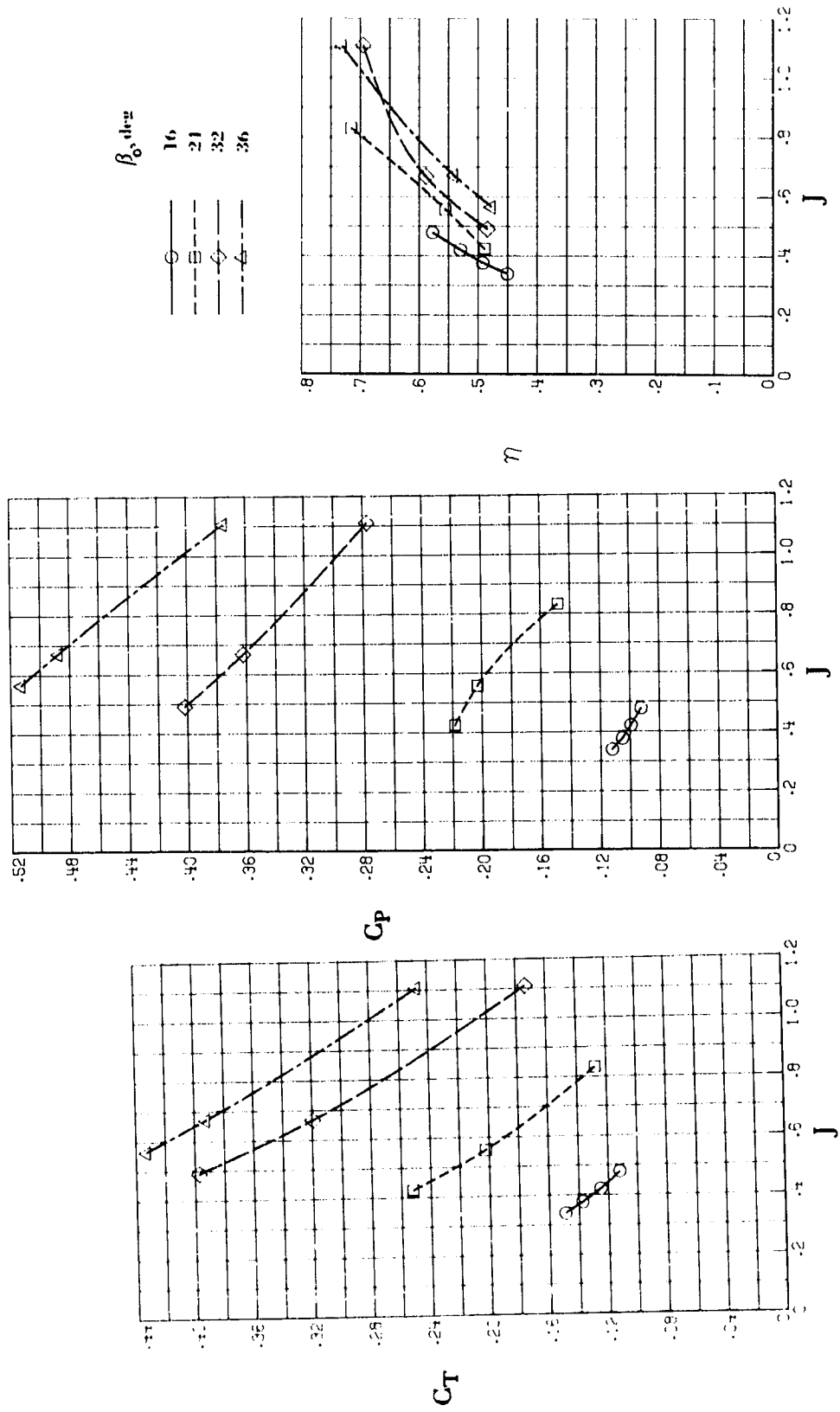
Figure 18.- Continued.

(c) $\alpha = 8°$.

Figure 18.- Continued.

73
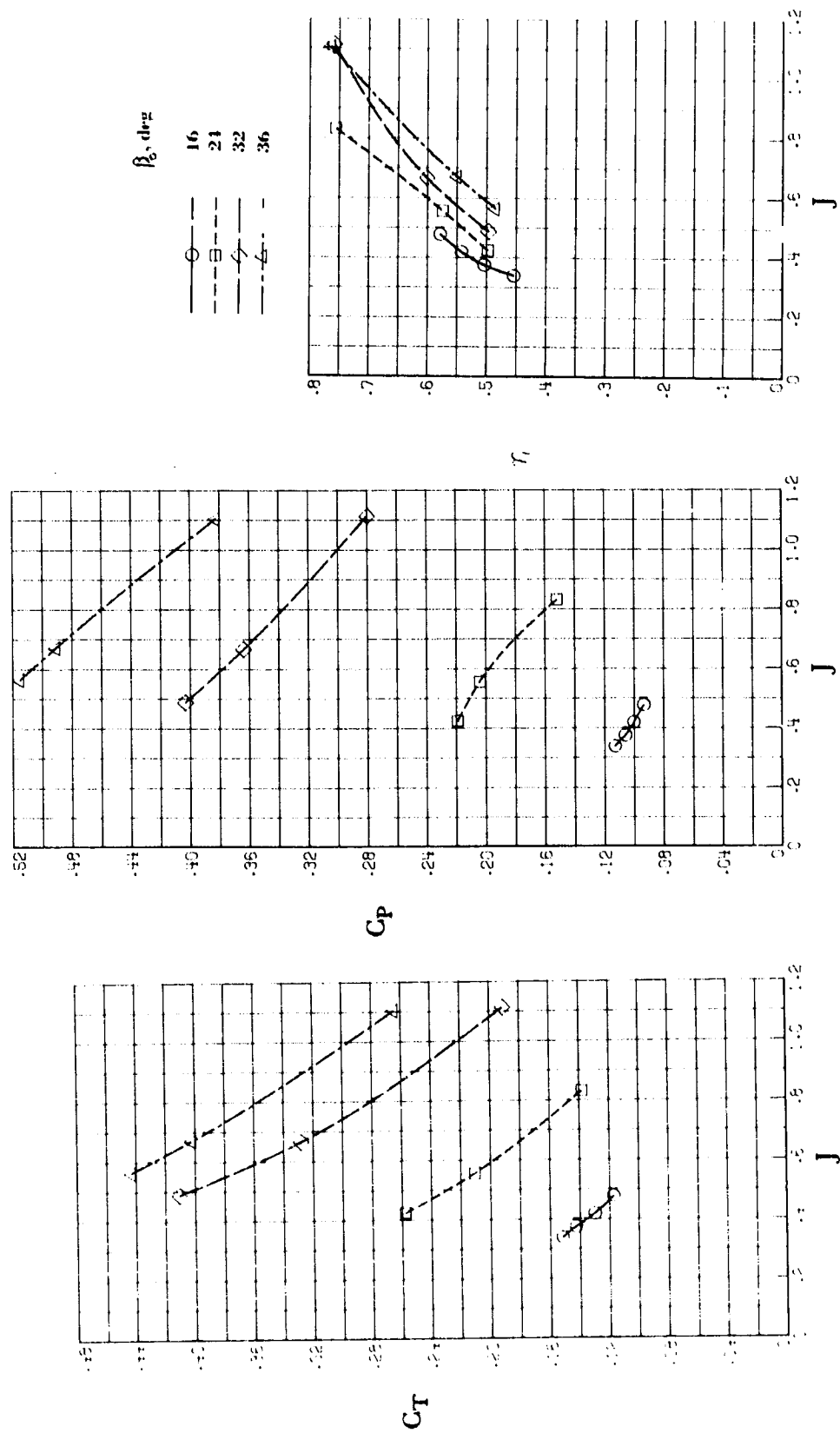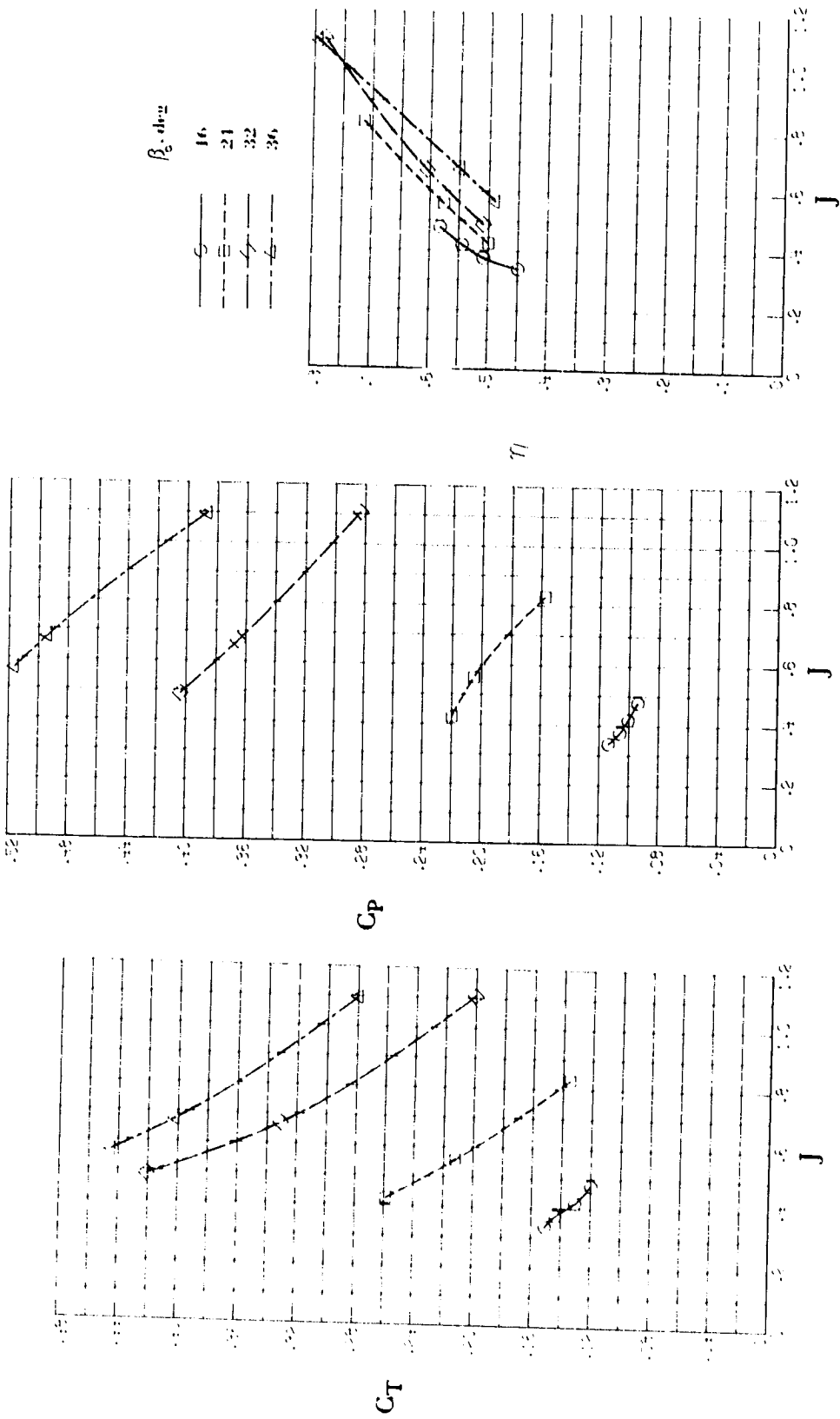
(d) $\alpha = 12^\circ$.

Figure 18.- Concluded.
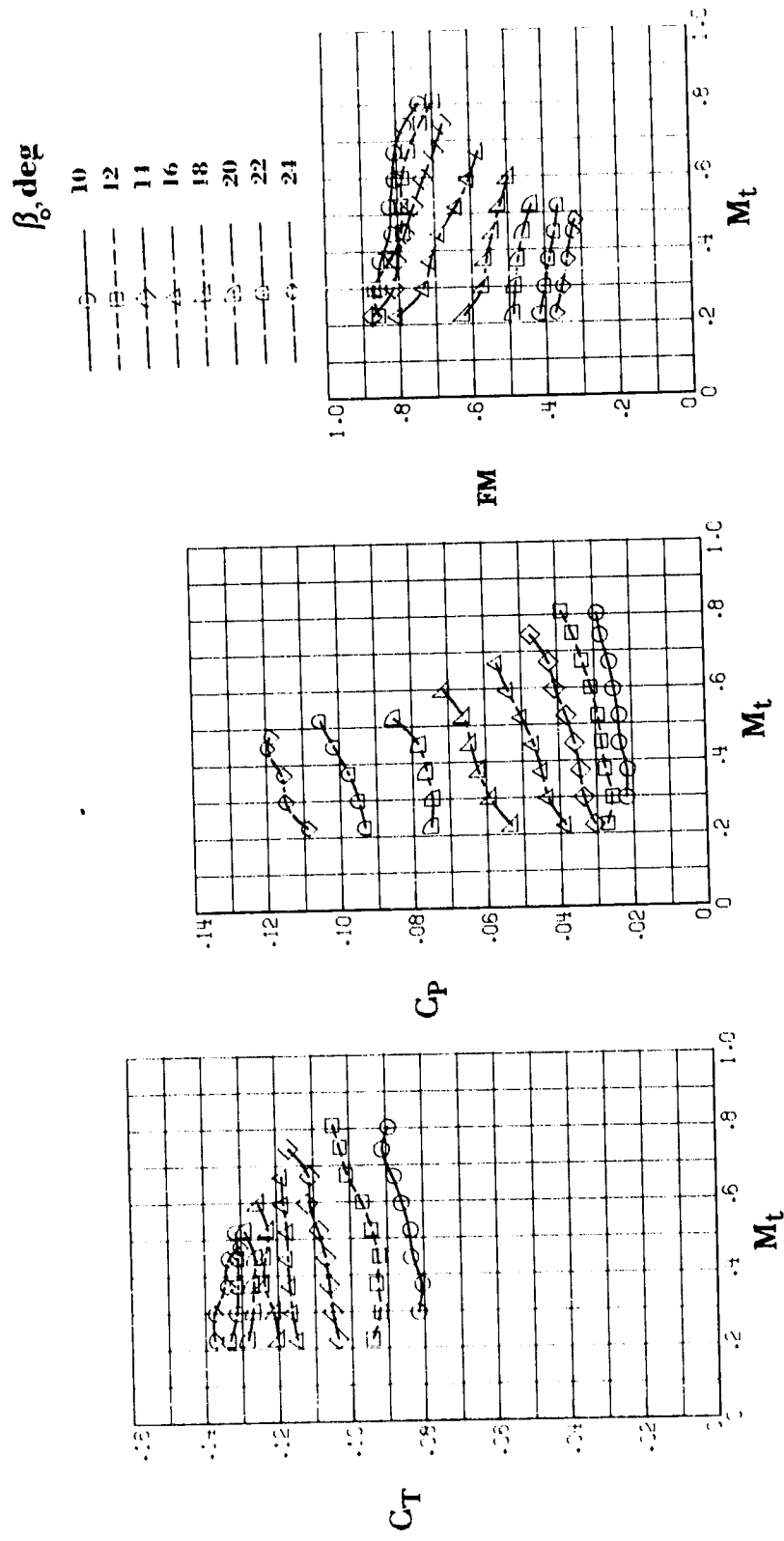
Figure 19.- Effect of blade angle and tip Mach number on static performance of 2-blade free propeller.
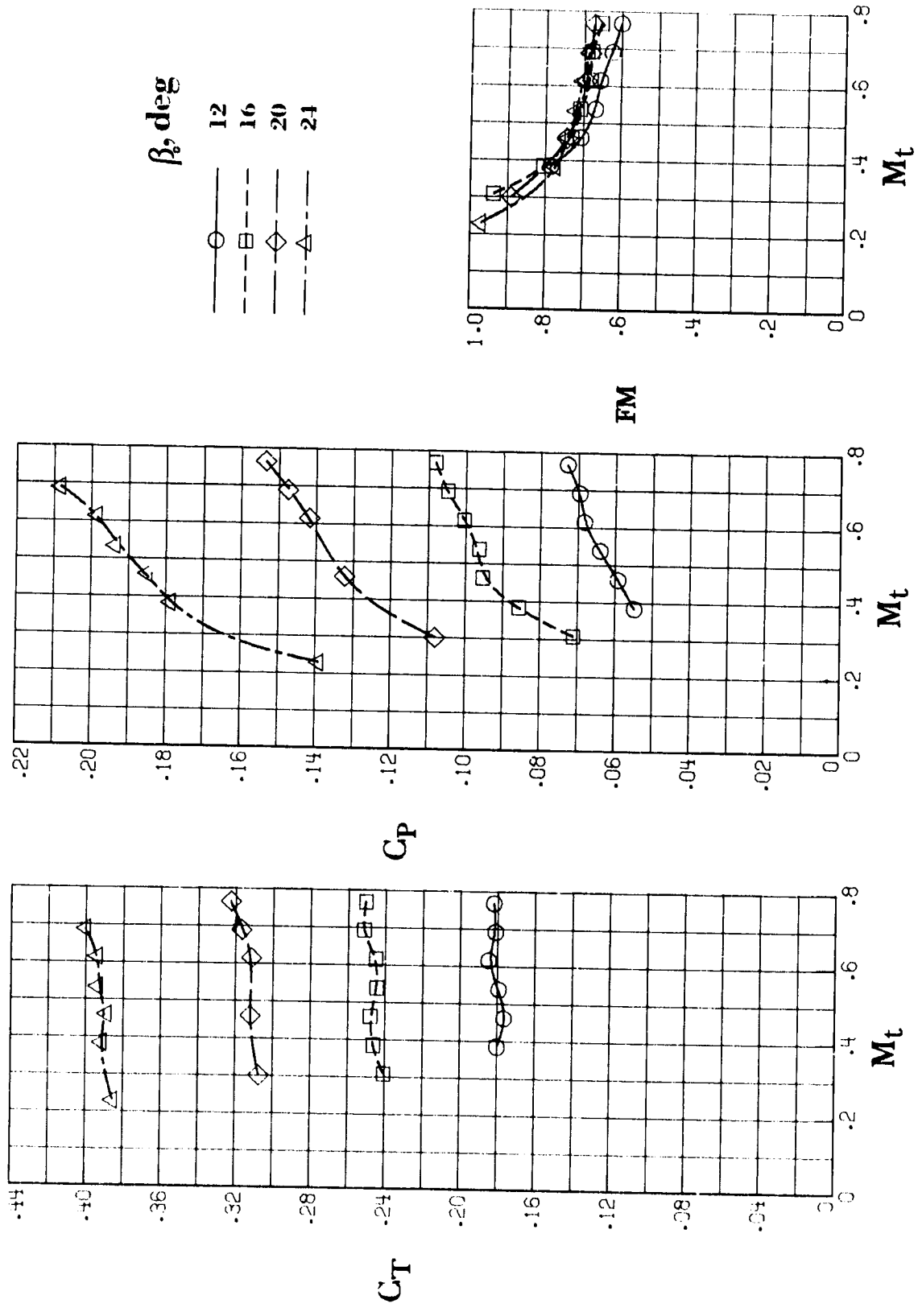
Figure 20.- Effect of blade angle and tip Mach number on static performance of 3-blade, shrouded, unloaded-tip propeller.
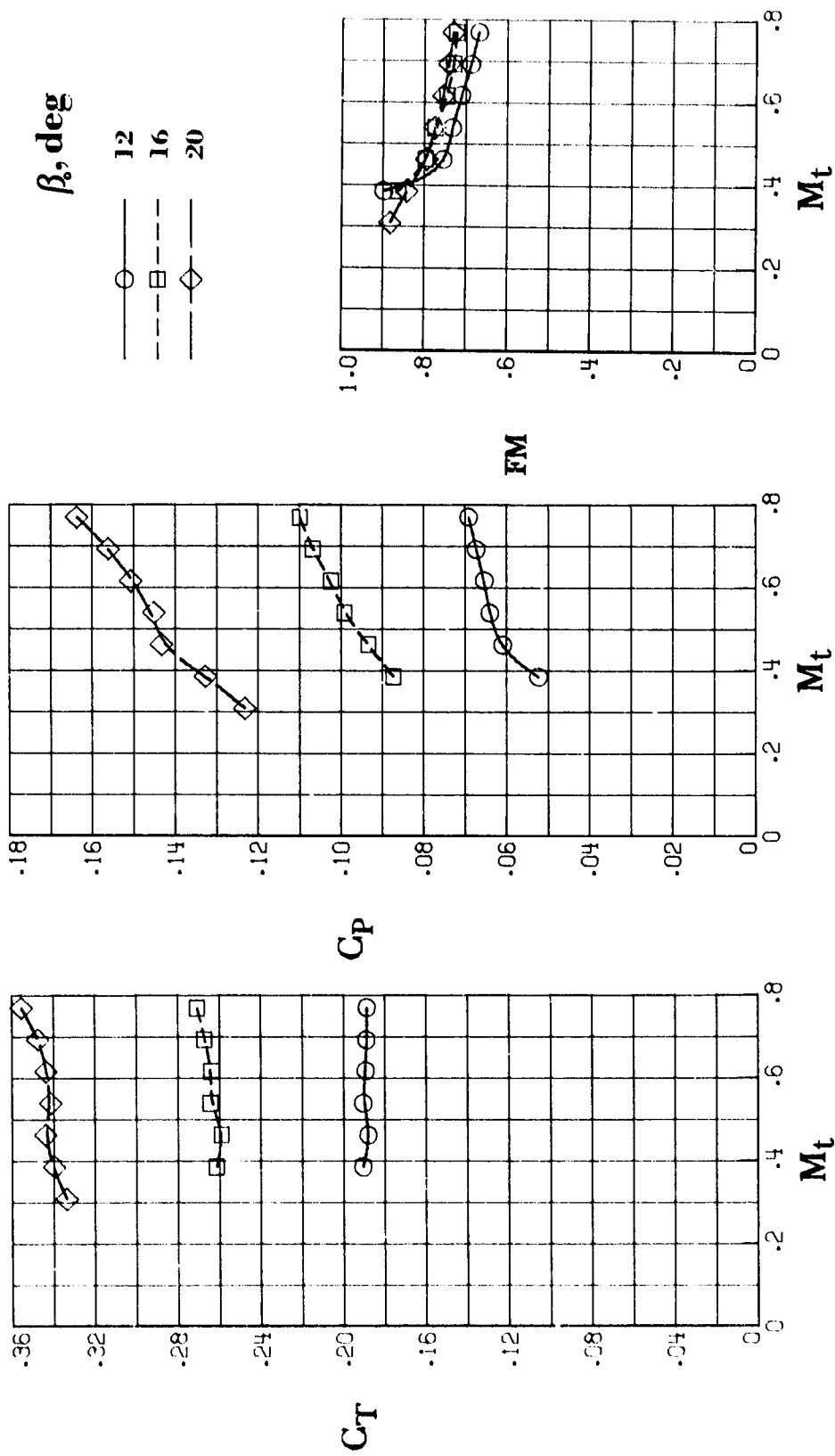
Figure 21.- Effect of blade angle and tip Mach number on static performance of 3-blade, shrouded, normal-tip propeller.

77
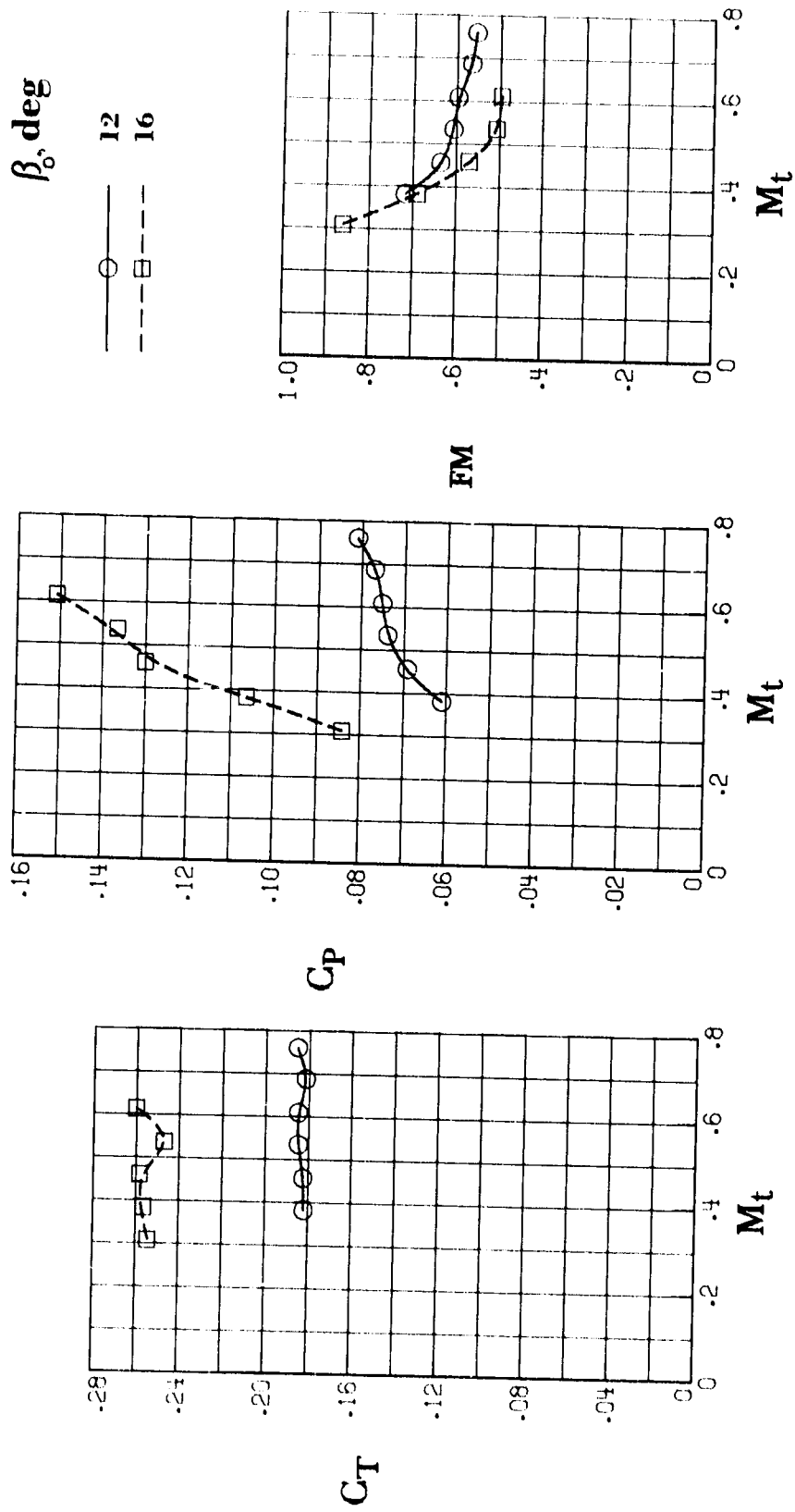
Figure 22.- Effect of blade angle and tip Mach number on static performance of 5-blade, shrouded, unloaded-tip propeller.
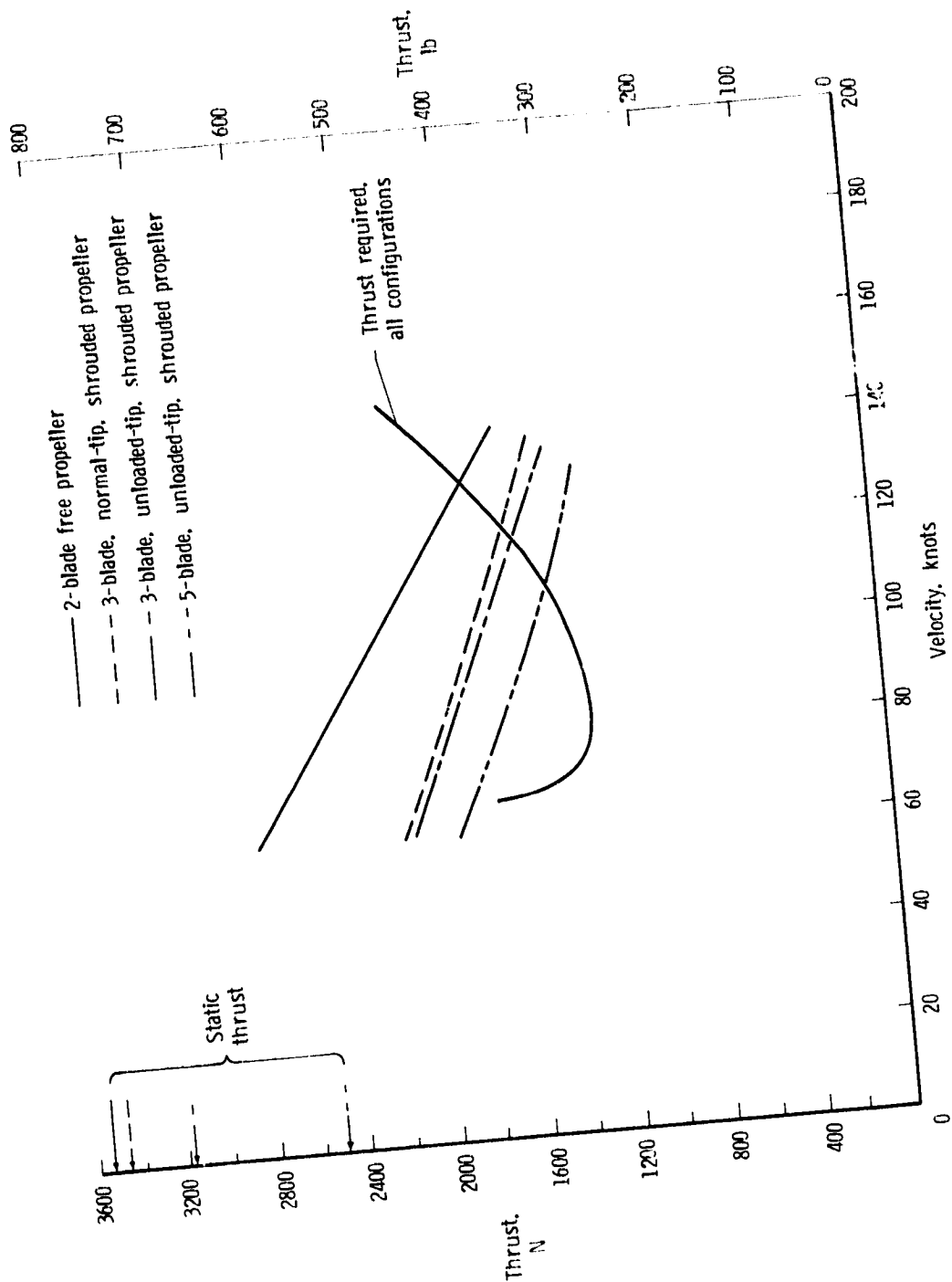
(a) Full-power conditions.

Figure 23.- Variation of thrust with velocity for four propeller configurations.
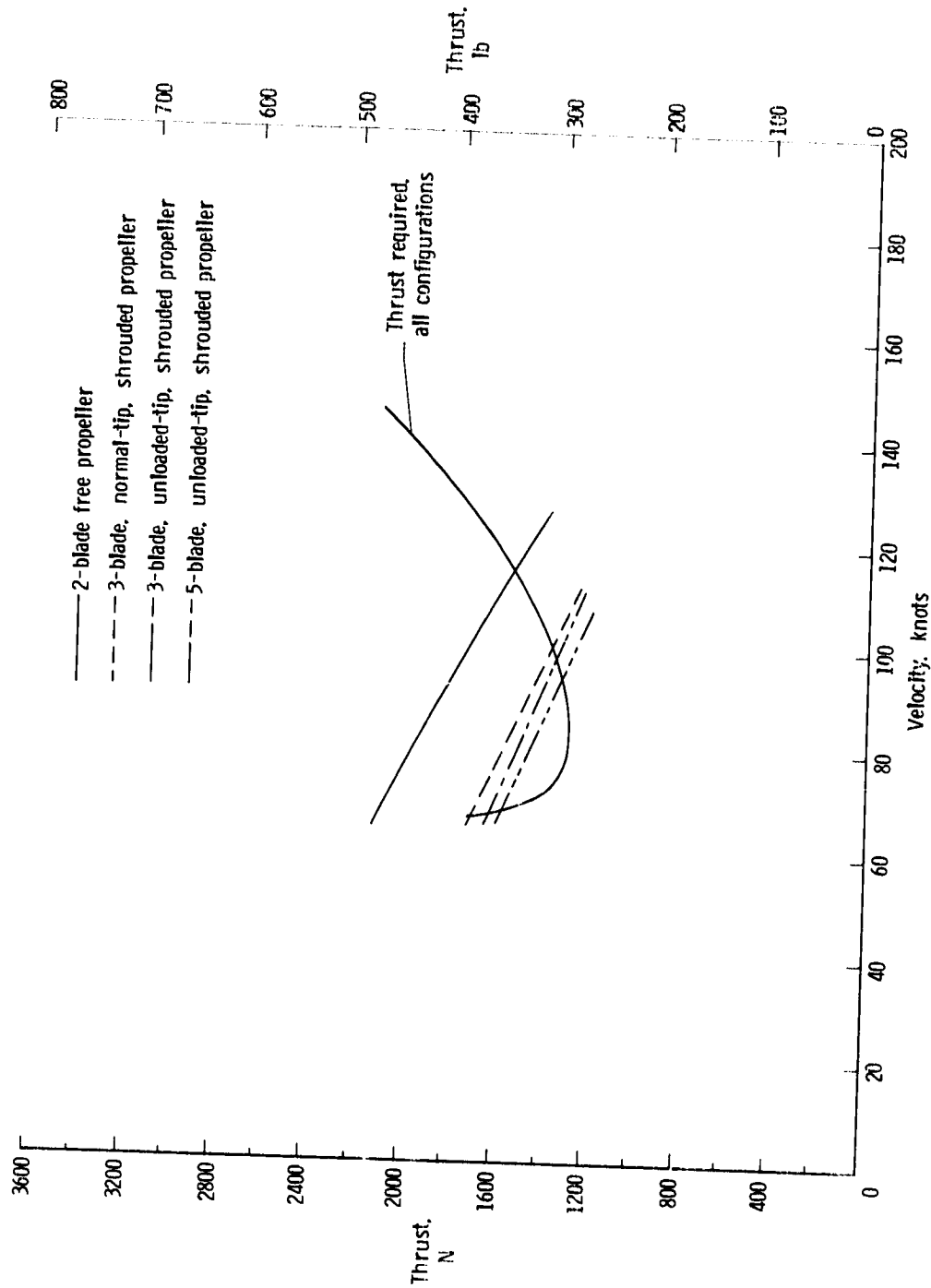
(b) Cruise conditions (0.75 power and 0.80 rpm).

Figure 23.– Concluded.

V = 0
Power = 128 kW (174 hp)
Thrust = 4014 N (902 lb)
2700 rpm

V = 25 m/sec (81 ft/sec)
Power = 112 kW (150 hp)
Thrust = 2678 N (602 lb)
2700 rpm
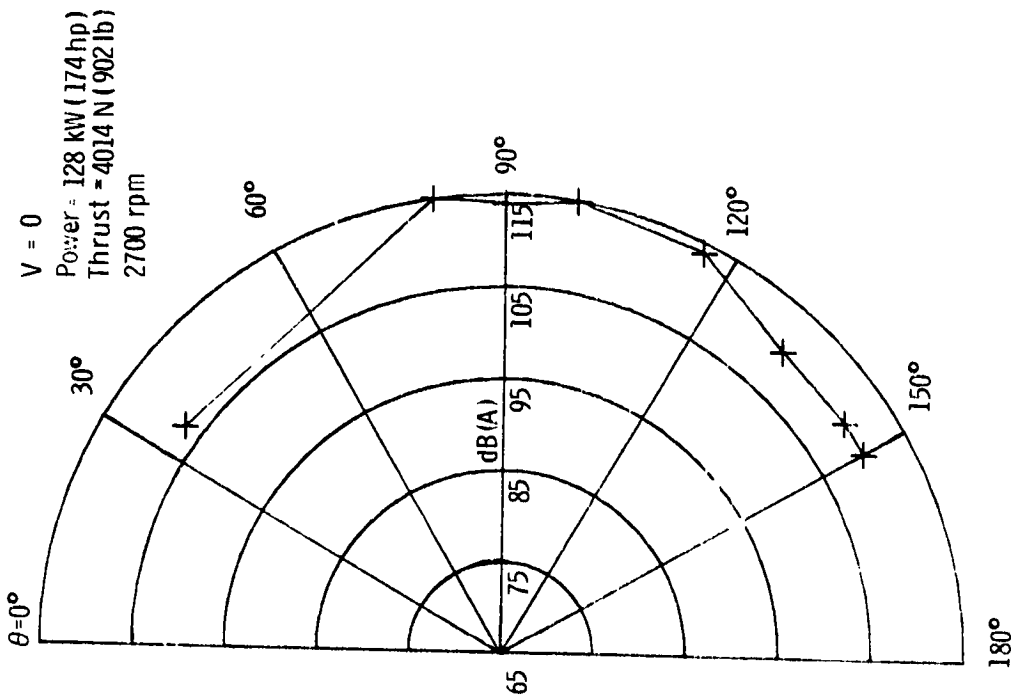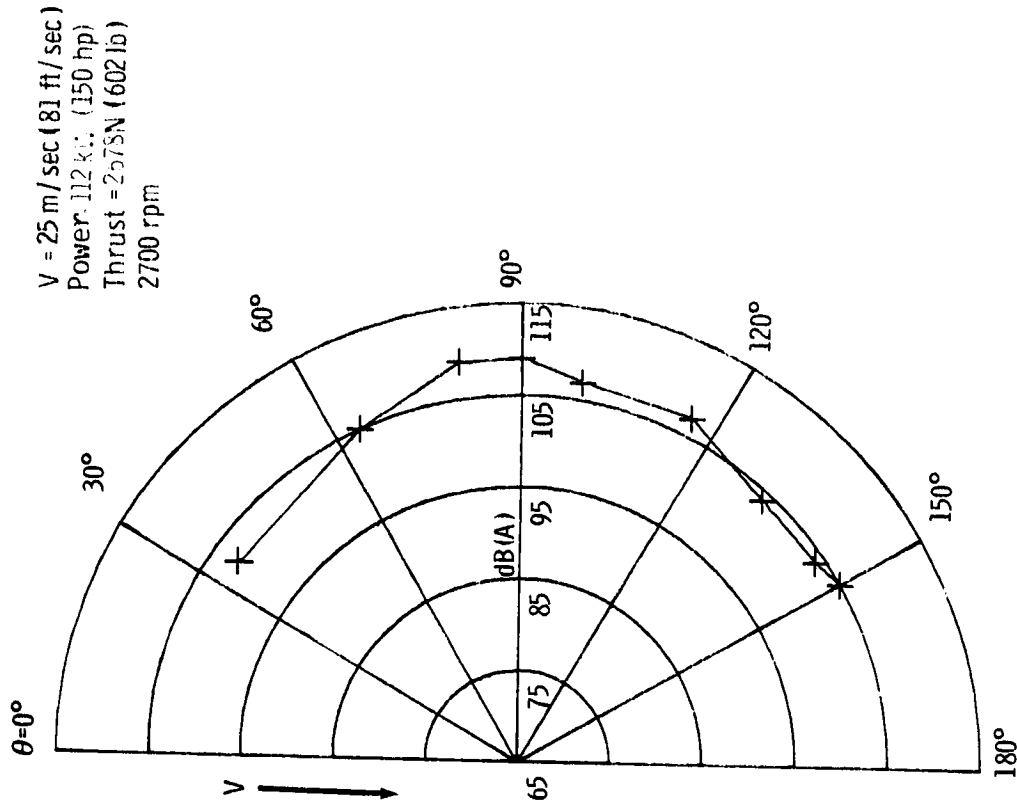
(a) Static (run 21(06)).

(b) Tunnel operating (run 54(01)).

Figure 24.- Acoustic directivity pattern for airplane with 2-blade free propeller operating.

81
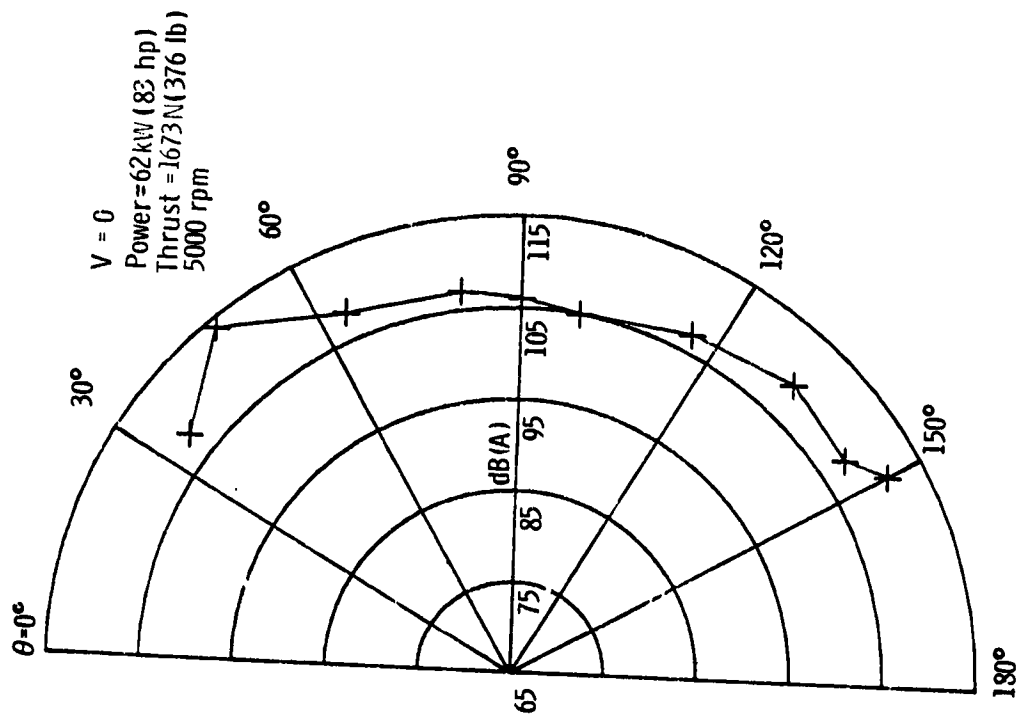
(a) Static (run 64(09)).

(b) Tunnel operating (run 77(01)).

Figure 25.- Acoustic directivity pattern for airplane with 5-blade shrouded propeller operating.

(a) Static.

(b) Tunnel operating.
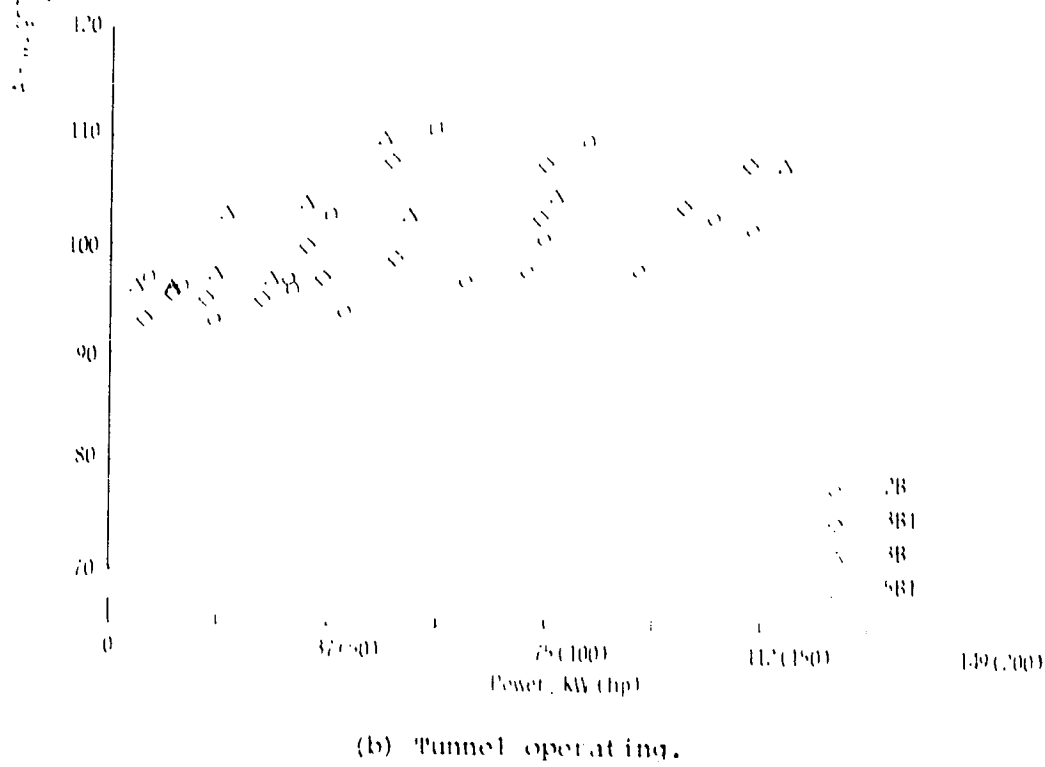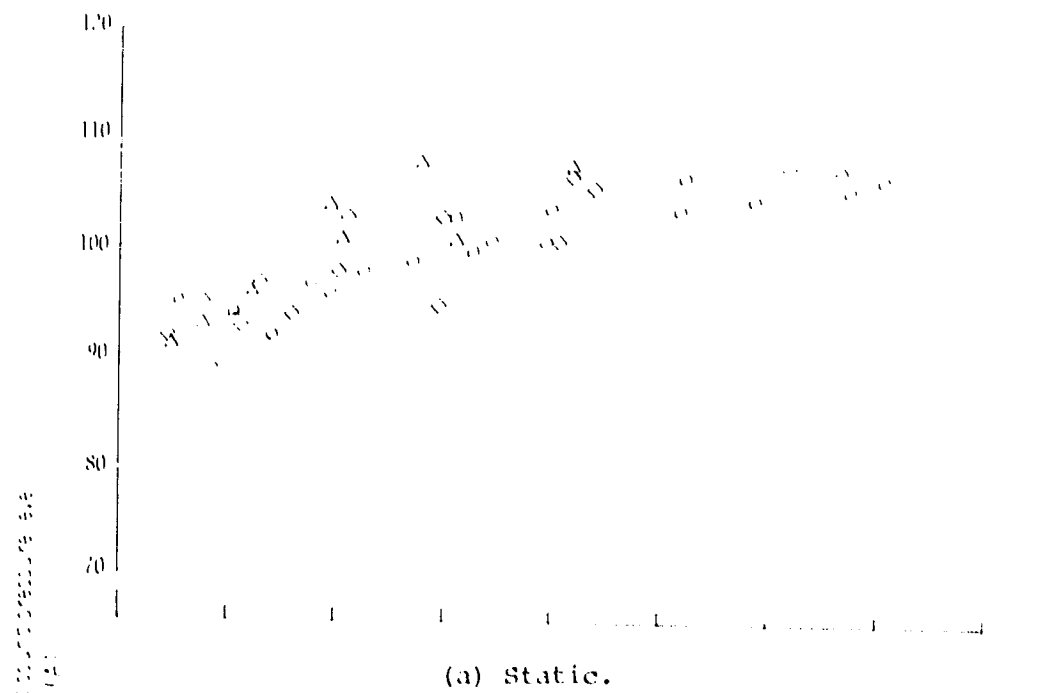
Figure 26.— A-weighted SPL measured at position 2 plotted against power as a function of propeller configuration.
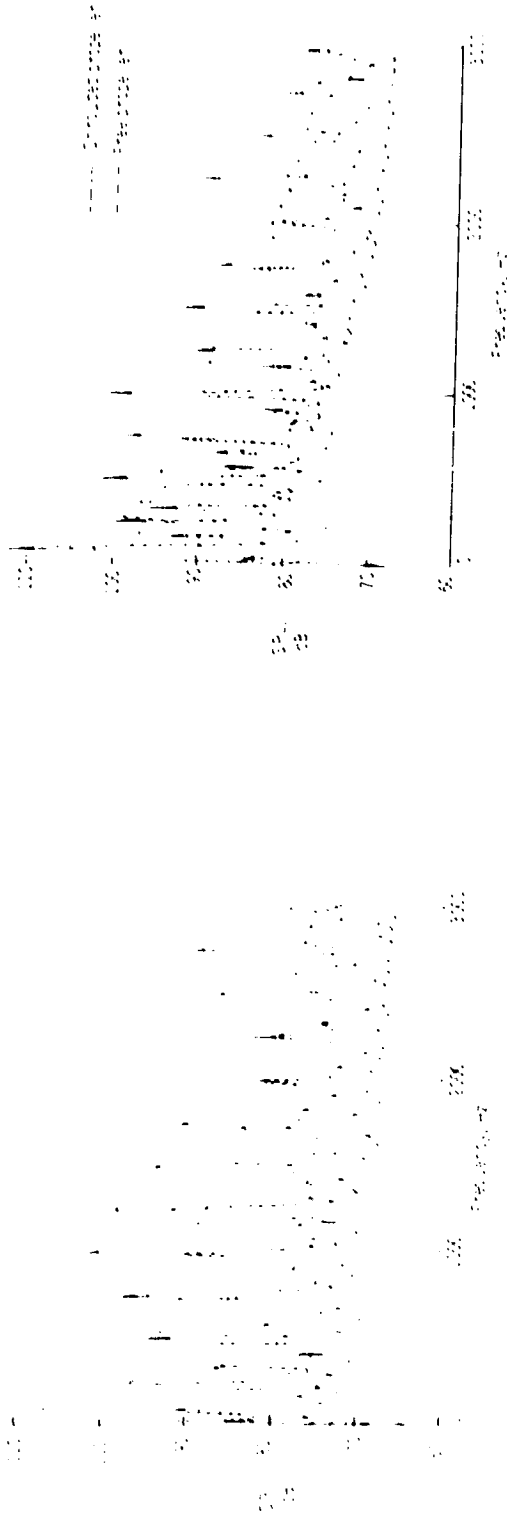
(a) 2-blade and 3-blade normal-tip propellers.

(b) 2-blade and 3-blade unloaded-tip propellers.

Figure 27.- Summary comparison of free and shrouded propellers under static conditions at maximum obtainable power.

84

PARAMETERS	PROPELLERS			
	2B	3B	3BT	5BT
DIAMETER, m (ft)	1.98 (6.50)	1.02 (3.33)	1.02 (3.33)	1.02 (3.33)
NUMBER BLADES	2	3	3	5
BLADE SPEED, rpm	2700	5000	5000	5000
ADVANCE RATIO, V/nD	0.270	0.341	0.340	0.345
THRUST, N (lb)	2678 (602)	1877 (422)	1761 (396)	1348 (303)
POWER, kW (hp)	112 (150)	114 (152)	111 (148)	84 (112)
NOISE LEVEL, dBA	102	111	110	105

Shrouded propeller
Free propeller
Tunnel noise
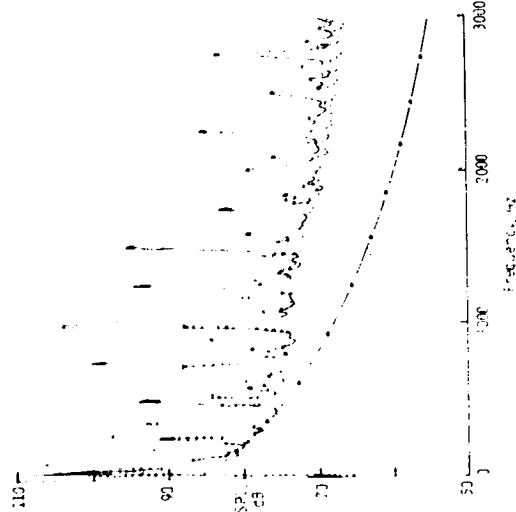
(a) 2-blade and 3-blade normal-tip propeller.
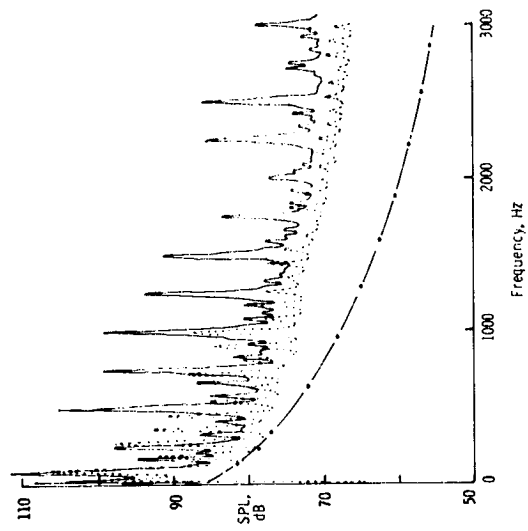
(b) 2-blade and 3-blade unloaded-tip propeller.
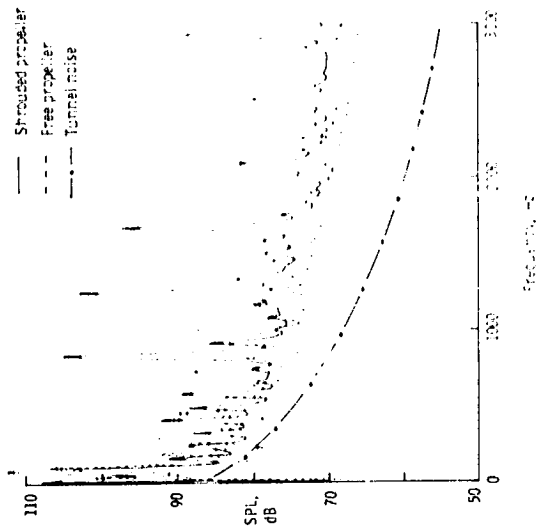
(c) 2-blade and 5-blade unloaded-tip propeller.

Figure 28.- Summary comparison of free and shrouded propellers under tunnel operating conditions at maximum obtainable power.

85